ENGINEERING FIBRIN MATRICES FOR ENHANCED VASCULARIZATION AND CELL INFILTRATION

A Dissertation

Presented to

The Academic Faculty

by

Alison McKissock Douglas

In Partial Fulfillment

of the Requirements for the Degree

Doctor of Philosophy in the

Department of Biomedical Engineering

Georgia Institute of Technology and Emory University

December 2015

ENGINEERING FIBRIN MATRICES FOR ENHANCED VASCULARIZATION AND CELL INFILTRATION

Approved by:

Dr. Thomas H. Barker, Advisor
Department of Biomedical Engineering
Georgia Institute of Technology

Dr. Andrés García School
School of Mechanical Engineering
Georgia Institute of Technology

Dr. Alberto Fernández-Nieves
School of Physics
Georgia Institute of Technology

Dr. L. Andrew Lyon
Schmid College of Science and Technology
Chapman University

Dr. Robert E. Guldberg
School of Mechanical Engineering
Georgia Institute of Technology

Date Approved: August 11th, 2015

To my mother and father for their constant support, love, and encouragement throughout this journey.

ACKNOWLEDGEMENTS

Over the last five years, many people have contributed to my success scientifically, intellectually, and emotionally, during my time here at Georgia Tech. I would like to thank them here and hope to not leave anyone out. First, I would like to thank Tom Barker for being my advisor and supporting me over the last five years throughout this experience. Not only has he provided scientific expertise throughout my journey as a student, but also he has truly been a constant source of support and encouragement. He also has pushed me to focus on the bigger picture of what my contribution to the field would be, for which I am grateful. He empowered me to reach out and develop relationships with other laboratories in order to generate the best interdisciplinary scientific research possible. I am thankful for Tom's support and mentorship, which has allowed me to drive my own project and grow intellectually to levels that many students may not experience depending on the environment of the lab and their relationship with their advisor.

I would also like to thank my thesis committee whose support, feedback, and scientific guidance has been critical to my time as a graduate student. Specifically, I would like to thank Alberto Fernandez-Nieves for being an incredible person and co-advisor (although not official) to me over the last several years. His passion for science and physics is simultaneously immeasurable and contagious. In the low times of this experience when I felt like I couldn't continue anymore, Alberto's excitement and belief in the work reinvigorated my psyche and kept me moving forward. For this, I am eternally grateful, and I would not be at this point today without him as a mentor. I also would like to thank Andrew Lyon, for his support throughout this process, especially in

the early stages of this project. I am grateful for his support and scientific expertise that he was able to share with me about microgels and their chemistry. Additionally, I would like to thank Andrés García for always asking questions, being a critic, raising concerns where appropriate, and pushing me to make the science better. I have always directly benefited from our conversations and am grateful for those experiences. I am also thankful for what I've learned from Andrés through his insight and perspectives on the bigger picture of the work and the biomaterials field. Finally, I would like to thank Bob Guldberg for taking the time to join my committee in the final stretch of the project. Without his guidance in helping design the *in vivo* studies and the technical support from his lab, the animal work (and thus any insight to how these materials would behave *in vivo*) performed in this dissertation would not have been possible.

I would like to thank members of the Barker lab past and present. Specifically, Vince Fiore, for being my graduate student mentor in my first year and helping me learn my way around the lab as well as serving as a constant resource (more on him later). I would also like to thank Allyson Soon for being an inspiration to me through being a true experimentalist and die-hard scientist. I would like to thank Ashley Brown for her support both technically and as the mother hen in the Barker lab for many (many) years. I would also like to thank Lizhi Cao for his technical expertise, making us laugh, and making us hungry when he would eat lunch at 10:30am. I would like to thank Dwight Chambers for being a great friend, a brilliant person, and for introducing us to Soylent. Other notable members include John Nicosia, Haylee Bachman, Michelle Gaines, and Vicky Stefanelli, who I would like to thank for bringing a friendly light energy to the group. Finally, I would like to thank Karisma Gupta and Keith Sellers, who contributed

hard work and were delightful undergraduates that I had the pleasure to work with on this project.

My project at Georgia Tech was truly a multi-investigator collaboration and through that, there were many other graduate students and post-docs along the way that helped make it possible. I would like to thank John Hyatt, from the Fernandez-Nieves lab, for helping me with rheology and also for performing the light scattering experiments. I am also thankful for the friendship we were able to achieve after spending many long days in the lab together (and for the times we were able to laugh and commiserate with each other – while we may have been sad, they were still fun). I am also thankful for Alex Fragkopoulos who wrote the MATLAB code that enabled the microgel network analysis and MVF assay sprouting analysis – the detailed characterization of my system would not have been possible without him so for that I am grateful. I would also like to thank other members of the Fernandez-Nieves lab that were extremely helpful (and great people/friends) including Miguel, Perry, and Winnie.

From the Guldberg lab, I would like to thank Laxmi Krishnan for being a great mentor to me and also for his interest in the project. Without his technical assistance with the MVF angiogenesis assay and the in vivo experiments, the work would not have been possible. Additionally, I'd like to thank Ashley Allen for her help performing the in vivo surgeries and also because she is a great person and friend. Other notable members include Hazel, Lauren, Albert, and Brennan, who were always happy to help me when I was over in their lab space. I would especially like to thank Angela Lin who helped me numerous times with micro-CT. Angela is also a great friend of mine and teammate on the Atlanta womens frisbee club team called Ozone.

My completion of this journey would not have been possible without the support of family and friends. I am thankful for my main group of friends in Atlanta, which is really just my frisbee team, Ozone. I joined the team in 2011 after my first year of graduate school and the rest is history (the club ultimate frisbee season lasts from May-October including many cross-country tournaments/trips and weekend practice… i.e. lots of time was spent with these people). Some of my closest friends who have kept me sane over the last several years include Dani Kaplan, Kate Wilson, Anna Hammond, Mira Walker, Emily Lloyd, and Angela Lin. For my fourth season on the team (in 2014), Angela and I captained together and led the team to a 5th place finish in the US National Championships held in Dallas, TX. It was awesome. I am grateful for all of those experiences and people – who helped lighten the load of graduate school.

Finally, I would like to thank my mom (and best friend) for her unwavering support and essentially serving as my therapist on many occasions. I am also grateful for her enthusiasm and for existing in general because she is one of my favorite people on this planet. Additionally, I would like to thank my father for being my number one fan and always being so proud of me. I would not be in the place I am today without the upbringing and support provided by my parents over the last 27 years. I would also like to thank my brothers Max and Timmy – for their support and friendship. And finally, I am grateful for Vince Fiore, for his love and support over the last 5 years – both scientifically and emotionally, Vince's contributions to my success and completion of this PhD are immeasurable.

TABLE OF CONTENTS

LIST OF TABLES

LIST OF FIGURES

LIST OF SYMBOLS AND ABBREVIATIONS

AAc	Acrylic acid
AF	AlexaFluor
APS	Ammonium persulfate
Arg	Arginine
Asp	Aspartic acid
BCS	Bovine calf serum
bFGF	Basic fibroblast growth factor
BIS	bisacrylamide crosslinked (2%)
$CaCl_2$	Calcium chloride
CAM	Chorioallantoic membrane
$CaSO_4$	Calcium sulfate
CLP	Cross-linking peptide
CMFDA	5-chloromethylfluorescein diacetate
CMV	Cytomegalovirus
D	Diffusion coefficient
DLS	Dynamic light scattering
DMEM	Dulbecco's modified eagle medium
DMF	*N,N*-Dimethylformamide
ECM	extracellular matrix
EDC	1-ethyl-3(3-dimethylaminopropyl)carbodiimide hydrochloride)
EGM	Endothelial growth medium
FBS	Fetal bovine serum
FpA	Fibrinopeptide A
FpB	Fibrinopeptide B
FXIII	Factor XIII, fibrin stabilizing factor
G'	Storage modulus
G"	Loss modulus
GDQ	Gly-Asp-Gln MMP cleavable amino acid sequence
GFP	Green fluorescent protein
Gly	Glycine
HDF	Human dermal fibroblast
HEPES	4-(2-hydroxyethyl)-1-piperazineethanesulfonic acid
HFF	Human foreskin fibroblast
HIF	Hypoxia inducible factor
HPF	1,1,1,3,3,3-Hexafluoro-2-propanol
HUVEC	Human umbilical vein endothelial cell
k_B	Boltzmann constant
LCST	Lower critical solution temperature
MAP	Microporous annealed particle
MMP	Matrix metalloproteinase
MSC	Mesenchymal stem cell
MVF	Microvessel fragment
n	Solvent refractive index
NA	Numerical aperture

NaCl	Sodium chloride
NHS	N-hydroxysulfosuccinimide
NIPAM	*N*-Isopropylacrylamide
PBS	Phosphate buffered saline
PCL	Polycaprolactone
PDGF	Platelet-derived growth factor
PEG	poly(ethylene glycol)
PEG-4MAL	Poly(ethylene glycol)-4 arm maleimide
PEGDA	Poly(ethylene glycol) diacrylate
PEO	Poly(ethylene oxide)
PGA	Poly(glycolic acid)
PLA	Poly(lactic acid)
pNIPAM	Poly(N-isopropylacrylamide)
pNIPAM-AAc	Poly(N-isopropylacrylamide-*co*-acrylic acid)
q	Momentum changes of scattered light
R_g	Radius of gyration
RGD	Arg-Gly-Asp cell binding tripeptide
R_h	Hydrodynamic radius
RhoA	Ras homolog gene family, member A
SLS	Static light scattering
SMC	Smooth muscle cell
Ugels	Microgels
ULC	Ultra low crosslinked
VEGF	Vascular endothelial growth factor
VPTT	Volume phase transition temperature
X-link	Crosslinked
ζ	Pore size
η	Viscosity
θ	Angle
λ_0	Wavelength of light in vacuum
τ	Correlation lag time
ϕ	Volume fraction
ϕ_c	Critical volume fraction

SUMMARY

Wound healing and revascularization of tissues at sites of injury are fundamental problems in the field of regenerative medicine. One promising approach to supporting vascularization is the use of fibrin polymers, the natural blood clotting protein, as an injectable biomaterial construct. Current fibrin matrices/sealants for wound healing applications use high concentrations of fibrinogen and thrombin, forming a dense matrix to facilitate stable clot formation. However, this limits the ability for endogenous cells to infiltrate the wound site for adequate tissue repair. The overall goal of this work is to design materials that are mechanically robust for ease of handling and clot stability, but allow for increased cell infiltration and tissue regeneration by modifying the fibrin network ultrastructure. This is achieved using colloidal assemblies of ultra low cross-linked poly(N-isopropylacrylamide) pNIPAm microgels (microgels), which we have shown can alter network architecture and mechanics. We hypothesized that by modifying microscale network structure we would enhance infiltrating cell motility, endogenous cell recruitment and angiogenesis, and tissue regeneration. Ultimately, it was shown that microgels enabled enhanced cell motility and infiltration *in vitro*, and in-growth of small diameter vessels *in vivo*. While, enabling larger vessel vascularization and multicellular processes involving collective cell migration still remain to be realized, this novel system represents a new method of modifying dense biomaterial systems for enhanced regenerative outcomes.

CHAPTER 1 INTRODUCTION

1.1 Specific Aims

A major challenge in tissue engineering and regenerative medicine is the ability to design materials with robust mechanical properties while simultaneously being permissive to cell invasion. This is difficult because the mesh size of a network is directly linked to the material's elastic modulus, with small mesh sizes being inhibitory to cell motility. Many tissue engineering approaches utilize natural protein-based polymer systems due to their enhanced endogenous bioactivity and potential for seamless integration with the host tissue. However, most natural biopolymers form weak hydrogels that do not fully match the mechanical properties of the target tissues making them difficult to apply in practice [1]. Thus, in order to strengthen these networks, higher concentrations of protein are used [2-4], exogenous crosslinkers are added [5], or synthetic polymers are incorporated into the matrices to form more mechanically robust networks [6, 7]. However, these approaches imply a smaller network mesh size, which physically inhibit cellular processes such as spreading and migration – prerequisites for cell infiltration and biomaterial integration. This establishes a significant discord in biomaterials design where one must either choose desirable tissue mechanical matching or cell infiltration and tissue ingrowth, while both together are difficult to achieve.

Fibrin is an attractive native protein used in tissue engineering and tissue sealant applications, but in order to perform as a sealant, it must be used at supraphysiological concentrations for stable clot formation. When used at these concentrations, cell infiltration is greatly reduced, hindering tissue remodeling and regeneration and ultimately leading to scar tissue formation. As opposed to engineering growth factor

delivery [8] or release of recombinant proteins [9], and inspired by the space-filling functions of high molecular weight proteoglycans within natural ECMs [10, 11], here we combined high volume fraction colloidal assemblies of ultra-low crosslinked (ULC) microgels with the natural extracellular matrix protein fibrin to make unique composite materials to allow for structural modifications to the polymer matrix to provide therapeutic benefit. Instead of remaining homogenously dispersed, microgels cluster within fibrin forming interconnected networks with properties similar to that of well-packed semi-fluid domains. We investigated the mechanisms of formation of these composite materials, and found them to assemble into interconnected networks within the composite, which is key to the observed enhanced cell and tissue phenotype. Additionally, the mechanical properties of the composite gels were indistinguishable from fibrin alone. We achieved these structures dynamically, via polymerization dynamics of the bulk polymer, or via depletion interactions and subsequent gelation.

Thus this dissertation focuses on two main objectives: 1) characterizing fibrin-microgel hybrid constructs and their ability to enhance cell motility and infiltration, and 2) understanding the fundamental biophysics of the formation of composite biomaterial-colloidal assembly hybrids. The overall hypothesis of this work was that by modifying the microscale network structure we would enhance infiltrating cell motility, endogenous cell recruitment and angiogenesis, and ultimately tissue regeneration. This was accomplished through the following specific aims:

Aim 1: Characterization of ultra-low crosslinked microgels and fibrin-microgel hybrid constructs. The generation of composite fibrin-microgel constructs was explored. *The hypothesis of this aim was that microgels would form interconnected structures*

within fibrin gels and that the mechanical properties of the composite would be maintained and comparable to the fibrin alone gel. The objective of this aim was characterize the system, using light scattering and viscometry[1], and study the effects of adding various concentrations of microgels to high concentration fibrin gels, through rheology, confocal microscopy, and image processing.

Aim 2: Determination of the effects of fibrin-microgel hybrid constructs on cellular phenotype, and investigation of the mechanism of microgel network formation in fibrin and other materials. This aim focuses on understanding how the composite materials are formed and the effect of these constructs on cellular phenotype when compared to fibrin only controls. *The hypothesis of this aim was that the addition of microgels would allow for increased cell spreading, motility, and infiltration.* This was assessed through quantitation of cell morphological outputs and live-cell imaging. Additionally, *the hypothesis of the mechanistic sub-aim was that the size and shape of microgel networks within fibrin would be dictated by the polymerization rate of fibrin.* This was tested through confocal imaging, image processing, and rheology.

Aim 3: Determination of the potential of fibrin-microgel hybrid constructs to enhance cell infiltration using *in vivo* systems. The angiogenic potential of these hybrid constructs was measured and quantified. *The hypothesis for this aim was that the presence of microgels would enhance angiogenesis and vascularization due to the ability of microgels to enhance migration.* A subcutaneous implant rodent model and several *in vitro* angiogenesis assays were tested to measure the regenerative effects of microgels.

[1] Portions adapted from Bachman et al. Ultrasoft, highly deformable microgels, Soft Matter, 11 (2015) 2018-2028. Adapted from with permission by The Royal Society of Chemistry.

Therefore, in situ assembly of these unique structures represents a simple, straightforward method for generating robust tissue integration and in growth of functional vascularization within dense polymer matrices.

1.2 Significance of Research

There is a great need to develop materials that aid in regeneration and subsequently promote the formation of a stable vascular network for long-term tissue survival. The field of tissue engineering and regenerative medicine is vast with much research being focused on designing elegant strategies to recapitulate the native ECM using engineered synthetic systems [12]. While these achieve some of the desired outputs, significant barriers and issues related to clinical feasibility still remain from these materials being translated to the clinic [13, 14]. Additionally, the use of growth factors and other proteins in synthetic systems significantly increases the cost, decreases the shelf life, and in some cases makes them cost-prohibitive in the healthcare system today unless they demonstrate extraordinary benefits.

Thus, the simplicity of the system described herein offers many advantages compared to more complex potentially over-engineered parallels. These include: the use of a natural polymer with inherent bioactivity, in situ polymerization of the composite to allow for filling of defects and shape matching, and minimal compositional changes to current FDA-approved products (fibrin sealants). We propose a simple strategy of forming composite materials through the mixing and subsequent gelation of fibrin-microgel constructs. These materials are also translatable and could be incorporated into fibrin sealant products or in other systems where the injury repair process and angiogenesis are compromised [15, 16].

The innovation of this work is that it provides the proof of principal concept that polymeric *soft* materials can generate novel functions relevant to biology (increasing cell-viewed porosity of a dense fibrin matrix) to both modulate the mechanics and ultrastructure of an environment without obstructing cellular processes, but instead accelerating them. This represents the first description of a porogen-like material being generated without the removal of the porogen itself. While microparticles have been incorporated into fibrin previously in order to deliver drugs [17-19] or other factors or mechanically reinforce the network [20, 21], there is no evidence of investigators using volume fractions of colloidal microparticles as high as explored in this work. Additionally, based on the physics of phase behavior of certain particle types [22, 23], it may be impossible for certain types of microparticles to be used at these high of concentrations, making this phenomena potentially unique to deformable soft materials. The idea of generating tunnels of deformable and yet water swollen colloidal assemblies for cells to explore within biomaterials is a fundamentally new concept in tissue engineering design. Others have used the softness of microgels in order to achieve desirable cell-mimicking properties [24], but particle softness has not been explored in the context of cell migration in composite networks. Therefore, the ins and outs of the system will be explored and explained in detail in the following pages.

CHAPTER 2 LITERATURE REVIEW

2.1 Biomaterials in tissue engineering

2.1.1 The extracellular matrix[2]

The essential non-cellular component of all tissues is the ECM, the protein scaffold and microenvironment in which cells reside [25]. A schematic representation of the ECM is presented in Figure 1. The protein composition and structure of the ECM can influence cell adhesion and signaling, as cells bind to specific ligand sites on ECM proteins via cell surface receptors, including integrins and proteoglycans [26]. Cell-ECM interactions are complex and dynamic in nature and can dictate cellular phenotype, influencing cell survival, proliferation, migration, and differentiation. Various ECM proteins also bind and sequester growth factors, which can lead to spatial and temporal control of the dynamics of cellular processes [27]. Additionally, the ECM can determine the mechanical properties of each organ through its compressive modulus, elasticity, and water retention, which can play a protective role in tissues to maintain homeostasis.

There are several canonical ECM proteins that are prevalent throughout many tissues in the body, each with their own complexities. Most tissues are heterogeneous mixtures of various proteins including collagens, laminins, and proteoglycans among others. A primary function of ECM proteins is to facilitate cell adhesion, in which they serve as ligands for one or many of the heterodimeric transmembrane cell surface receptors, termed integrins [28].

[2] Portions adapted from Clarke et al. Colloid-matrix assemblies in regenerative medicine, Current Opinion in Colloid & Interface Science, 18 (2013) 393-405. Copyright Elsevier 2013.

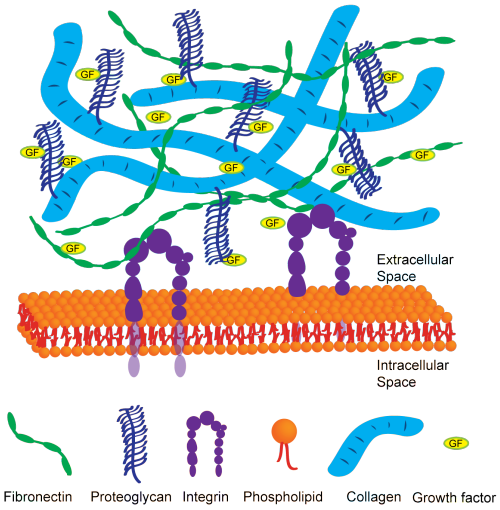

Figure 1: Schematic of the extracellular matrix. This cartoon illustrates the extracellular matrix proteinaceous structure found in tissues which cells interact with via cell surface receptors termed integrins. (Adapted from reference [171], Copyright Elsevier 2013.)

While most ECM proteins are slowly assembled and synthesized by cells within the surrounding tissue, an exception is fibrin, which is formed quickly through the initiation of the coagulation cascade. During this process, polymerization of soluble fibrinogen by thrombin cleavage forms an insoluble fibrin clot [29]. It is also important to note that the ECM is naturally in a non-equilibrium state as cells are constantly remodeling the network through deformations induced by cell contractile forces and degradation induced by numerous proteases, including the matrix metalloproteinases (MMPs), in addition to synthesizing new protein components within the tissue structure.

Proteoglycans are major components of many ECMs, where they act as fillers, contribute elasticity within connective tissues, and are important in molecular transport through the ECM [30]. Proteoglycans have a protein backbone with one or more

glycosaminoglycans or linear carbohydrate polymers covalently attached to the core protein. They are often sulfated, rendering them negatively charged under physiological conditions. This charge allows them to mediate signaling and regulate the movement of molecules through the matrix by binding cations and water molecules. Similarly, Microgels are highly swollen with water and can be synthesized to contain ionizable groups within the network [31].

Therefore the native ECM is an extremely complex, dynamic environment through which many cell fate processes are controlled. The fields of tissue engineering and regenerative medicine have sought to develop biomaterials capable of recapitulating the behavior of the ECM in the context of synthetic or biosynthetic hybrids of reduced complexity with the ability to regenerate severely damaged tissues either *in vitro* or *in vivo* remaining the primary goal. In addition, such materials can lead to the creation of accurate models to study cell behavior and fate under a multitude of environmental conditions. Hydrogels both synthetic and natural have been a main choice for ECM mimics because their mechanical properties and high water content resemble those of many tissues [12].

2.1.2 Engineering natural complexity into synthetic ECM mimicking materials[3]

As we know the ECM protein composition and structure can influence many important cell adhesion and signaling events. Synthetic systems lack essential ECM components, like integrin ligands, to foster cell binding and proliferation, and, therefore, require modification to include these molecules. Many have spent careers engineering strategies to overcome these challenges and incorporate complex biological moieties into

[3] Portions adapted from Clarke et al. Colloid-matrix assemblies in regenerative medicine, Current Opinion in Colloid & Interface Science, 18 (2013) 393-405. Copyright Elsevier 2013.

synthetic biomaterial systems [12, 13, 32-35]. While there are many different types of synthetic polymers that have been used as biomaterials in tissue engineering and regenerative medicine [36], here the focus will be on polymeric hydrogels. Hydrogels are a network of insoluble hydrophilic polymer chains that exhibit the ability to greatly swell in and retain water. Poly(ethylene glycol) (PEG) hydrogels have been extensively studied as candidates for tissue scaffolds because the hydrophilic nature of PEG prevents non-specific protein adsorption.

PEG acts as a blank scaffold where cell attachment, spreading, migration, and proliferation are mediated by specific molecules incorporated into the matrix. In the native ECM there are numerous sites for cell attachment, coupling cells and the ECM [37]. For this reason, cell-binding domains, the most common being RGD (the tripeptide Arg-Gly-Asp) [38], are often covalently bound to PEG networks to promote cell adhesion and motility. RGD represents the minimal integrin binding sequence found within many ECM molecules (fibrinogen, fibronectin) and is a convenient tripeptide used to functionalize many biomaterials [38-41]. In a typical example of this strategy, Gobin and West demonstrated the differing migration of human dermal fibroblasts (HDFs) in response to varying concentrations of RGD in synthetic ECM networks. With this approach, a balance must be struck between excessive ligand density, which may prevent cell detachment, and too low of a ligand density, where cells do not have enough adhesion sites for movement [42]. In further studies West and co-workers controlled the migration of human dermal fibroblasts in a three-dimensional PEG hydrogel by photopatterning a RGD peptide in defined spatial arrangements. HDFs moved in all directions when RGD was homogeneously incorporated in the network or in one

direction when only the photopatterned RGD gradient was present [43].

Additionally, for optimal success in vivo, synthetic materials must be rendered degradable to be fully integrated into a biological system. To meet this need and to decouple stiffness, pore size, and cell infiltration in synthetic hydrogels, investigators have engineered systems that enable cell-mediated degradation via protease-specific peptide crosslinkers [44-47]. This allows the material to maintain its scaffold shape and structure and only be structurally modified at points when cells degrade MMP sensitive cleavage sites in the gel backbone structure. These materials however rely on degradation for cell infiltration and thus can slow cell invasion and do not fully recapitulate native cell-ECM interactions. Hubbell and coworkers have demonstrated a biologically-inspired degradable matrix that incorporates MMP sensitive cross-linkers into PEG hydrogels [44, 47]. MMPs are naturally secreted by cells to break down ECM components during wound healing and tissue growth/remodeling. Therefore, the MMP-cleavable PEG matrix degrades in response to cellular activity, thereby more closely mimicking native processes. Moreover, the degradation of matrix mimetic hydrogels has been shown to be an important factor in cell migration [42, 48] and stem cell fate [49], making the inclusion of degradation sites important in the design of new matrices. Hydrolytically degradable scaffolds, like poly(lactic acid) (PLA) or poly(glycolic acid) (PGA), have also been employed as transient matrices or to control the release of bioactive molecules from scaffolds [50, 51]. Unlike protease sensitive hydrogels, PLA/PGA hydrogels degrade under physiological conditions resulting in scaffold break down that is not controlled by cellular activity. A consequence to the use of these polymers is the creation of acidic degradation products, which can result in inflammation in surrounding tissues.

A number of biochemical cues exist in ECMs, which impact cell proliferation, migration, and differentiation of stem cells. For example, angiogenesis, a necessary process in tissue development, requires a combination of growth factors presented with temporal and spatial control to promote the successful growth of vasculature. Growth factors are present in ECMs as soluble signaling molecules and tethered to the ECM, where release is governed by protease activity [52] or force mediated release [53]. Due to the importance of growth factors in tissue development there has been a significant effort to produce systems capable of delivering or presenting growth factors in a controlled manner [54, 55]. PEG hydrogels have been extensively studied as releasing scaffolds [56]. Mooney and co-workers have also used PLA/PGA copolymer hydrogels to deliver vascular endothelial growth factor (VEGF) and an inhibiting antibody (anti-VEGF) simultaneously to localize angiogenesis to specific zones [57].

Alternatively, growth factors can be covalently bound within synthetic scaffolds to influence cell behavior. West and colleagues immobilized basic fibroblast growth factor (bFGF) in a gradient within PEG hydrogels in addition to RGD. Inclusion of bFGF into the network enhanced smooth muscle cell (SMC) proliferation, and SMCs were found to align in the direction of increasing concentration of growth factor [58]. In native ECMs growth factors can be found bound within the network but are later liberated by cell secreted proteases. Similarly, Zisch et al. demonstrated the release of VEGF from PEG hydrogels using MMP degradable tethers. Thus growth factor release was governed by cell activity [59]. Efforts have also been made to enhance the binding of growth factors, as well as other proteins, through the incorporation of glycosaminoglycans into the matrix. One example is the addition of heparin, a sulfated glycosaminoglycan found

in ECMs, to PEG hydrogels to sequester molecules within the matrix and tune the release. Yamaguchi and Kiick fabricated a heparin-PEG gel, which was able to bind and control the release of bFGF. Growth factor release was sustained for over two weeks, while burst release was observed from a hydrogel lacking heparin [60].

In contrast to synthetic systems, protein based biomaterials derived from the extracellular matrix offer significant favorable benefits when compared to more inert materials, mainly enhanced endogenous bioactivity. In many systems, it has been shown that native matrix acts as a growth factor/cytokine depot, presents insoluble ligands and scaffolds biochemical cues in a way that enables synergistic signaling that can serve as cues to endogenous cells for recruitment to the site of injury for tissue repair and remodeling [27, 61, 62]. Natural ECM polymers (e.g. collagen, fibrin, hyaluronic acid, fibronectin, laminin) have cell adhesive domains present for binding, and can be degraded and remodeled using enzymes secreted by resident cells. In the case of fibrin, degradation products of the molecule have been shown to be pro-angiogenic [63, 64]. This is also mirrored by work from the Badylak group that has demonstrated the ability of the ECM degradation products from decellularized tissues used as regenerative scaffolds allow for the recruitment of pro-regenerative endogenous cell populations to the site of the implant [65-69].

2.1.3 Fibrinogen and Fibrin – The provisional matrix

Fibrinogen is the endogenous soluble blood clotting protein that circulates in our blood stream at a concentration of approximately 2.5 mg/mL. It is a 340 kD dimeric protein with three chains, Aα, Bβ, and γ [70]. Among these three chains are cell and growth factor binding regions, FXIII cross-linking sites, and enzymatic cleavage sites to

initiate the formation of insoluble fibrin. Pro-thrombin, also circulating in our blood stream is activated in response to the coagulation cascade (by clotting Factor X) and converted into active thrombin, which attacks fibrinogen molecules. Thrombin cleaves the fibrinopeptides (FpA, FpB) off of the fibrinogen N-terminal regions of the Aα and Bβ chains exposing 'knobs', which then are available to bind to complementary pockets (knob 'A' binds to hole 'a' and knob 'B' binds to hole 'b') on the C-termini of neighboring fibrin(ogen) molecules [71]. The molecules bind to one another and chains grow into protofibrils, which continually elongate and additionally begin to laterally aggregate [72]. Thrombin also activates the transglutaminase FXIII (forming FXIIIa), which aids in the formation of γ-glutamyl-ε-lysyl amide bonds between sites on the α and γ chains of adjacent fibrin(ogen) molecules. While it has been demonstrated that fibrin is an equilibrium polymer, when it is FXIII cross-linked, this process is halted completely and fibers must be proteolytically digested for dissolution to occur [73]. FXIII is thus known as a stabilizing factor, and with its ability to crosslink the α and γ chains of fibrin(ogen), a stronger more elastic clot is formed consequently [74, 75]. The activation of FXIII by thrombin exposes the active-site cysteine on the molecule, which enables the formation of γ-γ dimers within seconds (while α-α and α-γ crosslinks form more slowly as the clot matures) [76, 77]. Additionally, the crosslinking of other molecules such as fibronectin or α_2 plasmin inhibitor into a fibrin clot occurs at a slower rate compared to γ-γ dimerization [78]. Due to FXIII's large binding constant for fibrinogen ($K_D \approx 10^{-8}$), it circulates in the plasma mainly in association with fibrinogen and thus is often co-purified with plasma-derived fibrinogen used in most commercial fibrin sealants [79, 80].

It is known that several factors affect the formation of fibrin clots including fibrinogen concentration, thrombin concentration, calcium ions, and sodium chloride. Chloride ions are thought to interact with fibrinogen chains to inhibit or diminish molecular lateral aggregation during fibril formation, thus clots formed in the presence of lower salt concentrations generally produce thicker fibers [81]. Conversely, clots formed in high salt concentrations form translucent more highly branched networks with thinner fibers. It is also known that differences in fibrin fiber morphology affects clot mechanical properties. Thus, depending on the thrombin and/or calcium chloride concentration used during polymerization, clots of the same initial fibrinogen concentration can display dramatically different architectures. With respect to mechanical properties however, there is a balance between mesh size and fiber thickness, where the most mechanically robust clots come from gels with intermediate thrombin and calcium concentrations (thus intermediate fiber thicknesses and porosities) [82]. Additionally, clots with thinner fibers with more branching typically are less susceptible to lysis compared with those containing thicker fibers with more porous networks. This is typically related restricted or hindered diffusion of proteolytic molecules into these dense matrices.

Fibrin and its precursor, fibrinogen, present binding sites for other pro-coagulant proteins (thrombin and Factor XIII), pro-fibrinolytic proteins (plasminogen, tissue plasminogen activator), anti-fibrinolytic proteins (plasminogen activator inhibitor), growth factors (VEGF, PDGF, bFGF), ECM glycoproteins (fibronectin, heparin), and cell surface receptors (integrins, cadherins) [61, 83]. All of these components make up a network that is capable of transitioning the provisional wound network into a healed

tissue structure. During tissue repair, invading cells are able to migrate into the fibrin matrix and degrade/remodel the polymer over time [84].

2.1.4 Fibrin in wound healing and tissue engineering

As a classic example, fibrin serves as the provisional matrix formed at the site of injury through enzymatic activation with thrombin in response to the coagulation cascade [70, 83]. It initially aids in the process of halting bleeding, but then serves as a scaffold for regeneration, subsequent cell infiltration and tissue repair. Clinically, fibrin is used at supraphysiological concentrations (> 10 fold) as a hemostatic agent in events of trauma and as a sealant to glue tissues together or seal wounds [29, 85-87]. Fibrinogen can be conveniently isolated from serum proteins and is used clinically as a tissue sealant in combination with its activator, thrombin. It has also been extensively studied as a tissue construct for regeneration of many tissues including cardiac, muscle, skin, vascular and bone [88-90]. Current FDA-approved fibrin sealants on the market such as Tisseel® (Baxter Healthcare) and Evicel (Johnson & Johnson) typically contain supra-physiological fibrinogen concentrations ranging from 20-100 mg/mL, while the native human clot is approximately 2-4 mg/mL [7, 91]. In clinical formulations, fibrin sealants typically contain concentrated fibrinogen and thrombin in addition to FXIIIa [80], and fibronectin which are often co-precipitated with fibrinogen due to their high binding-affinity for the molecule [88, 92]. Additionally, these formulations are often supplemented with aprotinin, a protease inhibitor (which inhibits several serine proteases, including plasmin), which will allow for longer-term maintenance of the fibrin clot in vivo once it is exposed to the highly active enzymatic microenvironment [63, 93, 94].

When fibrin is utilized at these high concentrations, a dense matrix with nanometer scale pore size is formed, which is difficult for cells to infiltrate without significant degradation of the polymer [16, 86, 87, 95]. A basic study of neutrophil chemotaxis in various fibrin sealant clot formulations demonstrated that chemotaxis driven cell migration through clots at concentrations as low as 5 mg/mL were significantly dense enough to inhibit migration [16]. More specifically, when fibrin was used at high concentrations in a chorioallantoic membrane (CAM) assay to visualize blood vessel development, it was observed that cells were unable to directly invade the dense fibrin gel [96]. The CAM tissue degraded fibrin only along the polymer surface and replaced it with vascularized neo-tissue.

Not only is fibrin fundamental in hemostasis, but it also serves as a biologic scaffold that binds a multitude of factors, concentrating them to the wound microenvironment to enhance subsequent repair of the damaged tissue. However, if fibrin deposition and degradation processes are imbalanced (e.g. due to supra-physiological concentrations of fibrinogen), then cellular infiltration, ECM remodeling, and ultimately regenerative processes are hindered [84, 95, 97]. Mechanical and diffusional limitations of these supra-physiological clots impede cellular infiltration and remodeling [84, 96]. However, in order to generate fibrin gels with mechanical properties similar to osteoid for bone repair applications for example, or other applications requiring materials with an elastic modulus larger than a few hundred kilopascals, high concentrations of protein are necessary, resulting in networks that are extremely dense. Consequently, it has been shown that these concentrations can lead to poor regeneration of bone tissue *in vivo* [15]. The same issues hold for fibrinogen based tissue sealants that are used at high

concentrations to facilitate rapid wound closure, but then subsequently prevent host cell infiltration and remodeling [16].

PEG-fibrin constructs have also been investigated by groups in order to maintain the bioactivity of the fibrinogen molecule, while simultaneously taking advantage of the more robust mechanical properties, density, and biodegradability associated with PEG [62, 98-100]. Fibrinogen is PEGylated, purified, and polymerized into hybrid gels either through crosslinking of PEG or addition of thrombin, and these constructs have been shown to support cell adhesion and spreading. However, the constructs rely on higher PEG concentrations in order to produce the most mechanically robust gels (with Young's moduli >5-10 kPa). Thus, their ability to sustain complex morphogenetic processes such as angiogenesis in gels of increasing modulus has not yet been realized due to the strong dependence of network formation on gel crosslinking density [98, 101, 102]. In efforts to modulate the molecular architecture of PEG-fibrinogen gels, nanostructured composites were formed by incorporating Pluronic® F127 micelles into precursor gel solutions [103, 104]. Hydrogel network assembly was altered, however the micelles only had a modest effect on cell spreading in this system. PEG-fibrin constructs have been engineered in the Sugg's group using amine-reactive PEG to PEGylate fibrinogen [105, 106]. These same constructs have shown the ability of adipose-derived stem cells to undergo tubular network formation in PEG gels – thus simulating a crude form of angiogenesis. However, the structure of these gels has not been well characterized and their mechanical properties are on the order of 100s of Pascal's [107]. Thus, in order to be used in applications where stronger mechanical properties would be desired, the PEG or fibrin concentration would need to increase – thus limiting the mesh size and subsequent cell migration.

2.1.5 Challenges in biomaterial-host tissue integration

In order for an implanted or in situ forming biomaterial to maintain viability *in vivo*, the material and host tissue must interact at the interface. One of the crucial requirements for subsequent regenerative success is access to a blood supply for nutrient and waste exchange [108]. Previous work in the field has demonstrated that for cells within a material to remain viable, they must be within 200 μm of a vessel. Thus, the material must have a pre-templated vascular supply that can somehow anastomose with the host vasculature, or native cells must be able to infiltrate the material in order to establish its own supportive structures through angiogenesis and vascular sprouting. When studying host-biomaterial interactions, it is important to understand what will happen at the interface of the material and native tissue. Much work within the field of biomaterials has looked at the body's endogenous response to implanted synthetic materials [109-112]. Through this work it has been learned, that when a solid material is implanted in the body, the endogenous cells respond to the implant as non-self and the immune system undergoes what has been termed the foreign body reaction. The immune reaction starts upon material implantation where the acute response results in the recruitment of mononuclear leukocytes and neutrophils. Next they are followed by macrophages, which appear in increasing number in the chronic phase, while later fibroblasts infiltrate contributing to granulation tissue formation and fibrosis [109, 113]. At the implantation site, immune cells survey the area, and macrophages interact with the surface of the material. In efforts to 'eliminate' the foreign body, a key function of macrophages against bacteria and other small pathogens, the macrophages attempt to engulf the material. However, they are unable to do so and undergo 'frustrated

phagocytosis'. This results because the implant is likely much larger than the individual cells are capable of engulfing and thus it must be degraded to be removed (but many implants/devices are non-degradable). These frustrated phagocytic cells become large multinucleated foreign body giant cells, which completely surround the implant site. Subsequent steps of excessive matrix deposition and recruitment of activated fibroblasts result in the implant being effectively isolated and walled off from the host. Thus, this response must be overcome or manipulated when the desired therapeutic outcomes relies on interaction of host cells or tissue with the implant. Porous materials or those susceptible to degradation have been shown to mitigate this response in some cases, as they allow for macrophage and other immune cell infiltration/exploration within the material (and thus stave off foreign body giant cell formation and fibrous encapsulation) [114]. However, mechanisms of cell infiltration are still being studied in many systems. When studying cell infiltration and motility, for physical entry of the cells into the implant, there lies a delicate balance between the pore size of the matrix/material and the degradation of that material.

2.1.6 Modulating the pore size of biomaterials

The extracellular matrix provides the protein scaffold for which cells reside in native tissues. Typically, it has been shown that interstitial connective tissues comprised of mostly collagen have pore sizes range from 2-30μm [115, 116]. Biomaterials generated from natural ECM proteins (such as fibrin, collagen, matrigel, etc) are largely capable of recapitulating pore sizes on this same scale. However, when utilized at supraphysiological levels, these native protein gels can take on much smaller pore sizes.

The pore size of synthetic materials largely depends on the molecular building blocks of the system, or the method in which the material is generated. Thus, the pore size of the network in some cases is equivalent or on the same relevant length scale as the size of a monomer. Since most synthetic hydrogels have pore sizes on nanometer scale [46], there is a need for engineering of proteolytic degradable sites within the polymer backbone. Although great strides have been made in the development of cell-degradable polymers, in normal wound repair, regeneration, or embryonic development, matrix degradation is not a natural requisite to migration and invasion. Matrix degradation enables slow but persistent cell invasion into dense matrices, but most interstitial connective tissues allow for convenient migration through having much larger pore sizes [116]. Additionally, in the native ECM, the inclusion of high M_r proteoglycans within a more porous protein fibrillar mesh helps define the submicron pore size length scale, resulting in physically robust elastic materials with an inherent flow behavior at length- and time-scales relevant to cell invasion; this results in their permissive nature.

Alternatively, a bulk gel can be generated from a material with a small pore size around a network of sacrificial microparticles, which can be degraded away, resulting in an interconnected porous network of tunable sizes. Work from the Ratner group has determined design parameters of porous scaffolds for optimal biointegration and angiogenesis [117, 118]. However, most systems for formulating microporous scaffolds rely on either 1) photo-patterning [119] or 2) microsphere incorporation into the base scaffold during polymerization for subsequent microsphere degradation (with harsh solvents such as acetone [120]) and removal [89]. Furthermore, fibrin scaffolds for clinical use have an average pore size of ~ 100-600 nm [46], which is substantially below

the values that were found to be most amenable to angiogenesis and cell infiltration [114, 120]. It is clear from this that a potential exists to improve the regenerative properties of fibrin. Additionally, these current strategies to increase porosity lack the potential for *in situ* (i.e. injectable, shape-molding scaffold, *during* surgical procedures) scaffold formation for wound repair.

It has demonstrated that through engaging fibrin polymerization with 'b'-knob conjugates, a more porous structure can be formed with an increase in gel complex modulus, yet no significant differences in angiogenesis were displayed in a microvessel fragment sprouting assay [7]. Additionally, we have found this effect diminishes with increasing fibrinogen concentration. Therefore, fibrin(ogen) concentration is still the single most dominant factor in determining gel mechanical properties, raising the need for new strategies to modify this base scaffold for regenerative medicine.

2.1.7 Factors influencing 3D cell migration

Migration of interstitial cells is a multi-step process that relies on the physiochemical balance between cell deformability and physical tissue constraints [115]. Both chemical and physical properties of tissue composition and structure will influence these processes, including protein/molecular content, assembly and crosslinking state of the matrix [121-123], physical scaffold geometry and alignment (and thus the resulting pore size) [124, 125], and finally tissue stiffness [126]. During migration, initially, there is pseudopod protrusion at the leading edge of the cell driven by actin polymerization, which results in subsequent integrin-mediated adhesion to the ECM. Next proteases cleave ECM molecules in a contact dependent manner and contract their cell body in an actomyosin-mediated process to increase their tension [116]. Finally, the rear of the cell

retracts and the cell is able to translocate its body to move forward and migrate [127-129].

The mesh or pore size serves as a critical factor to help define the permissiveness of a material to enable 3D cell migration. Endogenous cells harness both proteolytic and non-proteolytic mechanisms to migrate through tissues, and they largely respond to cues from the external microenvironment to dictate their modes of migration [130]. It has been shown that metastatic cells can switch between an elongated mesenchymal migration that is adhesion dependent and an amoeboid adhesion independent phenotype [131-133]. Petrie and co-workers demonstrated that the elastic behavior of the ECM can also influence the migratory phenotype of fibroblasts, where activity of RhoA and linear elasticity of the matrix can switch cells between a lamellipodial based 3D migration and lobopodial-based migration [134]. Additionally, more recent work studying cells in confined microenvironments has further demonstrated how the effects of biophysical and biochemical can dictate these processes. It has been observed that typically slow mesenchymal cells can switch their migratory phenotype to an amoeboid-like stage under circumstances of low adhesion and high cortical contractility [130]. Wolf et al. demonstrated that cells are incapable of non-proteolytically migrating through pores smaller than ~10% of the diameter of their nucleus [115]. This comes out to a range of approximately 2-6 μm in diameter dependent on the cell type that is used and the associated nuclear deformability. Additional studies have confirmed the importance in the deformability of the nucleus in cell migration [135], specifically that nuclear lamin stiffness can be a barrier to motility [136]. Thus, there exist optimal matrix architectures that remain to be realized, displaying variable adhesivity and stiffness, from which cells

can harness these properties for angiogenesis and cell infiltration for improved biomaterial-host tissue integration.

In synthetic materials, cell migration is strongly influenced by the degradation properties of the matrix. Many biocompatible synthetic hydrogels degrade slowly via mechanisms such as hydrolysis, which enable them to maintain their structure and shape for longer periods of time *in vitro* and *in vivo*. However, synthetic hydrogels such as PEG which have pore sizes on the nanometer scale, and in order to permit cell motility, must be engineered to possess proteolytically cleaveable sites within the polymer backbone. Specific examples of these types of materials are described in section 2.1.2. This then enables network to degrade enough for cells to extend protrusions, spread, and initiate the same migration paradigm described above.

2.2 Microgels in regenerative applications

2.2.1 Fundamentals of microgels – chemical and physical properties

Microgels are colloidal hydrogel microparticles consisting of intramolecularly crosslinked polymers swollen by a good solvent [137]. These materials can be solid-like similar to traditional 'hard' colloids, but also portray the soft deformable properties inherent to many polymer systems. In contrast to solid colloidal particles such as those made from polystyrene or silica, microgels are stimuli responsive and able to change size by absorbing solvent through balancing internal and external osmotic pressures within their environment [137, 138]. The swelling properties of a microgel can be tuned through changing the solubility of the microgel polymer in the solvent. This can often be achieved through changing temperature or the chemical composition of the polymer backbone if there are ionizable groups present. Due to their more complex swelling properties

compared to hard spheres, microgels can display a rich range of behaviors. For example, the optical properties of microgels are unique and of interest because as the microgel becomes more swollen, its refractive index will converge towards that of the solvent [138]. However, as the particle becomes more deswollen by external stimuli, the microgels will deswell and thus increase their refractive index and at sufficient concentrations give rise to turbidity [139].

When thinking about the phase behavior of traditional hard spheres, volume fractions above $\phi = 0.55$ are considered within the crystalline regime and the densest close-packed arrangement of colloids (which is quite rare) corresponds to $\phi = 0.74$ [140]. Microgel swelling (or de-swelling) in response to environmental stimuli gives rise to complex phase behavior as the packing of microgels can theoretically reach volume fractions greater than one due to their deformability and ability to de-swell (which can be temperature, pH, or concentration dependent) [22]. It is also thought at sufficiently high volume fractions, microgels are so closely packed that interpenetration between adjacent particles can occur. Additionally, microgels of different polymer cross-linking densities (and thus stiffness) are able to display unique properties that have allowed for a better understanding of molecular glass formers and the glass transition. In work by Mattson et al, it was demonstrated that the fragility of a microgel suspension is dictated by the elastic properties of the microgel at the single particle level. Thus, the softer the particles, the stronger the suspension behavior, which corresponded to weaker growth of the elastic energy as packing fraction is increased [141]. The rheological properties of microgels are also unique when compared to those of hard spheres. Nanopore and micromechanical experiments have illustrated the deformability of microgels through observation of their

change in shape and volume under an applied stress [142]. These fundamental aspects of microgels that are enabled by the physiochemical properties of their structure allow for a wide array of possibilities for the application of microgels in many biomedical therapeutic strategies.

2.2.2 The use of microgels in biomedical applications

Colloids have been widely used in biomedical research due to their ease of synthesis, multi-functionality, and unique properties. More specifically, colloids have been heavily studied in the field of drug delivery, where they have served as carriers for small molecule therapeutics and biomacromolecules. Efforts have been focused on the development of formulations for intravenous administration for systemic circulation and release at a site of interest [143-150]. Display of ligands of the surface of the colloids allows for tunable targeting of microgels to therapeutic target receptors. Additionally, microgels have been employed to generate drug-eluting coatings or non-fouling surfaces on the surface of biomedical implants [151-153]. Colloids have also been utilized in modular systems in order to achieve structural complexity in addition to diversely patterned tissues [154-156]. As the next section will detail, colloids have the potential to provide a means of tailoring the mechanical properties of biologically derived hydrogels, which are easier to integrate into tissues than purely synthetic architectures.

2.2.3 Colloid reinforced matrices and composite gel systems[4]

Traditional synthetic hydrogels exhibit tunable mechanical properties that are similar to that of many tissues, making them widely studied for tissue engineering and

[4] Portions adapted from Clarke et al. Colloid-matrix assemblies in regenerative medicine, Current Opinion in Colloid & Interface Science, 18 (2013) 393-405. Copyright Elsevier 2013.

regenerative medicine applications. Reductionist ECMs, like collagen or fibrin gels, are useful for soft tissue applications where the elastic modulus needs to be on the order of Pascals to several kiloPascals. However, for tissues like bone, cartilage, and muscle, hundreds of kPa are required for proper cell growth, phenotypic maintenance, and tissue development [1]. A common issue in reductionist and synthetic ECM approaches is that the gels are often not mechanically robust enough for load-bearing tissue applications [157]. One of the primary challenges remaining in tissue engineering and regenerative medicine is the development of biomaterials that display robust mechanical properties while simultaneously being permissive to cellular invasion. It is currently typical that one can optimize either feature independently, but optimization of both simultaneously represents a significant challenge. A possible solution to increase the elastic modulus is to increase the polymer concentration or the number of crosslinks in the gel. However, this approach can be limiting, as simultaneous changes in gel porosity and, in some cases, ligand density influence material mechanical properties, cell migration and diffusion of molecules within the gel [158, 159]. For example, the ability to increase in the modulus of poly(ethylene glycol) (PEG) hydrogels without affecting mesh size has been demonstrated [160]; however, the mesh size is still on the order of tens of nanometers, which is not cell permissive.

Over the last few years, design of many new nanocomposite hydrogels for biomedical applications in regenerative medicine, biosensors, and drug delivery has gained interest in the biomaterials community [161]. In this new research area, various types of nanoparticles (including carbon-based, polymeric, ceramic, metal, etc.) are combined with a polymeric network where the particles either physically or covalently

interact with the hydrogel network to form a hybrid material. Many of these new composites or hybrids display novel functions and have the potential for further modifications/tuning to the application of interest.

One approach has been to develop synthetic additives that can increase the elastic modulus of hydrogels. This has been accomplished through the development of double network hydrogels and colloid reinforced hydrogels. Haraguchi *et al.* demonstrated the reinforcement of a poly(*N*-isopropylacrylamide) hydrogel by using inorganic clay disks as the crosslinking points within the gel [162]. A similar effect has been observed in poly(ethylene oxide) (PEO) hydrogels [163]. Additional approaches regarding nanoparticle-based reinforcement in composite materials have also been reported [164, 165]. In these nanocomposite gels, particles act as cross-linkers within the bulk gel, enhancing the mechanical toughness beyond that expected for traditional organic cross-linkers. Importantly, the presence of particulate cross-linkers creates more porous networks unlike their small molecule counterparts, which decreases the pore size of the gel as the cross-linker concentration increases. As natural ECMs are porous scaffolds, the incorporation of colloidal particles into synthetic ECMs could better mimic the native microstructured environment while simultaneously enabling controlled modulation if its mechanical properties.

While hard, inorganic particles have been successful in enhancing the elastic modulus of hydrogels, soft hydrogel colloids have also become a promising route [166]. A study reported by Richtering and co-workers demonstrated that temperature-responsive hydrogel microparticles (microgels) simply embedded in a hydrogel matrix resulted in a modest increase in the elastic and storage moduli and the strain and stress at break.

Temperature induced de-swelling of the particles resulted in a transformation from soft to hard particles, further enhancing the mechanical properties of the composite gel. An additional consequence of the induced volume change is the generation of a matrix with switchable porosities [167]. Saunders and co-workers have reported enhanced mechanical properties by chemically crosslinking stimuli-responsive microgels into a hydrogel network [168, 169]. Importantly, these doubly cross-linked μgel networks were shown to function in a load-bearing application: the reconstruction of deteriorated intervertebral discs. Degenerated discs injected with doubly cross-linked microgels had mechanical properties similar to those of normal intervertebral discs [170]. The authors proposed that the doubly cross-linked μgel network increased the swelling pressure within the discs because of the high water content, permitting the discs to behave in a manner similar to the natural system of collagen and proteoglycans – where collagen is the structural unit and the highly charged proteoglycans provide internal swelling osmotic pressure. Overall, biomaterial micro- and nanocomposites represent a growing area in regenerative medicine where there is much to gain through engineering colloid-matrix assemblies [171].

2.2.4 Ultra-low crosslinked microgels

Ultra-low crosslinked (ULC) poly(*N*-isopropylacrylamide) microgels are soft deformable microgels of approximately 500 nm radius. Their synthesis is based on precipitation polymerization without the presence of exogenous crosslinker, under reaction conditions that favor chain transfer. This allows NIPAm oligomers to self-crosslink and form soft, loose microgels [172, 173]. The addition of the co-monomer acrylic acid adds a negative charge to the microgels. This negative charge can then be

utilized for non-covalent binding of positively charged proteins with tunable release kinetics for therapeutic delivery [174]. As a result of their inherent softness, microgels can be concentrated above random close packing to form a space-filling colloidal glass [22]. Microgels in general are considered colloidally stable and demonstrate a strong resistance to aggregation because the surface of the particles often contains charges and 'hairy' surface chains [175]. Their ability to be lyophilized and easily re-dispersed in water additionally highlights their stable properties compared to other colloids. PNIPAm-based materials have been extensively studied for tissue engineering and drug delivery applications due to their thermoresponsivity, and studies have demonstrated the polymer and its degradation byproducts do not elicit cytotoxicity [176, 177]. Synthesis of microgels containing alternative polymers is additionally possible allowing one to pick and choose their base polymer of choice. The rheological properties of microgel suspensions are the focus of both fundamental and industrial applications and can be controlled to meet specific requirements by modifying their concentration, size, shape, cross-link density, surface properties, and solvent quality [178, 179]. Additionally, further characterization of the deformability of ultra soft microgels has been performed, and the size and acrylic acid content of these deformable microgels has been tuned [180].

2.2.5 Mechanisms of the formation of colloidal gel networks, i.e. depletion

Colloidal gelation and the formation colloidal networks that take on fractal morphologies is an entire field of study within soft condensed matter. Many different types of stimuli can initiate colloidal gelation. However, one method of induction is based on the entropic phenomenon of depletion. This phenomenon occurs between two larger colloids (order of microns in diameter, for example) that are surrounded in a

suspension of other smaller colloids (or depletants, on the order of nanometers in diameter). Depletion is a net attractive force between these two larger colloids of interest that are driven together based on an osmotic pressure induced by the smaller colloids. Under normal conditions, the space between the two larger colloids is large enough to fit a smaller particle, i.e. the diameter of a smaller colloid within the system. However, due to entropy and thus the desire for the smaller colloids to occupy more volume, the two larger colloids are brought together increasing the effective volume of the smaller colloids. This phenomenon has been described in detail for hard sphere colloids [181] and the interaction potential of the larger colloids is related to the volume fraction of the depletant and the size of the two constituents. If the interaction potential is on the order of k_BT, then the interaction is not strong enough to sustain clustered particles and thermal fluctuations will release the transient interactions the particles may encounter. However, is the interaction potential is substantially large, i.e. > 5-10 k_BT, then depletion will be expected to occur and the larger colloids will interact, flocculate, and grow into colloidal gel networks throughout the system. Others have mixed non-adsorbing polymers with colloidal suspensions to induce an effective attraction between the particles to generate fluids of clusters [182]. While these studies give insight to food and cosmetic/personal applications where colloidal stability of products is critical, rich information regarding the physics of these interactions can be gained. Additionally, although often overlooked, the depletion attraction force has many implications in cell biology/intracellular organization, as the molecularly crowded environment likely gives rise to these attractions and drives assembly between larger proteins/complexes within the cell [183].

2.3 Angiogenesis and vascularization of implanted materials

2.3.1 Angiogenesis

Vascularization is defined as the process of becoming vascular – or the development or extension of blood vessels. There are several designations of vascularization that are important to distinguish between when considering blood vessel formation in various biological processes. Vasculogenesis is the *de novo* formation of new vessels from endothelial cells and is generally thought to only occur in the developing embryo, where mesoderm-derived endothelial precursors (angioblasts) fuse to form a primitive capillary plexus [184, 185]. However, there exists controversy in the field, as there have been recent studies in the literature suggesting circulating or bone-marrow derived endothelial progenitor cells may contribute to adult vasculogenesis [186-188], while results from other studies contradict this fact [189]. Ateriogenesis is the growth of functional collateral arteries from pre-existing arterio-arteriolar anastomoses that is normally triggered by physical forces such as altered shear forces [190]. Angiogenesis is the process in which new blood vessels sprout from existing blood vessels. Distinct biological triggers occur to stimulate angiogenesis such as tissue expansion (for example, in growing tumors) and hypoxic tissue microenvironments. In response to hypoxia in tissues, hypoxia-inducible transcription factors (HIF) bind to enhancer elements in the promoter region of certain genes to regulate expression. Of particular importance is VEGF, which can increase its expression up to 30 fold within minutes [191]. Sprouting is initiated by these angiogenic signals from the surrounding tissue, including growth factors like VEGF and chemokines released from an inflammatory cell [192]. Pericytes will detach from the surrounding vessel basement

membrane via proteolytic digestion (regulated by MMPs), the endothelial cells will loosen their junctions, and the vessel will dilate. This dilation and VEGF signaling to the endothelial cells causes the extravasation of plasma proteins such as fibrinogen and fibronectin, which will form an ECM surface for endothelial cells to migrate. Subsequent proteolysis of matrix in the surrounding area will liberate additional nascent pro-angiogenic growth factors bound to the matrix such as VEGF and FGF. As the angiogenic tube lengthens, one cells is designated as the tip cell to lead the way and degrade the matrix as it infiltrates the surrounding tissue. Complex signaling pathways critical to a detailed molecular understanding of angiogenesis are described elsewhere [185] and designate cells on either side of the tip cell as stalk cells, which divide in order to maintain cell junctions and advance the growing vessel forward.

Therapeutic angiogenesis or therapeutic vascularization is a regenerative strategy focused on targeting blood vessel infiltration and reperfusion of ischemic tissues. Due to the high number of people with peripheral artery disease [193] and those with coronary heart disease [194], engineering strategies to promote therapeutic vascularization represents a significant area of research in regenerative medicine [195-199].

2.3.2 Collective cell migration and mechanisms endothelial cell migration

Collective cell migration is a process in which groups of cells engage in modes of motility together as a unit. The three main points central to collective cell migration are as follows: 1) the functional and physical connections between the cells are maintained and the integrity of the cell-cell junctions are kept during motion, 2) supracellular organization or polarity is maintained within the group of cells, and there is a global organization of the actin cytoskeletons among the cells, 3) groups of moving cells

structurally modify the matrix into which they move through degradation and subsequent remodeling with deposition of new ECM [200-202]. *In vivo*, many developmental and wound healing processes utilize collective cell migration to respond to environmental cues and mobilize groups of cells to perform a specific function. Examples of processes in which collective cell migration occurs include branching morphogenesis (morphogenic duct/gland formation, i.e. mammary gland), cancer metastasis (multicellular 3D invasion strands, or a detached cluster of cancer cells), 2D sheets (epithelial development and wound healing), and vascular sprouting, to name a few.

During the collective cell migration of vascular sprouting in newly forming or regenerating vessels, collections of 3D strands will invade the provisional fibrin-fibronectin matrix in the wound microevironment. Migration is initiated by the tip cell, which exhibits many filopodial protrusions to probe the surrounding matrix, degrade it where necessary, and allow for subsequent matrix remodeling and deposition to form a track for stalk cells and the vessel behind it to follow. Stalk cells are connected to each other and the tip cell through VE-cadherin cell-cell junctions. VEGF is the most potent pro-migratory factor for endothelial cells during angiogenesis and the signaling pathways and mechanisms are described in more detail elsewhere [203].

It is known that the extracellular microenvironment, specifically the ECM structure and mechanical properties, can influence the modes of cellular migration [130, 134]. In fact, it has recently been shown that ECM density can influence a switch between single cell migration versus collective cell migration in *in vitro* cancer cell invasion models, where higher density ECM networks generated more invasive collective cell strands compared to individual migratory cells [204]. Thus, not only does cell type

and cell-specific properties influence cell motility, but there is also a role for ECM organization to influence cell fate.

2.3.3 Engineering strategies for enhancing vascularization

Due to the need to develop strategies to vascularize biomaterials, many investigators have explored this field. The main strategies that have been explored include pre-fabricating vessel conduits, embedding vascular cells within materials upon implantation to enable microvessel network formation and anastomoses with host vasculature, and engineering degradable synthetic matrices with growth factors to recruit endogenous cells to invade the matrix. Miller and co-workers developed a method to pre-form vascular networks using 3D printing. In this system, 3D complex grid networks were printed using a carbohydrate glass [205]. A hydrogel was then formed around the 3D printed sugar structure. Flowing water through the conduits then resulted in the dissolution of the sugar creating an open vessel network within the hydrogel biomaterial. Subsequently, cells could be embedded in the hydrogels or seeded within the vessel conduits to form multicellular vascularized tissues. Additionally, other patterning techniques were used to demonstrate enhanced cell viability in larger gel constructs and enable anastomoses with host vasculature upon *in vivo* implantation [206, 207].

Human umbilical vein endothelial cells (HUVECs) have been studied over the past 25 years and shown the ability to spontaneously form vessel networks in vitro when culture with ECM hydrogel substrates [208-210]. Additionally, primary microvessel fragments isolated from digested adipose tissue have been extensively studied [211-217]. These multicellular fragments containing endothelial cells, pericytes, and red blood cells have been shown in culture to form interconnected networks and anastomose with host

vasculature *in vivo*. One could imagine an autologous or allogeneic therapy where fat is isolated, digested, and capillaries are acquired, minced, and embedded within a hydrogel for tissue engineering or soft tissue reconstruction. Thus, this represents an interesting alternative to pre-fabrication of vessel conduits, where implanted cells form the networks on their own in response to microenvironmental stimuli.

Many groups have investigated the release of growth factors, in particular VEGF, from dense biomaterials in order to provide a vascular signal to endogenous cells to induce angiogenesis within an implanted material or ischemic tissue [218, 219]. However, VEGF delivery has not yet been translated into the clinic successfully – as the dose, duration, and delivery method of VEGF needs tight control. This is critical to the therapeutic outcome, where low levels or a short half-life of VEGF will result in no benefit and high levels of VEGF can cause aberrant angiogenesis (preventing stable vessel formation) [220, 221]. Hubbell and co-workers have worked to overcome this challenge through utilizing the native ECMs ability to bind growth factors as a delivery vehicle in both natural and synthetic systems [8, 199, 222]. Additionally, work from Phelps et al. demonstrated the ability to incorporate tethered $VEGF_{121}$ for controlled release from RGD modified PEG-DA hydrogels, where increased material vascularization was observed in groups containing VEGF [223]. Work from West and co-workers illustrated the in growth and formation of blood vessels in three-dimensional engineered MMP-degradable VEGF-loaded PEG gels both *in vitro* in a co-culture of HUVECs and 10T1/2 cells and *in vivo* when engineered gels were implanted in mouse cornea [224]. More recently, Sacchi et al. demonstrated an increase in vascularization of long-lasting fibrin implants that were engineered with a degradable protease inhibitor

sequence. When degradation and release of recombinant $VEGF_{164}$ from the construct was tuned to optimal levels, they were able to achieve functional and stable vessels demonstrated when implanted intramuscularly [9]. While a few groups have displayed some success in certain pre-clinical models and systems, there is still work to be done to determine how these therapies can ultimately be translated to the clinic in a safe, efficient, and cost-effective manner. Thus, inducing vascular growth into materials for regeneration remains an important challenge within the field that will likely not be solved by one approach yet will require multiple strategies and tweaks for different applications.

CHAPTER 3 CHARACTERIZATION OF ULTRA LOW CROSSLINKED MICROGELS AND FIBRIN-MICROGEL HYBRID CONSTRUCTS

3.1 Introduction

There is a great need to generate materials-based strategies for regenerative medicine and tissue engineering where implanted materials can quickly and easily integrate with host tissue and to enable the establishment of a functional vasculature. In this work, fibrin was used as a model system, as it is a relevant ECM scaffold that is often utilized due to its endogenous bioactivity and its prevalence in the wound microenvironment as the native provisional matrix. Drawing inspiration from proteoglycans within the native ECM, which have a space-filling role and are water-swollen structures that add compressive strength to tissues, microgels were added to dense fibrin matrices to mimic these properties and promote enhanced cell infiltration and vascularization. Thus, the generation of composite fibrin-microgel constructs was explored. The hypothesis of this aim was that microgels would form interconnected structures within fibrin gels and that the mechanical properties of the composite would be maintained at the same levels as the fibrin alone gel.

The objective of this aim was to study the effects of adding various concentrations of microgels to high concentration fibrin gels (at fibrinogen concentrations where normal cell motility and infiltration were inhibited). In order to do this, a careful characterization of the microgels used in this system was completed. This included size measurements of the particles including both the hydrodynamic radius and radius of gyration. Additionally, microgels with varying crosslinking density were investigated. Specifically, pNIPAM

microgels synthesized in the absence of exogenous crosslinker termed ultra low crosslinked (ULC) microgels were studied, in addition to those synthesized with 2% methylene-bisacrylamide (BIS) crosslinked microgels. In order to compare results between the two types of microgels, measurements of microgel suspension viscosity were necessary to calculate the volume fraction of microgels at certain concentrations to control this parameter when forming composite fibrin-microgel constructs. Furthermore, structural and mechanical properties of the composite materials were measured and analyzed to understand the composition and behavior of the system. Computational analysis of reconstructions of the three-dimensional structures further allowed for an understanding of the architecture of the materials and quantitative measures of relative volume fractions, network sizes, and connectivity of microgel domains. These findings facilitated the understanding of the system for generation of future hypotheses with respect to how cells will interrogate and interact with these composite materials.

3.2 Materials and Methods

3.2.1 Microgel synthesis

Ultra low crosslinked microgels of poly(N'isopropylacrylamide-*co*-acrylic acid) (95%pNIPAM/5%AAc) were synthesized from standard precipitation polymerization techniques as previously described [24, 172, 173, 180]. Briefly, sterile filtered solutions of NIPAm monomer (recrystallized from n-hexanes) and acrylic acid were mixed at 450 rpm in a reaction vessel at 70 °C before the addition of an initiator, ammonium persulfate (APS). For BIS crosslinked microgels, 2% bisacrylamide was added to the reaction as an exogenous crosslinker to produce more highly crosslinked, and thus stiffer particles. In both cases, the reaction proceeded for 6 hours, after which the solution of microgels was

cooled, filtered through glass wool, and purified by ultra-centrifugation. Purified microgels were lyophilized for future use. Fluorescent microgels were generated through labeling of AAc groups with cadaverine conjugates of AlexaFluor dyes (cadaverine AF488, 555,647, Life Technologies) via EDC/NHS chemistry. ULC microgels were resuspended in 25 mM HEPES (4-(2-hydroxyethyl)-1-piperazineethanesulfonic acid) 150 mM NaCl pH 7.4 (HEPES buffer) at stock volume fractions of either 0.28 or 0.56 (10 or 20 mg/mL for ULC) for future experiments.

3.2.2 Microgel characterization with static and dynamic light scattering

3.2.2.1 Multiangle static light-scattering[5]

Multiangle static light-scattering (3DDLS-Pro Spectrometer) was performed by collaborators in the Fernandez-Nieves groups. To compare to previous findings, a 90° setup for dynamic light scattering was additionally executed. To perform the static and dynamic light scattering measurements (SLS and DLS, respectively) for 5% AAc ULC and 2% BIS crosslinked particles, we used a 3D cross-correlation (for removing multiple-scattering) setup (LS Instruments). The 3D DLS system allowed for removal of multiple scattering from the data, enabled the measurement of R_g (in addition to R_h), and also allowed for more precise fit of the form factor to different model functions, which gave information about the radial distribution of polymer density in the particles. Laser light incident onto the sample was scattered into a detector that was positioned at different angles to the incident beam. Different angles correspond to different momentum changes q of the scattered light, according to $q = \frac{4\pi n}{\lambda_0}\sin(\theta/2)$, where λ_0 is the wavelength of the

[5] Portions adapted from Bachman et al. Ultrasoft, highly deformable microgels, Soft Matter, 11 (2015) 2018-2028. Adapted from with permission by The Royal Society of Chemistry.

light in vacuum and n is the solvent refractive index. In SLS, the average intensity scattered into a particular q is analyzed to provide information about the internal structure of the particles. In our case, the accessible q-range included the Guinier regime, in which the intensity decays according to $e^{-(qR_g)^{2/3}}$, where R_g is the particles' radius of gyration, defined as $(R_g)^2 = \frac{\int_0^R drr^4\rho(r)}{\int_0^R drr^2\rho(r)}$ [225]. By fitting this to the observed low-q intensity, we obtained R_g values for our particles at different conditions. If instead of averaging, the time-dependent intensity fluctuations are cross-correlated, we obtained the electric field cross-correlation function, defined as $g_E(\tau) \propto e^{-Dq^2\tau}$, [226] where τ is the correlation lag time and D is the particles' diffusion coefficient. The hydrodynamic radius of our particles was given by the Stokes-Einstein equation, $R_h = k_BT/6\pi\eta D$, where k_B is the Boltzmann constant, T is the temperature in Kelvin, and η is the solvent viscosity [225]. The ratio R_g/R_h is a measure of the mass distribution inside the particles. For a sphere with homogeneous density, R_g/R_h has the analytical value $\sqrt{3/5}$; for a particle with mass concentrated at the center, such as a core-shell particle, this value is lower, while for a particle with mass concentrated at the outside, such as a hollow sphere, this value is higher. We measured R_g and R_h for our particles over a range of temperatures both above and below the pNIPAm LCST of ~33 °C in pH 7.4 HEPES buffer. Note that although the acrylic acid co-monomer is ionized at this pH, which should increase the LCST [227], its low concentration in the microgels (5%) and screening by the dissolved salt ions minimized any such LCST perturbation.

3.2.3 Viscometric measurements of dilute microgel suspensions[6]

Since the particle volume fraction, Φ, is the relevant measure of concentration in colloidal suspensions, viscometry was performed to determine this quantity for both ULC and BIS crosslinked μgel suspensions. An Ubbelodhe viscometer was used to measure the time it takes for dilute suspensions of various microgel weight percentages to travel through a capillary. Temperature was controlled by immersing the viscometer in a water bath for the duration of the measurements. The time read out, constant for the viscometer, and density of the solvent was used to calculate the dynamic viscosity of the suspensions. The data were fit to the Einstein-Batchelor equation ($\eta/\eta_0 = 5.9\Phi^2+2.5\Phi+1$) and plotted as the ratio of dynamic viscosity measured to that of the solvent, η/η_0, vs. the microgel weight percent (Figure 1C), to solve for Φ [228]. We note that Φ is proportional to the microgel concentration c, $\Phi = k * c$, where the constant k can depend on pH, salt concentration and temperature, for a given microgel, since these variables can potentially affect the particle size. The variables k and η can also be used to understand how the solvent quality affects the solvation/swelling of the particles.

3.2.4 Determination of effects of microgels on fibrin gel formation

3.2.4.1 Fibrin and composite gel formation

Human fibrinogen (CSL Behring) was used to form fibrin gels. All gels were formed in HEPES $CaCl_2$ buffer (150 mM NaCl, 5 mM $CaCl_2$, 25 mM HEPES; pH 7.4) and thrombin (0.1-10 U/mL). Composite gels were formed through mixing of ULC microgels with the fibrinogen/HEPES/$CaCl_2$ mixture prior to the addition of thrombin

[6] Portions adapted from Bachman et al. Ultrasoft, highly deformable microgels, Soft Matter, 11 (2015) 2018-2028. Adapted from with permission by The Royal Society of Chemistry.

(0.1, 1, or 10 U/mL). Clots were allowed to polymerize for 1 hour prior to imaging or other experiments.

3.2.5 Mechanical measurements of fibrin-microgel composites

3.2.5.1 Rheological measurements of composite gels

In order to study construct mechanics, a Physica MCR 501 cone and plate rheometer (Anton-Paar) was used (2.014° cone angle, and 24.960 mm tool diameter) to measure the viscoelastic properties of fibrin clots. Clots were formulated as described previously. Both frequency (0.01Hz-10Hz measuring 6pts/decade, 0.5% constant strain) and strain sweeps (0.1-100% strain measuring 6pts/decade, 1Hz constant frequency) were performed to record the storage (G') and loss modulus (G") of at least 6 gels from each group.

3.2.5.2 Statisical Analysis

Statistical analyses were performed in GraphPad Prism (GraphPad Software, San Diego, CA). Differences storage moduli between groups measured were analyzed using a ordinary one-way ANOVA with a Tukey's multiple comparison post-test.

3.2.6 Fluorescence confocal microscopy of hybrid gels

Clots with and without Microgels were formulated as described above and polymerized for one hour between a glass slide and no.1 coverslip [72, 73]. Laser scanning confocal microscopy (LSM 700, Carl Zeiss, Inc.) with a 63X oil immersion objective (NA, 1.4) was used to visualize fibrin matrices using 5% AlexaFluor 647-labeled fibrinogen and AF555 or AF488-microgels. Gels were imaged at least 25 μm

above the glass interface to avoid heterogeneities in the network near contact with the glass surface.

3.2.7 Three-dimensional computational analysis of network architecture of fibrin-microgel composites

3D confocal images were imported into MATLAB for custom processing and analysis. Using a custom in house built script, images were thresholded using the Otsu method, binarized, and run through a median filter. Next, the skeleton of the structure was obtained, which consisted of a central line having the same topology, branching, and overall shape of the initial structure. The skeleton was calculated by solving the eikonal equation and detecting all its singularities, which form a set that correspond to the seek skeleton [229]. The eikonal equation was solved using the fast marching method, which gave very accurate results in Cartesian coordinates [230]. From there the arc length of the skeleton was extracted and the connectivity of the sample was quantified. In particular, the number and location of the branches within the skeleton, as well as the branching number of every branch point and the average distance between branches was calculated.

3.3 Results

3.3.1 Microgel size and viscosity characterization

ULC microgels were synthesized from pNIPAm and 5% AAc. The size and viscosity of ULC particles or 2% BIS crosslinked pNIPAm microgels (also containing 5% AAc) were analyzed through dynamic and static light scattering (DLS/SLS) and viscometry. These techniques were utilized to gain a thorough understanding of ULC size

and polymer distribution. The hydrodynamic radius is a measure of entire particle radius that can be obtained from the Stokes-Einstein equation, $R_h = (k_B T)/(6 \pi \eta D)$. Their results are comparable to previous findings and demonstrated a particle diameter of approximately 1 μm for the ULC microgels. More specifically, at physiological conditions, ULC and 2% BIS particles were found to have similar hydrodynamic radii and radii of gyration of 562 ± 8 nm/445 ± 5 nm and 382 ± 6 nm/313 ± 9 nm, respectively. Measurements were acquired in 25 mM HEPES 150 mM NaCl pH 7.4 at various temperatures, and little temperature dependence in radius was observed (Figure 2).

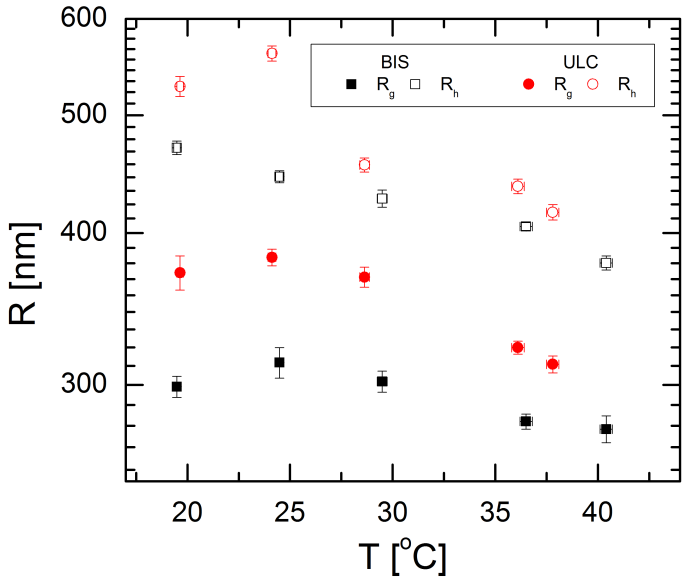

Figure 2: Hydrodynamic radius (R_h) and radius of gyration (R_g) of ULC and BIS microgels under physiological conditions. Dilute suspensions of microgels in 25 mM HEPES 150 mM NaCl pH 7.4 were analyzed using light scattering and their radii as a function of temperature are reported, ULC (in red) and BIS (in black).

Typically, as pNIPAM is a thermoresponsive polymer with a volume phase transition temperature (VPTT) around 31-33°C, one would expect to see a collapse of the particle structure across this temperature regime. However, the microgels contain 5% acrylic acid, which is deprotonated at physiological pH. Additionally, the presence of NaCl at relatively high concentrations effectively deswells the microgel even at temperatures below the VPTT, when comparing R_h of the microgels in water. In order to gain an understanding of the microgel structure, a plot of R_g/R_h versus temperature was generated (Figure 3).

The radius of gyration is the root mean squared distance between monomers within a polymer, and it gives a measure of particle internal structure. The ratio of radius of gyration to hydrodynamic radius is a measure often used to understand a particles structure (homogenous sphere versus core-shell, etc.). Despite the low density of the ULC microgels, they approximate homogenous spheres well with data points clustering around a value of 0.77 or $\sqrt{3/5}$ (theoretical value for homogenous sphere, dotted line in Figure 3) with a slight increase in core versus outer density at lower temperatures (lower R_g/R_h), and a bump near the transition temperature. This indicates that most of the particles' mass migrates to the particle periphery before homogenizing throughout the particle. It is important to note that while it can be assumed multiple scattering is not present in sufficiently dilute samples, there's an important exception that was meaningful for these measurements. Depending on the form factor, there can be minima in the angular scattering intensity. This is particularly true of the homogeneous sphere case, where the minima are very sharp. Even for a dilute sample, where multiple scattering is negligible at most angles, a significant portion of the intensity at these minima is

multiple-scattered. This is true no matter how dilute the sample is, and can be proved (in 3D cross-correlation measurements) by looking at the intercept as a function of angle: there are minima in the intercept that correspond to those of the form factor. Using the 3DDLS we were able to correct the form factor for this multiple scattering. Without the correction, the minima will appear considerably less sharp, and the result would be that we would not have seen such a good fit to the homogeneous sphere form factor, and could have been led to believe that it was more of a core-shell morphology.

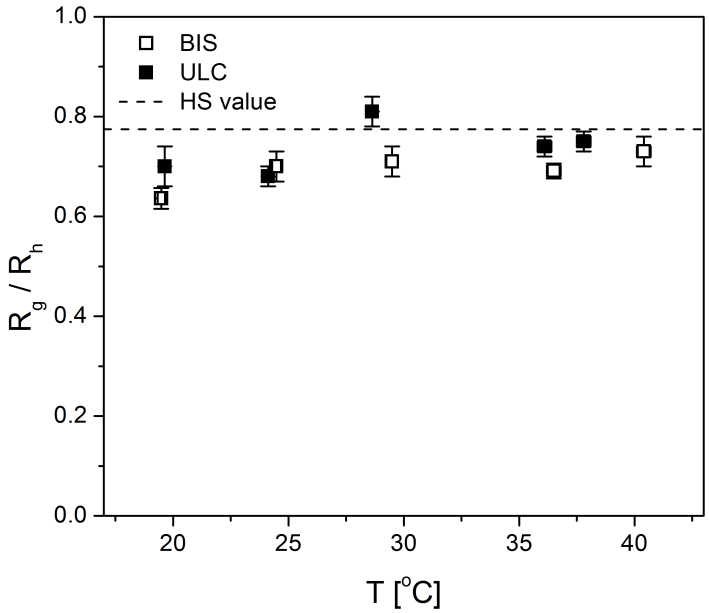

Figure 3: Ratio of radius of gyration (R_g) to the hydrodynamic radius (R_h) for ULC and BIS microgels under physiological conditions. Dilute suspensions of microgels in 25 mM HEPES 150 mM NaCl pH 7.4 were analyzed using ligh scattering. The dotted line represents the theoretical value for a homogenous sphere. Reproduced by permission of the Royal Society of Chemistry from [180].

On average the BIS microgels R_g/R_h values are slightly lower, thus indicating a slightly more core-shell based structure, but overall these particles can be viewed as largely having relatively constant mass distribution throughout the particle structure.

3.3.2 Determination of microgel volume fraction from mass concentration

In many cases, specific properties of suspensions of microgels are dependent on the effective volume fraction occupied by the dispersed component. Volume fraction can also serve as a unifying measure to understand the concentration and phase behavior of a suspension. Thus, we performed viscometric measurements to determine this quantity for both ULC and 2% BIS crosslinked microgel suspensions. Viscometric data (Figure 4) were fit using the Einstein-Batchelor equation.

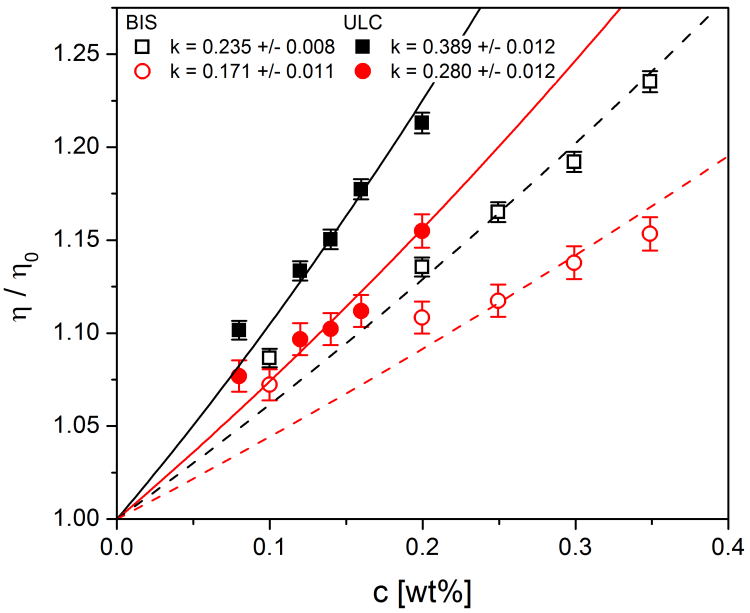

Figure 4: Viscosity of microgel suspensions at various concentrations at physiologial conditions. The viscosity of dilute suspensions of microgels in 25 mM HEPES 150 mM NaCl pH 7.4 were measured using viscometry. Samples were tested

at 25° C or 37° C. Reproduced by permission of the Royal Society of Chemistry from [180].

From these data, k values were calculated to allow conversion between concentration and volume fraction. It was found that the lowest concentrations of microgels tested deviated systematically from the quadratic fit, which likely represents the sensitivity limits of the viscometer. The fit was constrained to go to one at zero volume fraction, and as a result we found that the deviations in fit at low microgel concentrations have negligible effects on the overall fit. K-values for each of the ULC and BIS microgels at 25 °C or 37 °C were derived and are illustrated in Table 1 in the form of mL/mg.

Table 1: Viscometry K-Values (mL/mg) in 25 mM HEPES 150 mM NaCl pH 7.4.

Microgel Type	25 °C	37 °C
ULC	0.0388	0.0280
BIS	0.0234	0.0171

Calculated k values were approximately 1.64 times higher for ULC microgels than 2% BIS crosslinked microgels of similar size. One way to conceptualize this is that 1.64 times more BIS particles by mass must be utilized to reach equivalent volume fractions of ULC particles. This is another demonstration of the low density of these particles compared to more traditionally crosslinked microgels.

3.3.3 Rheological properties of fibrin gels with and without microgels

The properties of fibrin alone and composite gels were measured at both 8 and 25 mg/mL fibrin concentrations with and without ULC or BIS microgels at ϕ=0.112.

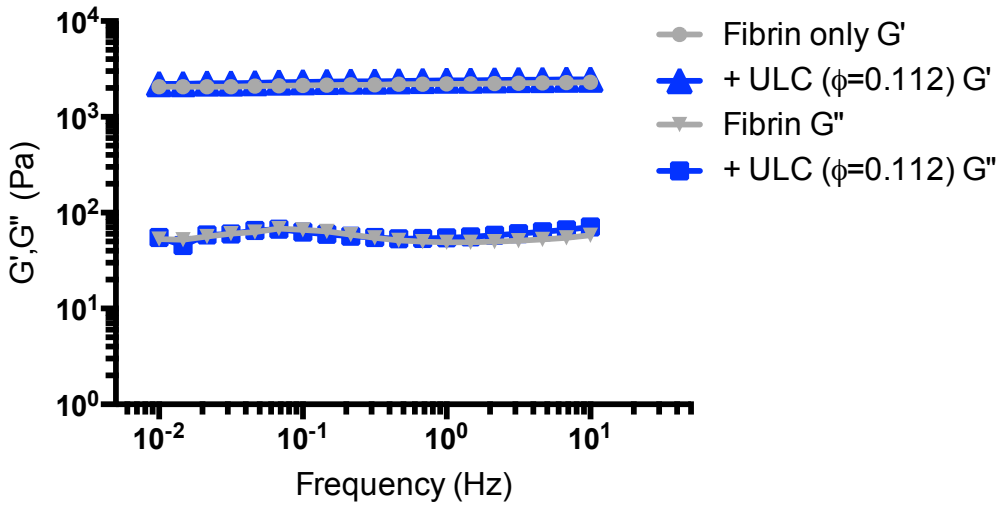

Figure 5: Rheological properties of fibrin and hybrid fibrin-microgel constructs. Storage and loss moduli of gels were measured within the linear regime at 0.5% strain over a frequency range of 0.01 to 10 Hz. Representative curves are shown for fibrin 8 mg/mL alone and fibrin 8 mg/mL with ϕ=0.112 ULC microgels.

Initially, a strain sweep at constant frequency of 1Hz was performed to determine the linear regime, as fibrin is known to be strain stiffening [231]. From this test, a strain of 0.5% was determined to be appropriate for subsequent tests. The frequency response was measured within the linear regime of G'G" of the 8 mg/mL fibrin gels with or without microgels, and found to be indistinguishable from one another. The behavior was typical of a viscoelastic solid. Data from 8 mg/mL fibrin samples with and without microgels at ϕ =0.112 is shown in Figure 5 and illustrates that microgels have no dramatic effect on the rheological properties of the fibrin composite gels.

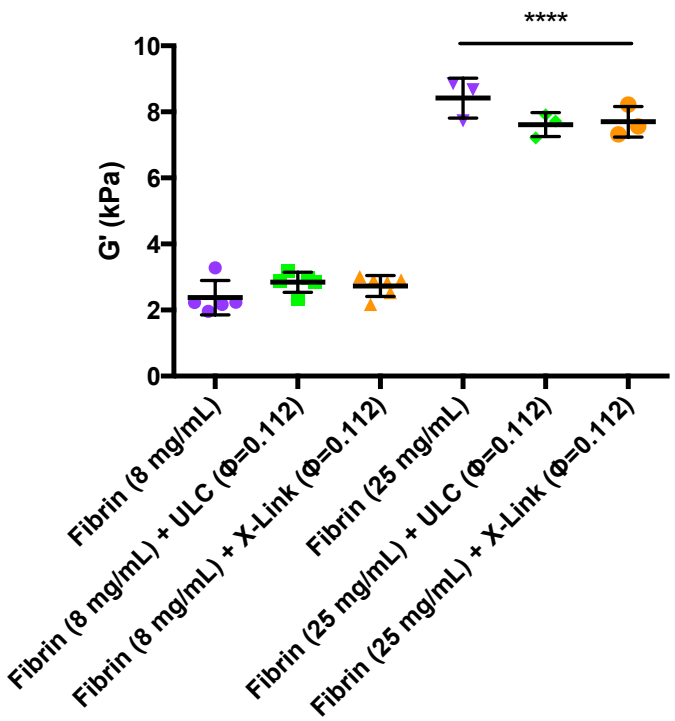

Figure 6: Storage modulus of fibrin and hybrid fibrin-microgel constructs. Storage and loss moduli of gels were measured within the linear regime at 0.5% strain over a frequency range of 0.01-10 Hz. Statistics were measured using a Ordinary one-way ANOVA and Tukey's multiple comparison test, bars represent mean ± standard deviation. While there are significant differences between all of the 8 mg/mL and all 25 mg/mL groups ($p<0.0001$), there are no significant differences between no microgels, ULC, or BIS groups at either fibrin concentration.

The storage modulus of fibrin gels with and without microgels at various fibrin concentrations were measured and are displayed in Figure 6. G' values were averaged across the frequency regime tested (0.01-10 Hz) for three individual gels per group (n=3). As expected, there were significant differences in the average storage moduli between the two fibrin concentrations tested (measured by an ordinary one-way ANOVA $p<0.0001$).

However, within each fibrin concentration, no significant differences were found between the groups with and without microgels. This demonstrated that the presence of the microgels did not affect shear rheological properties of the materials compared to fibrin alone.

3.3.4 Visualization of hybrid fibrin-microgel composite gel structure

The gel structures were imaged using clots that were doped with 5% fluorescent fibrinogen in addition to fluorescently labeled microgels. Individual slices within the 3D volume are shown in Figure 7.

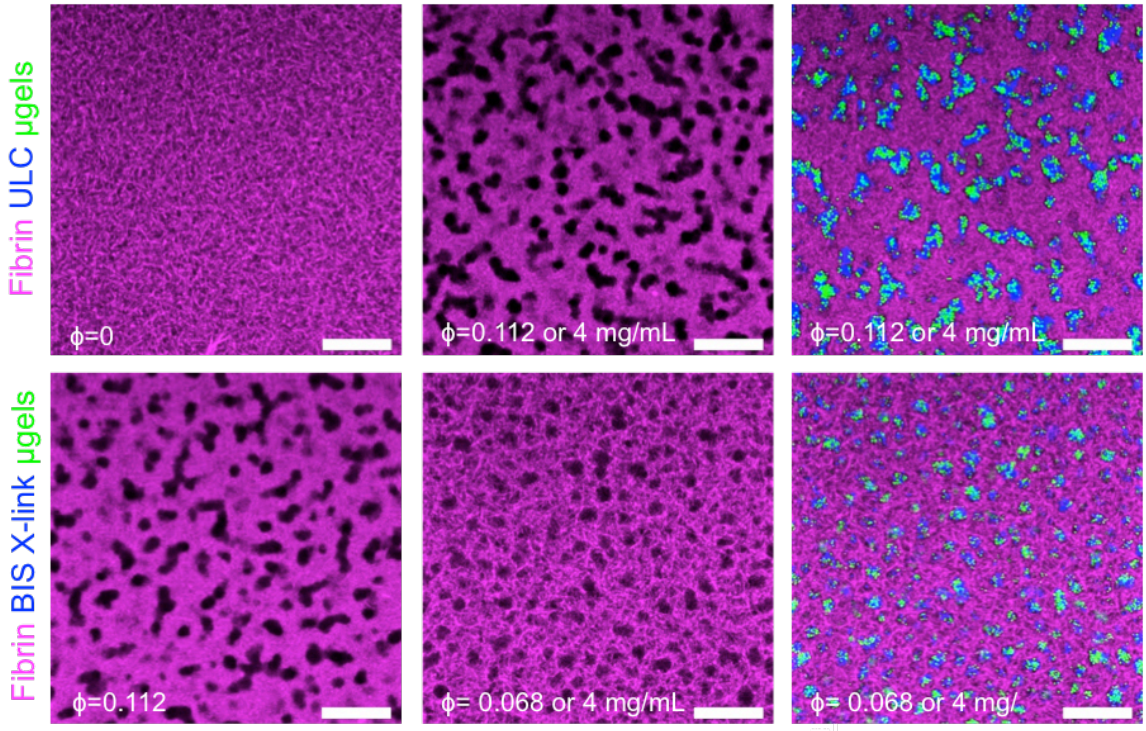

Figure 7: Confocal images of fibrin gels with and without ULC or BIS microgels. Single confocal slices of fibrin 8 mg/mL alone and fibrin 8 mg/mL with ϕ=0.112 ULC microgels (labeled and unlabeled) (top row). Fibrin 8 mg/mL with ϕ=0.112

BIS microgels, or ϕ=0.068 BIS microgels (labeled and unlabeled) (bottom row), scale bar 20 µm.

In the fibrin alone clot, it can be appreciated that the fibrin mesh is dense and even difficult to distinguish pore size in these matrices. However, when microgels are added to the networks to form composite gels, spaces within the fibrin mesh are generated, which are filled with microgels that have clustered into multi-microgel domains, as opposed to remaining a homogenous dispersion of microgels in the polymer matrix. It is also of note that controlling volume fraction between the ULC and BIS microgels is the relevant parameter to control and that strikingly similar networks are formed irrespective of microgel crosslinking density. However, if microgel weight percent or mass based concentration is controlled, this results in different network structures due to the differences in mass and size of the ULC and BIS microgels.

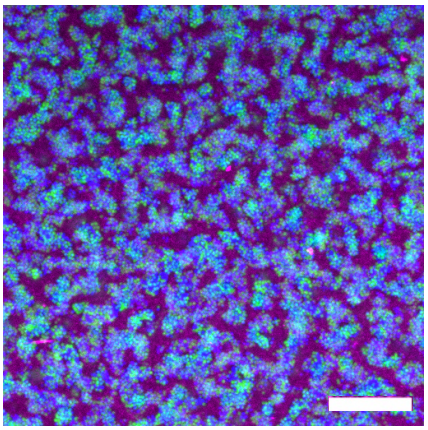

Figure 8: Maximum intensity projection of interconnected microgel network formed in fibrin 8 mg/mL with a mixture of fluorescently labeled ULC microgels. Labeled with AF488 and AF555 (ϕ=0.112), scale bar 20 µm.

Above, in Figure 8, a maximum intensity projection of the interconnected microgel network within the dense fibrin 8 mg/mL gel is shown. This image illustrates the packing and arrangement of microgels within the 'tunnels' that are formed in fibrin.

3.3.5 Quantification of microgel network structure using MATLAB computational analysis of confocal images of fibrin-microgel composites

Confocal z-stacks of hybrid matrices were acquired for samples containing 8 mg/mL fibrin with various concentrations of microgels (ϕ=0.028, 0.056, 0.112, 0.168). The stacks were analyzed with the MicrogelNetworkAnalysis m-file in matlab in order to process the image, generate a skeleton, and output variables of interest. From the skeletonized data, the number of connected volumes (or connected microgel domains) was calculated, with fewer networks indicating a larger degree of network connectivity. Additionally, the radius, length, and volume percent of these connected volumes was calculated, as additional characterization parameters. A schematic of the summarized process can be found in Figure 9.

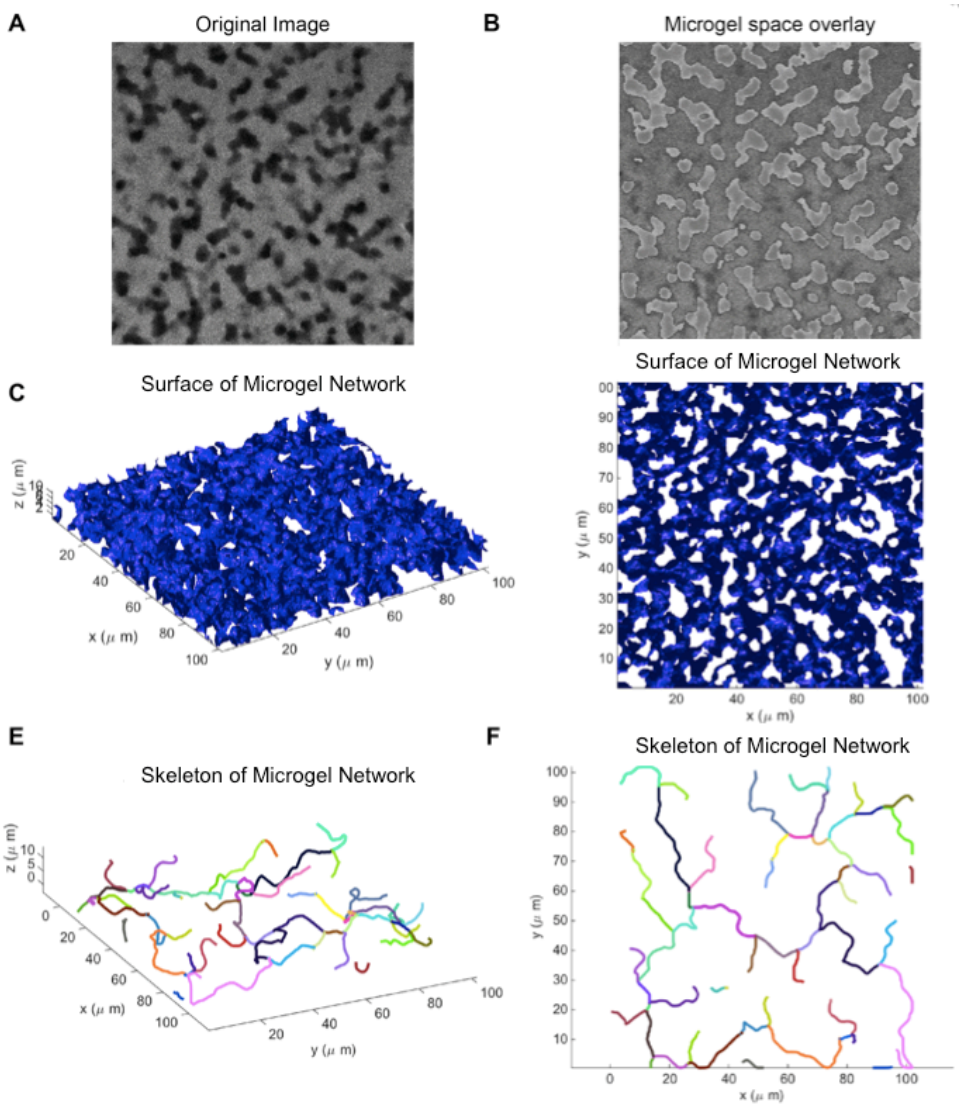

Figure 9: Network analysis process, 3D reconstruction, and skeletonization image processing. Confocal z-stack of fluorecently labeleded fibrin 8 mg/mL with ϕ=0.112 ULC microgels and 1.0 U/mL thrombin was analyzed. A) Initial image, B) image with overlaid found microgel spaces, C-D) 3D reconstruction/isosurface of microgel network, and E-F) found skeleton-tracing the centroid of the network are shown.

Results from the network analysis described in Figure 9 of representative data is summarized in Table 2. Overall, it was observed that the radius of microgel domains averaged around 4.5 μm for this gel formulation.

Table 2: Network analysis results for fibrin 8 mg/mL with ULC microgels ϕ=0.112 and 1.0 U/mL thrombin.

Connected Volumes	Average Radius (μm)	Volume Percent (%)	Arc Length (mm)	Branches per volume (#)
1	4.5	0.916	1.23	77
2	3.41	0.017	0.034	1
3	5.16	0.013	0.033	3
4	4.1	0.009	0.011	1

Additionally, as initial microgel volume fraction was increased shown in Figure 10, the microgel domains grew into interconnected networks. Clusters of microgels associated in pockets, which then eventually grew to a point to join with other pockets and form a percolating network throughout the 3D volume.

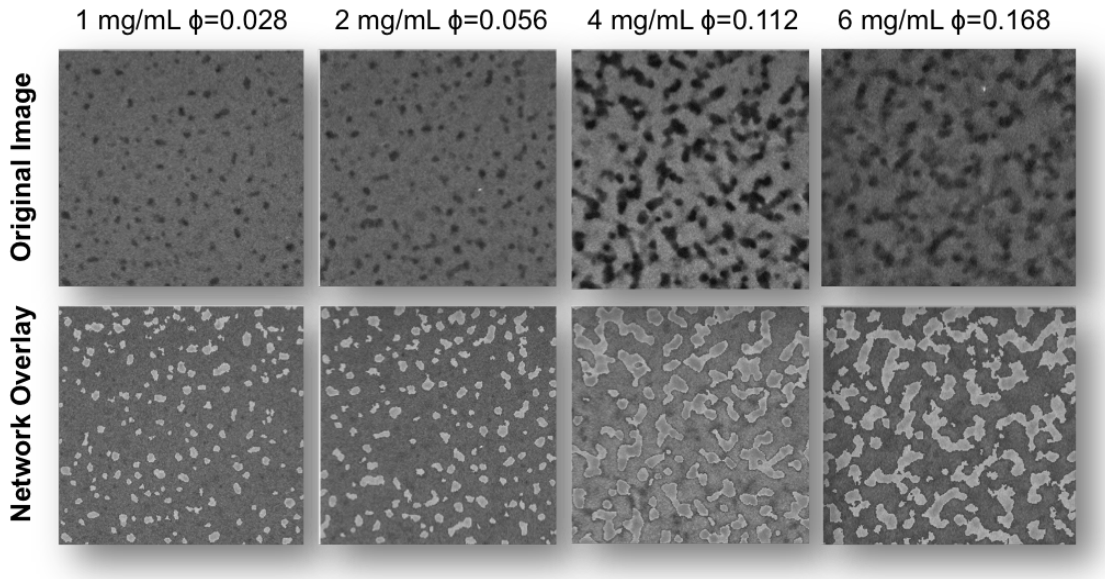

Figure 10: ULC concentration modulation. Confocal slices of fluorecently labeleded fibrin 8 mg/mL with increasing volume fractions of ULC microgels (left to right) at 1.0 U/mL thrombin. Initial images (top row), image with overlaid found microgel spaces (bottom row).

This interconnectivity is further illustrated by the decrease in number of detected connected volumes (converging towards 1) and increase in length and volume percent (reaching values in the 90+ % range) of the main connected volume with increasing microgel volume fraction (Data in Tables 3-6 for increasing microgel volume fractions).

Table 3: Network analysis results for fibrin 8 mg/mL with ULC microgels ϕ=0.028 and 1.0 U/mL thrombin.

Connected Volumes	Average Radius (μm)	Volume Percent (%)	Arc Length (mm)	Branches per volume (#)
1	4.32	0.090	0.206	19
2	3.83	0.089	0.293	43
3	3.62	0.071	0.158	15
4	4.43	0.039	0.120	10
5	4.25	0.015	0.0001	8
+ 279 others				

Table 4: Network analysis results for fibrin 8 mg/mL with ULC microgels ϕ=0.056 and 1.0 U/mL thrombin.

Connected Volumes	Average Radius (μm)	Volume Percent (%)	Arc Length (mm)	Branches per volume (#)
1	3.31	0.045	0.112	11
2	3.31	0.023	0.0548	2
3	4.28	0.021	0.0534	4
4	4.21	0.019	0.0408	5
5	3.49	0.017	0.0466	4
+ 264 others				

Table 5: Network analysis results for fibrin 8 mg/mL with ULC microgels ϕ=0.112 and 1.0 U/mL thrombin.

Connected Volumes	Average Radius (μm)	Volume Percent (%)	Arc Length (mm)	Branches per volume (#)
1	4.5	0.916	1.2320	77
2	3.41	0.017	0.0344	1
3	5.16	0.013	0.0329	3
4	4.1	0.010	0.0114	1
5	4.02	0.009	0.0121	1
+ 12 others				

Table 6: Network analysis results for fibrin 8 mg/mL with ULC microgels ϕ=0.168 and 1.0 U/mL thrombin.

Connected Volumes	Average Radius (μm)	Volume Percent (%)	Arc Length (mm)	Branches per volume (#)
1	4.36	0.998	1.2639	
2	4.62	0.0007	7.47E-03	
3	5.33	0.0007	4.91E-03	
4	3.95	0.0006	2.97E-03	

Upon closer look of the data, there appears to be a switch somewhere between ϕ=0.056 and 0.112 where the network becomes percolated, i.e. individual domains begin to connect and grow to a point where there is a single path that can be followed

throughout the volume from one side to another (Figure 11). Thus, it was determined that at a critical volume fraction of microgels, the network becomes interconnected and that value was found to be ϕ_c=0.112.

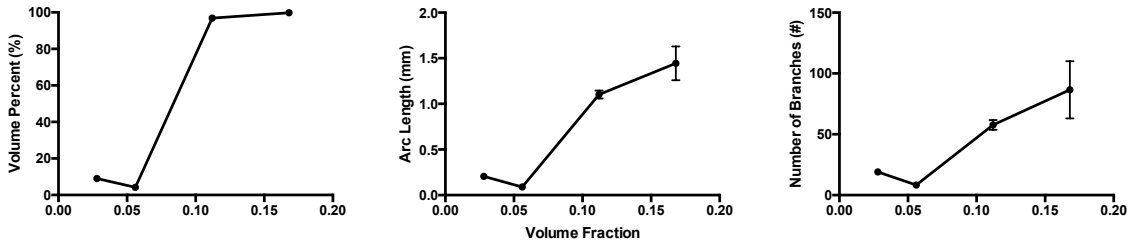

Figure 11: Demonstration of critical threshold of microgel volume fraction where network percolation occurs. Analysis of confocal data is summarized here for hybrid constructs. From left to right, volume percent of the main connected volume, arc length, and number of branches are shown for various volume fractions of microgels.

3.4 Discussion

In this aim, microgels were characterized as well as the fibrin-microgel hybrid constructs utilizing a variety of imaging and mechanical methods. It was found that both the ULC and BIS microgels are approximately 1 μm in diameter and have a structure similar to that of a homogenous sphere. The microgels do not display strong temperature dependent swelling behavior due to the high concentration of salt under physiological conditions in addition to the presence of acrylic acid, which is deprotonated under physiological pH. Fibrin gels at 8 mg/mL form dense matrices and when microgels are incorporated into these clots, polymerization is not inhibited and clustered microgel domains are generated that grow into percolated networks with increasing initial microgel

volume fraction. Additionally, similar 3D architectures were formed independent of microgel crosslinking density as long as volume fraction was controlled illustrating that this phenomenon is not necessarily microgel specific, but is dominated by fibrin polymerization in the absence of any known fibrin-microgel interactions. Interestingly, the presence of microgels does not affect the storage or loss moduli of the composite gels compared to fibrin only controls. This was hypothesized to be due to the maintenance of the characteristic length scale of the pore size, as $G' = k_BT/\zeta^3$. The microgels are maintained within fibrin and their size is on the same order as the fibrin mesh size, thus G' is conserved. However, if the microgel networks were instead – empty voids, then the characteristic pore size of the composite network would increase, thus decreasing G' (since they are inversely proportional). Additionally, because the microgels are maintained with the fibrin networks, as opposed to being cleared out like many porogen systems [89, 120], they are able to add a compressive strength to the matrices and hold water within their structure, as opposed to fibrin alone clots which collapse under significant applied force. Additionally, it should be noted that microgels display dramatically different rheological properties in shear when compared to those of a bulk gel. When a strain is applied to a suspension of microgels, they have the capability to rearrange their structure and organization around one another, unlike bulk gels where crosslinks inhibit relaxation. However, because the microgels are contained within the fibrin network, the rheological measurements that we acquired do not display these properties (likely because the fibrin pore dominates). From a cellular perspective, this could be a potentially useful characteristic within the tissue construct, because the mechanics of the construct are conserved; yet at the micro-scale, semi-fluid microgel

domains could possibly structurally rearrange and adjust with applied force or cellular interrogation.

Finally, there appears to be a critical initial microgel volume fraction, above which clustered microgel domains become connected to form an interconnected percolated network. This information allowed for a better understanding of the base system to allow a better understanding of how biological processes many potentially harness these composite materials for enhanced phenotypic outputs.

CHAPTER 4 DETERMINATION OF THE EFFECTS OF FIBRIN-MICROGEL HYBRID CONSTRUCTS ON CELLULAR PHENOTYPE

4.1 Introduction

When designing a material for tissue engineering applications, one design criteria to consider is to match the mechanical properties of the implant material to the host tissue to promote recruitment and specification of host cells to facilitate repair or regeneration [32]. This design criterion is supported by the literature [232], which shows that material mechanical properties affect cell fate *in vitro* [233-236] and *in vivo* [235, 237, 238]. In seminal work from Discher and Engler, it was discovered that substrate elasticity directed mesenchymal stem cell phenotype through the cell's ability to 'mechanosense' via the actin-myosin cytoskeleton and cell-matrix adhesions [233, 239]. More specifically, Engler observed when MSCs were plated on soft substrates, they differentiated towards a neurogenic lineage, on an intermediate stiffness they displayed myogenic markers, and on stiff substrates they displayed osteogenic characteristics [234]. Work from Helen Blau's group has also demonstrated the effect of matrix elasticity on cell fate *in vitro* through rescuing muscle stem cell potency when culturing the cells on softer substrates mimicking muscle (12kPa) compared to tissue culture plastic (10^6 kPa) [236, 240]. Translating the 2D matrix elasticity findings to cell fate into 3D tissues using proteomic profiling, Swift et al. demonstrated that expression of the nuclear intermediate filament protein lamin-A changed in response to changes in tissue elasticity (increased expression with increasing stiffness). Thus cells can transduce mechanical signals through nuclear

lamin-A to enhance tissue-specific differentiation *in vivo* [238]. Additionally from a mechanics perspective, matching mechanical properties of an implanted material to that of the target tissue diminishes any differences in stress profiles that the tissue may experience during applied force. Fibrin matrices can be pre-formed and implanted at a site of injury, or polymerized in situ to fill a physiological site of interest. In the previous chapter, it was demonstrated fibrin mechanical properties could be tuned through alternation of fibrinogen concentration, but microgels do not have a significant effect on the shear modulus. Fibrin degradation products are pro-angiogenic [63, 64], making it suitable choice for the base polymer system. An engineering strategy was developed to overcome the shortcoming of utilizing fibrin gels with high fibrinogen concentrations, and a thorough characterization of the fibrin-microgel hybrid matrices was performed. Thus, this aim focuses on understanding the effect of these constructs on cellular phenotype when compared to fibrin only controls.

The engineering goal of these composite materials was to enable enhanced cell spreading and motility compared to dense fibrin only constructs that impeded these processes. Cellular morphological outputs, such as spreading, are prerequisites to enabling cell migration and thus cell infiltration, which ultimately leads to host-material integration [32]. The hypothesis of this aim was that the addition of microgels would allow for increased cell spreading, motility, and infiltration.

4.2 Materials and Methods

4.2.1 Cell culture

NIH 3T3 fibroblasts (ATCC) were cultured according to manufacturer's recommendations and sub-culturing protocols in Dulbecco's modified eagle's medium

DMEM with 4.5 g/L glucose, L-glutamine, sodium pyruvate and supplemented with 1% penicillin/streptomycin and 10% bovine calf serum.

4.2.2 Fibrin gel formation

4.2.2.1 Preparation of fibrin gels with and without microgels

Gels were formed as described previously in Chapter 3. Human fibrinogen (CSL Behring) was used to form fibrin gels in HEPES (N-2-hydroxyethylpiperazine-N-2-ethanesulfonic acid) $CaCl_2$ buffer (150 mM NaCl, 5 mM $CaCl_2$, 25 mM HEPES; pH 7.4). Composite gels were formed through mixing of ULC microgels with the fibrinogen/HEPES/$CaCl_2$ mixture prior to the addition of thrombin (0.1, 1, or 10 U/mL). Clots were allowed to polymerize for 1 hour prior to imaging or the addition of media. When applicable, cell suspensions in culture media were added to the fibrinogen mixture prior to mixing with thrombin as 10% of the total clot volume.

4.2.3 Cell spreading assay

4.2.3.1 Experimental set-up and cell staining

For cell spreading assays, NIH 3T3 fibroblasts were incorporated into polymerizing fibrin only and fibrin-microgel gels in media at a density of 200,000 cells/mL comprising 10% of the gel volume. Gels were formed as described previously with fibrin alone or fibrin with ULC microgels (ϕ=0.014, 0.028, 0.056, 0.112, or 0.168). After incubation over night, the samples were rinsed with cold 1X PBS, fixed with 4% formaldehyde (Sigma-Aldrich) for 20 minutes, permeabilized with 0.2% Triton X-100 for 10 minutes, rinsed again with 1X PBS, and incubated with AF488 Phalloidin (Life Technologies) to stain the actin cytoskeleton and Hoechst 33258 (Life Technologies) to

stain the nucleus. Confocal z-stacks (100 μm) were imaged with a 10X objective and maximum intensity projections were created.

4.2.3.2 Image acquisition and Quantification of cell morphology

Cell area was measured from maximum intensity projections using NIS Elements Software (Nikon) and other morphological parameters were calculated including circularity (=4*π*Area/Perimeter^2) and elliptical factor (major/minor axis), which were measured from at least 50 different cells in 3 different gels.

4.2.4 Cell motility assay

4.2.4.1 Experimental set-up and cell labeling strategy

For motility studies, cells were stained with 10 μM of Cell Tracker Dye Green CMFDA (Invitrogen) for 15 minutes in growth media according to manufacturer's instructions prior to encapsulation in gels. Cells were incorporated into polymerizing fibrin and fibrin-microgel gels in media at a density of 200,000 cells/mL comprising 10% of the gel volume. Two gels (fibrin +/- microgels, ϕ=0, 0.014, 0.028, 0.056, 0.112, or 0.168, or BIS X-link microgels ϕ=0.112) per experiment were formed in a 35 mm dish side by side and were allowed to polymerize at 37C in the incubator for 1 hour prior to the addition of media on top of the composite gels. Cells were allowed to grow and spread overnight before beginning time-lapse experiments the next morning. Live cell imaging was performed with a Nikon BioStation IM-Q Live-Cell incubation chamber and microscope. Images of cells at least 25 μm above the interface were acquired with a 10X objective in phase-contrast and FITC every 10 minutes over the course of 12 hours in 6-10 regions per gel from 2-3 independent experiments.

4.2.4.2 Image acquisition and Quantification of migration speed

Fluorescent images of labeled cells were imported into FIJI (ImageJ) and cells were manually tracked (recording x and y coordinates) over the duration of the experiment. Summed distance over time and average instantaneous speed was calculated for each cell over the course of the experiment and plotted. Dividing cells and cells that moved out of the viewing field for more than ½ of the experimental duration were neglected. At least 50-100 cells were tracked per experimental and control group from 2-3 independent experiments.

4.2.5 Cell infiltration assay

4.2.5.1 Preparation of inner cell-laden fibrin gel

A dense cell laden gel was generated with 10^6 cells/mL in an 1 mg/mL fibrin gel according to fibrin gel formation protocols described previously. These gels were small volume (2ul) clots placed on the bottom of a 96 well plate and were polymerized for 15 minutes prior to encapsulation with a second gel.

4.2.5.2 Preparation of outer gel with or without microgels

After 15 minutes, the inner gel was then covered in a cell-free 8 mg/mL fibrin gel with or without microgels (ϕ=0.112). After allowing the second gel to polymerize for 1 hour, cell culture media was added and the cells imaged with phase contrast microscopy at 4x magnification over the course of three days.

4.2.5.3 Quantification of migration/infiltration distance

Infiltration/migration distance of the outgrowths into the surrounding gel from the core was measured from phase contrast images using ImageJ. Three random cell streams

migrating out from each gel were measured and averaged on each day, with data pooled from 9-12 gels per group over two independent experiments.

4.2.5.4 Statisical Analysis

All statistical analyses were performed in GraphPad Prism (GraphPad Software, San Diego, CA). For cell morphology specifically, circularity– a one-way ANOVA was performed with a Tukey's multiple comparisons post-test. For cell spread area and elongation, the data was not normally distributed and thus a Kruskal-Wallis non-parametric test was used with Dunn's post-test for multiple comparisons was performed. For analyzing cell infiltration in the outgrowth assay, a two-way ANOVA was performed with Bonferroni's multiple comparisons test. For migration speed, the data did not fit a normal Gaussian distribution and thus the Kruskal-Wallis non-parametric test was used with Dunn's post-test for multiple comparisons. Data is represented in box and whisker plots, which extend from the 25th to 75th percentiles with a line at the median and error bars to the minimum and maximum values.

4.3 Results

4.3.1 Cell morphological phenotype in fibrin-microgel composite gels

After overnight growth and spreading, cellular morphology and spreading in fibrin (8 mg/mL) constructs was examined, through visualization of the actin cytoskeleton as shown below in Figure 12.

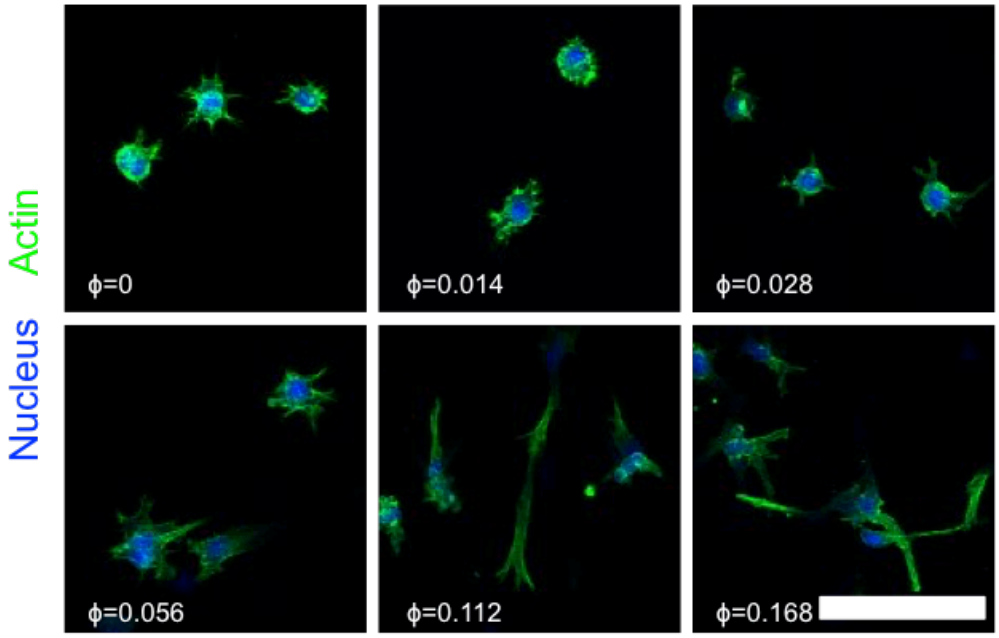

Figure 12: Representative confocal maximum intensity projections of NIH3T3 fibroblast morphology in fibrin-microgel constructs. Maximum intensity projections of staining of the actin cytoskeleton at various initial microgel volume fractions listed on the image are shown, scale 100 μm.

In the fibrin alone groups, cells displayed a rounded morphology, as expected within these dense polymer scaffolds where cells must degrade the matrix around them in order to spread due to the small pore size of the network. However, when ULC microgels are incorporated into the network, a 1.85 fold increase in cell spreading is observed in a microgel concentration dependent manner (Figure 12, 13A). At the transition to a critical volume fraction ϕ_c the cell spread area jumps from an average of 728.5 μm^2 in the fibrin only group to 1352 μm^2 at $\phi = 0.112$.

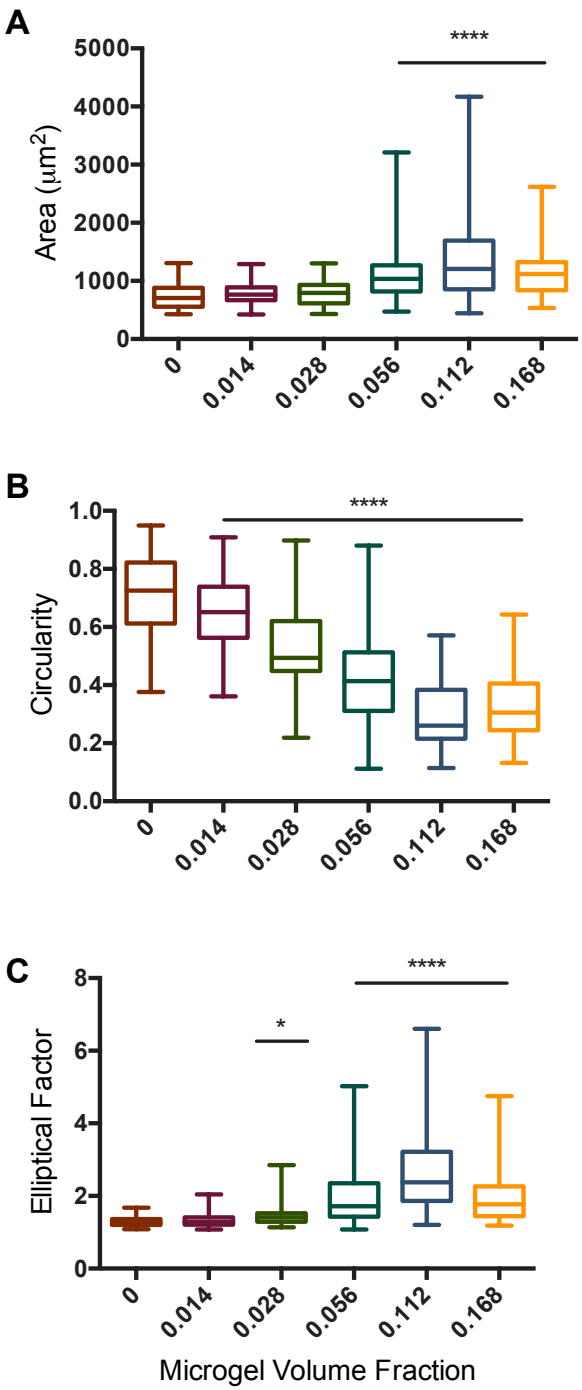

Figure 13: NIH3T3 fibroblast morphological analysis in hybrid fibrin-microgel constructs. Analysis of confocal data is summarized here for hybrid constructs. Average cell spread area measured from maximum intensity projections from 4 gels (n=55-79 cells) A) Cell spread area measured from maximum intensity projections,

box and whiskers plot extends from the 25th to 75th percentiles with a line at the median and error bars to the minimum and maximum values, Kruskal-Wallis non-parametric test was performed with Dunn's post-test, **** $p<0.0001$ compared to $\phi=0$ group; B) Circularity analyzed, box and whiskers plot extends from the 25th to 75th percentiles with a line at the median and error bars to the minimum and maximum values, data passed normalcy test and one-way ANOVA with Tukey's post-test for multiple comparisons was performed **** $p<0.0001$ compared to $\phi=0$ group. C) Elongation (min feret/max feret) was calculated and box and whiskers plot extends from the 25th to 75th percentiles with a line at the median and error bars to the minimum and maximum values, Kruskal-Wallis non-parametric test was performed with Dunn's post-test, * $p<0.01$, **** $p<0.0001$ compared to $\phi=0$ group. For all parameters n= 55-79 cells analyzed per volume fraction in a minimum of 3 separate gels.

As the volume fraction of ULC microgels increases, cells lose their circularity becoming more elliptical and their overall spread area increases (Figure 13B,C). These findings demonstrate that the cells are able to leverage the microgel domains in order to extend protrusions and spread in three-dimensions.

4.3.2 Cell motility in fibrin-microgel composite gels

In order to determine if these 3D interconnected microgel tunnels could affect cellular phenotype and motility in vitro, NIH3T3 fibroblasts were incorporated into the composite hydrogels during polymerization and were monitored over the course of 12 hours after an initial 16 hours of growth and spreading. Time-lapse microscopy of

fluorescently labeled cells and manual tracking of random cell migration was performed on each of these constructs. Plotting migration distance versus time, cells were seen to follow a linear trend with increasing slopes for samples containing microgels compared to fibrin only controls (Figure 14), indicating steady and persistent random migration through the network.

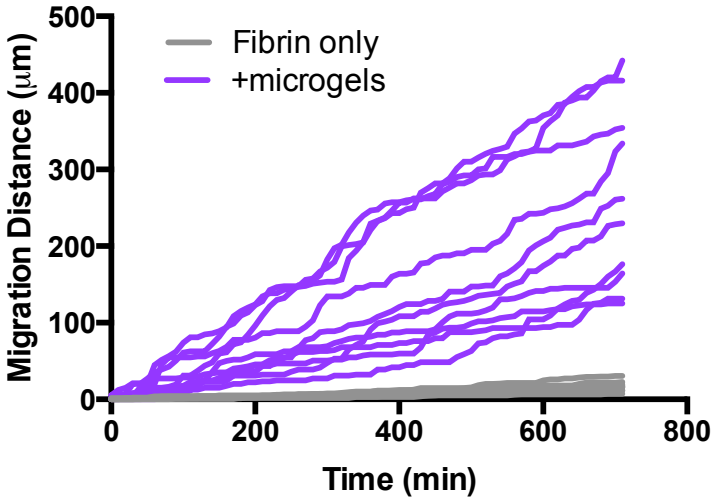

Figure 14: NIH3T3 fibroblast migration distance versus time in hybrid fibrin-microgel constructs. Summed migration distance over the course of twelve hours is shown for a representative set of cells (n=10 per condition) for fibrin 8 mg/mL with and without ϕ=0.112 ULC microgels.

An increase in average migration speed was observed in a microgel dose-dependent manner (Figure 15), for example an increase was observed from an average of 1.78 μm/hr in a fibrin only control to 15.82 μm/hr with the addition of Φ=0.112 ULC microgels.

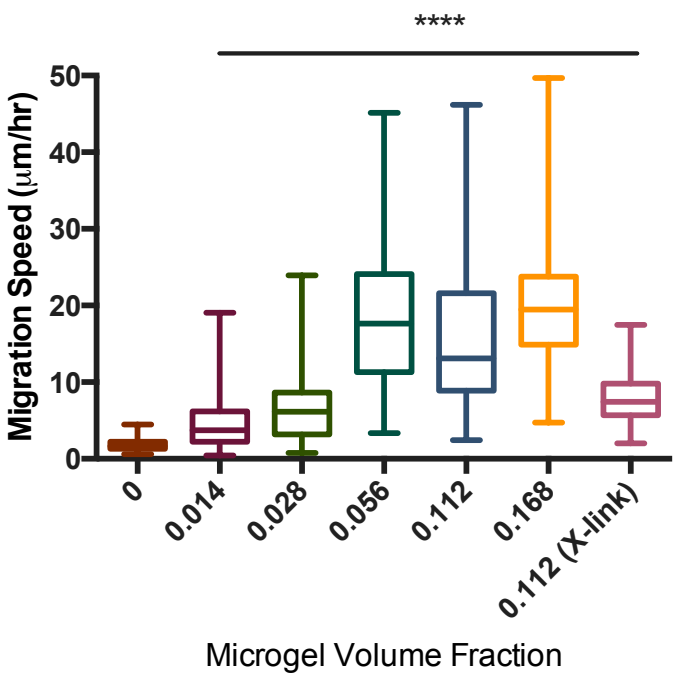

Figure 15: NIH3T3 fibroblast average migration speed in fibrin 8 mg/mL with increasing microgel volume fraction. Averge migration speed per cell is shown for fibrin 8 mg/mL with increasing volume fractions of microgels. Averages are calculated from the instantaneous speed of a cell over the course of the 12 hour experiment n = 2-4 gels (47-184 total cells analyzed per group). Box and whiskers plot extends from the 25th to 75th percentiles with a line at the median and error bars to the minimum and maximum values; Non-parametric Kruskal-Wallis test was performed with Dunn's multiple comparisons test p<0.0001.

Increases in average migration speed through fibrin were also observed with the addition of equivalent volume fractions of BIS crosslinked microgels, but only reaching an average of 7.93 μm/hr, strongly suggesting that the deformability of ULC microgels greatly enables cell infiltration, as shown in Figure 16.

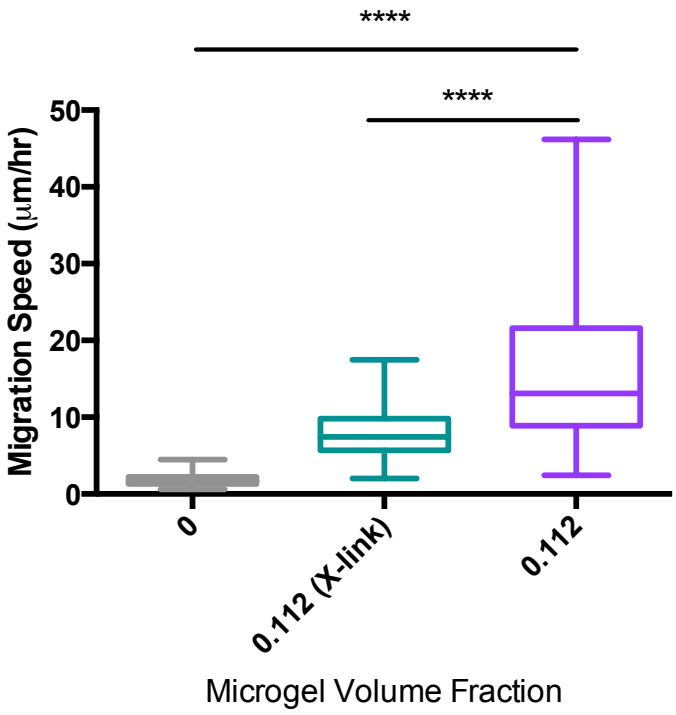

Figure 16: NIH3T3 fibroblast average migration speed in fibrin 8 mg/mL with and without microgels (ϕ=0.112). Average migration speeds are shown for cells polymerized in fibrin alone (gray), fibrin with BIS crosslinked (X-link) microgels (green) (n=51), or ULC microgels (purple) (n=184). Box and whiskers plot extends from the 25th to 75th percentiles with a line at the median and error bars to the minimum and maximum values; Kruskal-Wallis non-parametric test was performed with Dunn's multiple comparisons test, **** p<0.0001.

This indicates a role for microgel composition, specifically deformability, in dictating cellular phenotype (both motility and morphology) within these composite materials. Additionally, at more clinically relevant fibrin concentrations of 25 mg/mL an increase in migration speed was observed with the addition of Φ=0.112 ULC microgels (Figure 17).

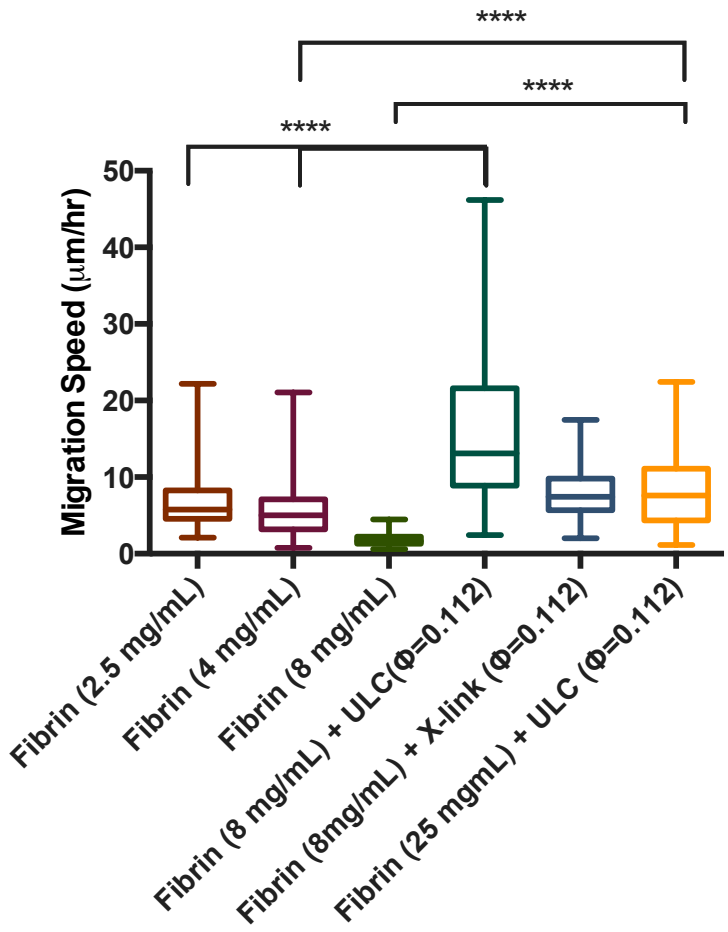

Figure 17: NIH3T3 fibroblast average migration speed in fibrin gels of various concentrations in comparison with those containing microgels (ϕ=0.112). Average migration speeds are shown for cells polymerized in fibrin alone, or various fibrin-microgel hybrid constructs (n = 2-4 gels, 47-184 total cells analyzed per group). Box and whiskers plot extends from the 25th to 75th percentiles with a line at the median and error bars to the minimum and maximum values; Non-parametric Kruskal-Wallis with Dunn's multiple comparisons test was performed, **** p<0.0001.

Additionally, cells within fibrin 8 mg/mL + ULC microgels ϕ=0.112 are able to migrate at significantly higher speeds than physiological controls of 2.5 or 4 mg/mL fibrin alone.

4.3.3 Effect of microgels on cell infiltration in an outgrowth assay

To look more specifically at infiltration, an in vitro outgrowth assay was performed to monitor migration of cells from a dense cell pellet into an outer fibrin gel 8 mg/mL with or without microgels. Over the course of three days, significant migration (hundreds of microns) into the outer gel containing ULC microgels was observed compared to the fibrin only gel, which maintained a strict unchanged border as shown in Figure 18. Specifically, after 3 days, cells encapsulated by a fibrin only gel had only migrated on average 9.2 microns, whereas cells encapsulated by a hybrid gel containing microgels had migrated an average of 260.9 microns.

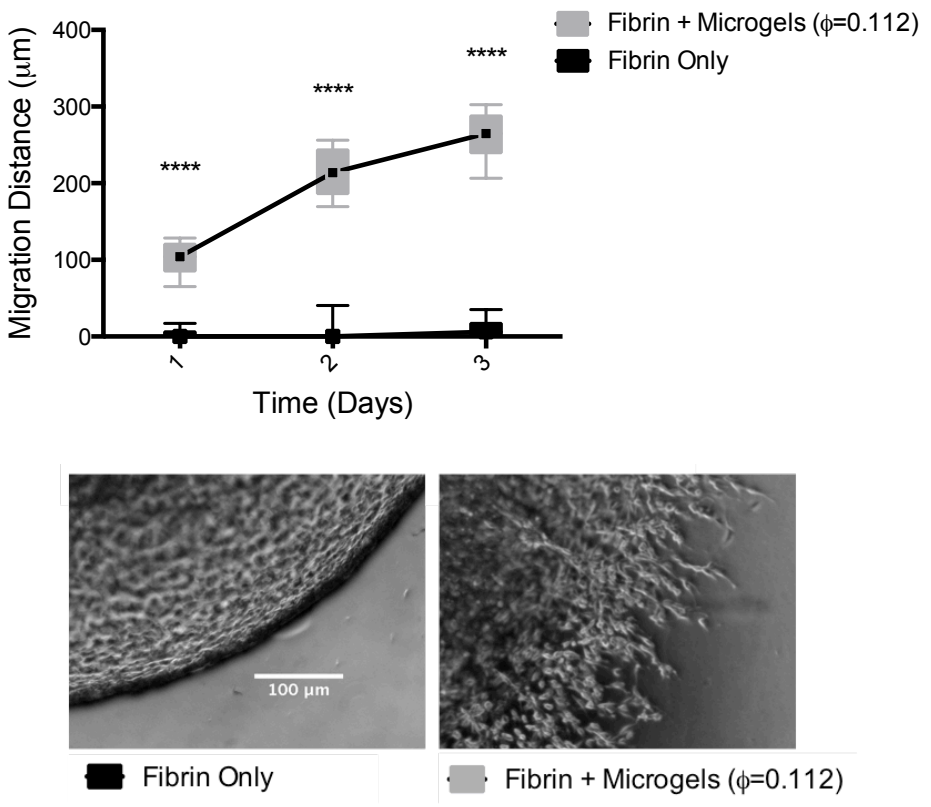

Figure 18: NIH3T3 fibroblast average migration speed in fibrin gels of various concentrations in comparison with those containing microgels (ϕ=0.112). Average migration speeds are shown for cells polymerized in fibrin alone, or various fibrin-microgel hybrid constructs. Box and whiskers plot shown, migration distance averaged from 5 measurements from n=12 gels from two independent biological replicates (represented as median with 75/25% percentile with minimum and maximum). A two-way ANOVA with Bonferroni's multiple comparisons test was performed and statistically significant differences were found between ± microgels ($p<0.0001$) at each time point.

4.4 Discussion

In this aim, it was observed that microgels enabled cell spreading, motility, and infiltration in a microgel dose-dependent manner. The switch in phenotype began to

occur at a similar initial volume fraction where the formation of an interconnected percolated network would be observed, around ϕ_c. This observation mirrors generally accepted engineering strategies from the literature where a highly interconnected network is known that to facilitate tissue integration and cell infiltration [13]. However, the microgels are maintained within the composite structure raising interesting questions for future studies about how the cells may be leveraging the microgel networks for enhanced motility.

With respect to cell migration speed measurements, it was observed that microgels were able to enhance average speeds to values above those found at physiological fibrin concentrations and even those at half the fibrin concentration of the composite gel. The incorporation of microgels (ϕ=0.112) to even higher concentration fibrin gels (25 mg/mL) was able to rescue migration speed to levels commensurate with physiological fibrin concentrations. It should be noted that all of these experiments were performed in the absence of a protease inhibitor, in order to more closely mimic the *in vivo* microenvironment. Therefore, some degradation is likely occurring and enabling migration. When the protease inhibitor aprotinin is added to the gels and media solutions, as commonly performed with fibrin *in vitro* cell culture assays [7], the presence of microgels still enables motility to degrees significantly greater than fibrin alone. However, the increase in migration speed is muted compared to data where no protease inhibitor is applied. Thus, microgels may enable degradation independent spreading and motility; however, their effect is more dramatic when degradation can proceed normally.

While the specific cellular mechanism is not well understood, the hypothesis is that somehow, the cell is able to harness the microgel-filled space to extend protrusions

and bind to fibrin at more distant locations from the cell body. Subsequently, the cell is able to generate more contractile forces as it is more spread. This could be through enhanced local deformation surrounding the individual cell. While it is unlikely that the presence of microgels alone upregulates the expression of proteolytic enzymes by the encapsulated cells, there is evidence in the literature, that cell spreading/contractility and MMP expression are linked [241]. Thus, cells with increased contractility that are able to extend protrusions (in the cancer field, termed invadopodia) increase their proteolytic activity and have enhanced expression of MMPs [242].

Additionally, cells could be harnessing the microgel suspension characteristic relaxation time in order to extend protrusions through the microgel-filled domains within the composite gel. This hypothesis could be compared to the analogy of a child playing in a ball pit at a playground with a fixed volume. If one were stuck in a packed suspension of balls, the ability for motion to occur would depend on the ball pit packing fraction, the deformability of the balls, and the ability of the balls to move/rearrange with respect to one another. Evidence from this aim suggests that particle crosslinking density (i.e. ULC microgels compared to BIS microgels) affects migration speed of NIH 3T3s in these composite gel systems. Thus, microgel deformability or microgel relaxation time (rearrangement time) could be a logical mechanism that the cells are utilizing to move through these composite materials.

As a final hypothesis, cells theoretically could be phagocytosing microgels and effectively 'eating' their way through the composite matrix. This hypothesis is difficult to test due to the inability to image microgels in their native unmodified chemical form (since fluorescently labeling the particle occupies the acrylic acid site and thus may

change the net charge of the particle). Individual unmodified microgel particles of this size cannot be visualized in phase contrast or DIC under high magnification unless they are present at high volume fractions in a microgel suspension. Cellular detail likely prevalent due to the structure of organelles within the cell body made it impossible to discern differences in the internal structure (i.e. whether microgels were present) in cells incubated in hybrid constructs. Literature in the phagocytosis of particles is quite rich, and it has been shown that negatively charged unmodified particles are typically not internalized by cells [243-246]. Flow cytometry experiments of cells incubated in fibrin-microgel composite gels, which were then digested to release the encapsulated cells, showed no observable differences in forward scatter or side scatter (data not shown). Large concentrations of fluorescently labeled microgels were incubated with cells in 2D culture and no particles were visualized within the cells after 4 hours (data not shown). However, when imaging cells embedded in hybrid matrices with fluorescently labeled microgels, microgels appeared to co-localize with the cell body. As large amounts of microgels are present, the delineation of microgels inside versus outside the cell is difficult to appreciate. Additionally, it is unclear if this is an artifact of the chemical modification of these specific microgels for fluorescent confocal microscopy visualization experiments. Consequently, experimental confirmation of this hypothesis has been a challenge and the results are unclear, but may be suggestive of another mechanism cells could use to navigate in confined tissue spaces in the presence of molecular crowding.

CHAPTER 5 INVESTIGATION OF THE MECHANISM OF MICROGEL NETWORK FORMATION IN FIBRIN AND OTHER MATERIALS

5.1 Introduction

Why do microgels cluster into interconnected domains in fibrin materials? Upon polymerization, what drives the microgels into these networks as opposed to remaining homogenously dispersed within the gel? In efforts to better understand how these interconnected composite materials are formed and what dictates their structure, this chapter focuses on investigating the mechanism of microgel network formation. This is important because if we understand how the system is functioning in the example of fibrin, then potentially we can translate our findings to other biomaterial systems. This could enable significant benefits in material systems that suffer from the drawbacks of small pore sizes (which includes many synthetic materials). Using fibrin as a model system where the reaction kinetics can be tuned by adjusting the concentration of the catalytic enzyme, thrombin, we studied how these composite materials form and the factors that dictate their resulting architecture. The hypothesis of this sub-aim was that the size and shape of microgel networks within fibrin would be dictated by the polymerization rate of fibrin.

Based on evidence in the hybrid-fibrin microgel system, it was hypothesized that the architecture of the resulting microgel network structure was connected to the method of gel polymerization or crosslinking. This was investigated in fibrin by modulating thrombin concentration and observing polymerization in real-time. To further test the

hypothesis that polymerization or gel crosslinking method would determine the resulting microgel network architecture, experiments were performed with PEG gels as well as Alginate. PEG hydrogels can be formed using different gelation strategies, and in this work UV free radical polymerization of PEG diacrylate and Michael-type addition of PEG-maleimide were explored [247]. Alginate, an anionic polysaccharide derived from brown seaweed, was also tested as it has frequently been studied as a tissue engineering scaffold or synthetic ECM material [248]. Alginate gels crosslink through alternative mechanism known as ionic crosslinking [249]. Thus, when alginate molecules are exposed to divalent cations such as Ca^{2+}, the gel structure becomes crosslinked [250]. These reactions important to materials such as PEG and alginate represent a fundamentally different method of polymerization or crosslinking when compared to materials like fibrin. Through this study, the mechanisms of microgel network formation were explored to allow for a better understanding of the system and facilitate translation of this technology into other materials.

5.2 Materials and Methods

5.2.1 Composite gel formation with thrombin modulation

5.2.1.1 Preparation of composite gels with varying thrombin concentrations

Fibrinogen (CSL Behring) purified from human plasma (containing FXIII and fibronectin) was used at various concentrations throughout the study. For the formation of fibrin clots, fibrinogen was mixed with 25 mM HEPES 150 mM NaCl (HEPES buffer) pH 7.4, and 5 mM $CaCl_2$ prior to the addition of thrombin (0.1, 1, or 10 U/mL). Composite gels were formed through mixing of ULC microgels with the

fibrinogen/HEPES/CaCl2 mixture prior to the addition of thrombin (0.1, 1, or 10 U/mL). Clots were allowed to polymerize for 1 hour prior to imaging.

5.2.1.2 Rheological measurements of composite gels with varying thrombin concentrations

In order to measure the gel point of the hybrid matrices, a time sweep was performed after the addition of thrombin to the composite fibrin-microgel suspension. Measurements were acquired at a fixed strain of 0.5% every second, and G', G" were recorded for 3 independent gels. The gel point was calculated as the total time required after initiation of polymerization at which G' became greater than G".

5.2.1.3 Real time polymerization of composite gels imaged with spinning-disk fluorescence confocal microscopy

A Cell Observer Spinning Disk (SD) confocal (Carl Zeiss Microscopy Ltd) was used for the acquisition of time-lapse videos of real time microgel network formation in 3D composite gels with varying thrombin concentrations. Gels were formed as previously described using AF488 fluorescently labeled ULC microgels. Briefly, fibrinogen (8 mg/mL) and ULC microgel (ϕ=0.112) solutions were pipetted onto the glass bottom dish for initial visualization of microgels in the fluid suspension and adjustment of the focal plane. Thrombin was then added to the mixture at the desired concentration and measurements were recorded immediately after mixing. Images were acquired at the fastest frame rate possible through the three dimensional volume. Using a 63 X (plan Apochromat NA 1.46) objective, the optimal sampling for 25 μm thick stacks gave images every 0.25 microns resulting in 100 images per stack. Acquisition proceeded continuously until the system halted and appeared to reach a gelled equilibrium state.

5.2.1.4 Three-dimensional computational analysis of network architecture with modulation of thrombin concentration

Composite gels with fluorescently labeled fibrinogen were prepared as described previously, but were polymerized with varying concentrations of thrombin, either 0.1, 1.0, or 10 U/mL. Confocal z-stacks were acquired as previously described (in Chapter 3) using a 63X objective and MATLAB image processing was performed. The custom network analysis script described in Chapter 3 was then additionally utilized to measure the architectural parameters of the microgel networks, as described previously.

5.2.1.5 Cell motility experiments in composite gels with varying thrombin conentrations

Composite gels containing NIH3T3s were polymerized as described previously, but with 0.1, 1.0, or 10 U/mL thrombin. Similarly as outlined in Chapter 4, cells were tracked over the course of 12 hours and migration speed was quantified.

5.2.2 PEG-microgel composite gel formation

First, free radical polymerization of PEG diacrylate (PEGDA) was performed using Igracure 2959. Briefly, PEGDA (Mw = 2500 Da) was dissolved in PBS at a final concentration of 10 wt %. AF488 ULC microgels at a final concentration of $\phi = 0.112$ were added to the PEG mixture, followed by the addition of I2959 at a final concentration of 0.05 wt%. The solution was mixed and pipetted onto a glass bottom dish and polymerized under UV exposure at 10 W/cm^2 for 10 minutes. The microgels within the resulting gel was then imaged using confocal microscopy.

As another example, PEG-4MAL [247] was generously obtained from the García Lab and utilized for composite PEG-ULC microgel composites. In these materials, PEG-4MAL (Mw = 20 kD) was utilized and resuspended in PBS for a final concentration of

4%. AF488 ULC microgels were added at a final concentration of $\phi = 0.112$ in 25 mM HEPES 150 mM NaCl, which would additionally facilitate the addition reaction as HEPES is a nucleophilic buffering reagent. The peptide cysteine reactive peptide crosslinker GDQ was added at a 1.45:1 molar ratio of crosslinking peptide to PEG at physiological pH. Crosslinking was initiated for the formation of a gel and immobilization of microgels within the PEG structure was visualized within a few minutes. For later depletion experiments, PEG-4MAL was resuspended at 100 mg/mL as a stock solution in PBS and added at varying concentrations to microgel suspensions.

5.2.3 Alginate-microgel composite gel formation

5.2.3.1 Alginate source and characterization

Sterile irradiated alginate generously obtained from the Guldberg Lab sourced from FMC Biopolymer (FMC Biopolymer, Sandvika, Norway) with a high G to M ratio was utilized [251, 252]. It was resuspended at a concentration of 5 wt% in alpha-MEM for composite gel formation experiments. Cross-linking of alginate can be achieved through the addition of divalent cations to the polymer in solution, specifically, calcium (and calcium sulfate was used in these studies). AF488 Microgels (ϕ=0.112) were mixed with the alginate solution reaching a final concentration of 1% alginate and a final concentration of 6 mM $CaSO_4$ was added to induce crosslinking.

5.2.3.2 Composite alginate-microgel confocal imaging

Confocal imaging of the 3D alginate composite gels with fluorescently labeled ULC microgels indicated that crosslinking had occurred and microgels were immobilized. In order to determine the mechanism of clustering in alginate, AF488

labeled microgels in HEPES buffer were pipetted on the LSM 700 fluorescent confocal microscope (Carl Zeiss Microscopy, Ltd) for continuous real time imaging with a 60X objective. Alginate alone was added to the solution of microgels at different concentrations to determine if depletion induced pre-clustering was occurring prior to the addition of $CaSO_4$.

5.3 Results

5.3.1 Effect of modulating thrombin concentration on composite gel formation

To determine the mechanism of formation of these microgel assemblies, we performed and imaged polymerization in real-time using fibrinogen (8 mg/mL) and fluorescently labeled ULC microgels (ϕ=0.112) to observe assembly. We observed that the ULC microgels were homogenously dispersed prior to polymerization and were driven to form packed interconnected networks with the addition of thrombin. Representative images at the endpoint of the experiment of the gels formed with different thrombin concentrations are shown in Figure 19.

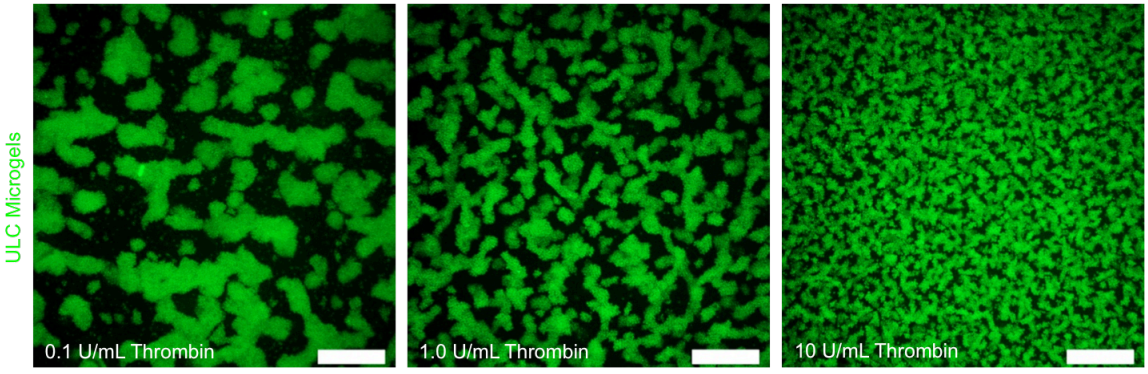

Figure 19: Incorporation of fluorecently labeled microgels (ϕ=0.112) in fibrin 8 mg/mL polymerized with varying concentrations of thrombin. Maximum intensity

projections of fibrin gels with AF488 ULC microgels polymerized with either 0.1, 1.0, or 10 U/mL thrombin.

When polymerizing a fibrin gel, it is known that changing thrombin concentration affects the polymerization rate [72, 81] and thus changes the gel point of the material. This was confirmed in Figure 20, where it is shown that increasing thrombin concentration decreases the time for G' to overcome G", the transition point for the material where it becomes more solid-like than fluid-like.

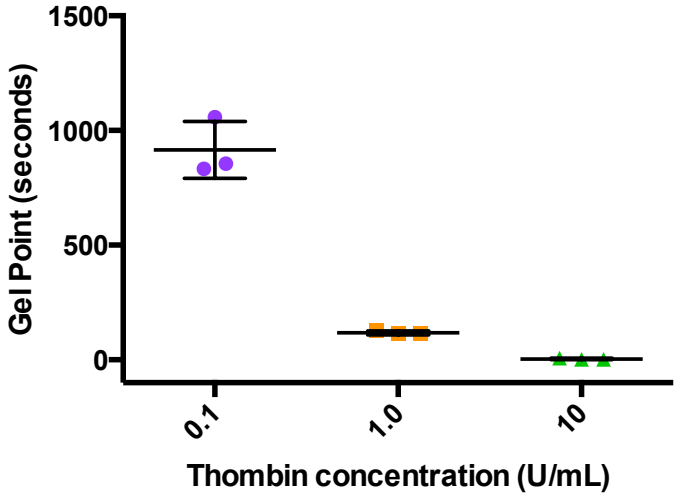

Figure 20: Rheological measurement of gel point of hybrid fibrin-microgel constructs with varying concentrations of thrombin. G',G" of polymerizing gels was measured immediately after the addition of thrombin every second at 0.5% strain. Gel point was calculated as the time (seconds) at which G' became > G".

Analysis (similar as described in Chapter 3) of composite networks formed with fluorescently labeled fibrinogen 8 mg/mL and ULC microgels (ϕ=0.112) at various thrombin concentrations allowed for determination of the average network radius and

volume percent of the main connected volume. It was observed that the average radius of these domains could be modulated through changing thrombin concentration (Figure 21A) while the connectivity is maintained (Figure 21B).

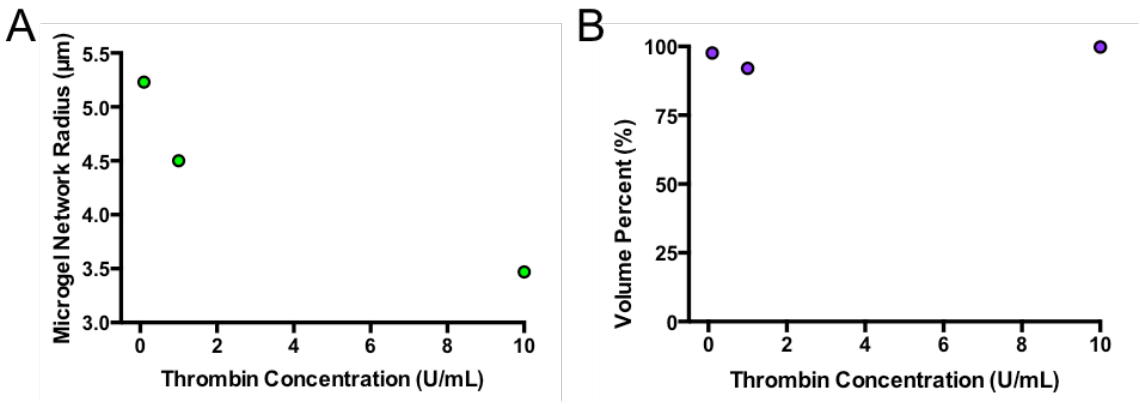

Figure 21: Network analysis of 3D hybrid fibrin-microgel networks polymerized with varying concentrations of thrombin. Confocal z-stacks of gels polymerized with fluorescently labeled fibrinogen were analyzed. A) Demonstrates the change in average microgel network radius with increasing thrombin concentration. B) Shows the volume percent of the main connected volume for increasing thrombin concentrations.

Details of the network analysis data for representative composite gels (fibrin 8 mg/mL + ULC microgels ϕ=0.112) formed at various thrombin concentrations (0.1, 1.0, and 10 U/mL) is outlined in Tables 7-9. ‘

Table 7: Network analysis results for thrombin modulation of fibrin 8 mg/mL with ULC ϕ=0.112 and 0.1 U/mL thrombin.

Connected Volumes	Average Radius (μm)	Volume Percent (%)	Arc Length (mm)	Branches per Volume (#)
1	5.23	0.976	1.327	82
2	4.36	0.013	0.029	2
3	3.94	0.003	0.007	1
4	1.23	0.002	0.008	1
5	4.92	0.001	0.004	1
+ 5 more				

Table 8: Network analysis results for thrombin modulation of fibrin 8 mg/mL with ULC ϕ=0.112 and 1.0 U/mL thrombin.

Connected Volumes	Average Radius (μm)	Volume Percent (%)	Arc Length (mm)	Branches per Volume (#)
1	4.5	0.916	1.2320	77
2	3.41	0.017	0.0344	1
3	5.16	0.013	0.0329	3
4	4.1	0.010	0.0114	1
5	4.02	0.009	0.0121	1
+ 12 others				

Table 9: Network analysis results for thrombin modulation of fibrin 8 mg/mL with ULC ϕ=0.112 and 10 U/mL thrombin.

Connected Volumes	Average Radius (μm)	Volume Percent (%)	Arc Length (mm)	Branches per Volume (#)
1	3.47	0.9983	2.4	187
2	3.2	0.0008	0.0037	1
3	6.23	0.0005	0.0082	2
4	5.18	0.0004	0.0023	1

It is observed that the percent volume occupied by the main connected volume is consistently > 90% indicating that all formulations form interconnected microgel networks. Additionally, the average radius for the main detected volume of each condition (0.1, 1.0, 10 U/mL thrombin) decreases from 5.23 μm to 4.5 μm to 3.47 μm, respectively. Because lower thrombin concentrations resulted in the formation of larger clustered microgel assemblies, the data suggest that the assembly results from the polymerization dynamics. The polymerizing fibrin represents multiple growing and branching rigid rod-like structures, which drive the microgels into confined domains/percolating networks. The particles are being forced into a smaller volume as fibrin is formed. The microgels then adopt a structure within the composite, which is dictated by concentration and the strength/length scale of the particle-particle repulsive forces.

5.3.2 Effect of fibrin-microgel network architecture on cell motility

Migration speed was analyzed as described previously and results from fibrin 8 mg/mL gels with ULC microgels ϕ=0.112 polymerized with either 0.1, 1.0, or 10 U/mL thrombin. In the 0.1 U/mL thrombin group, slow polymerization of the hybrid gels resulted in settling of cells to the gel-culture dish interface, and thus these materials could not be analyzed. Results from 1.0 and 10 U/mL thrombin samples are displayed below in Figure 22.

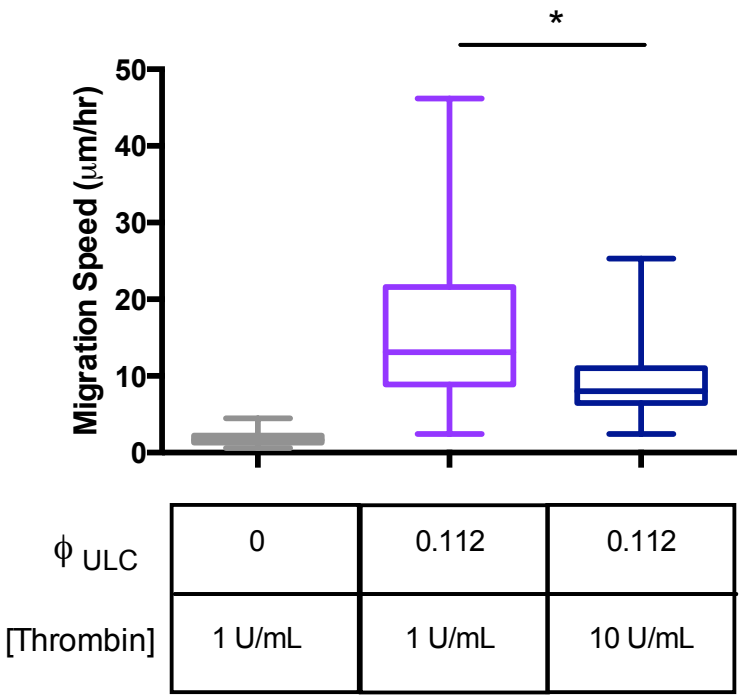

Figure 22: Comparison of migration speed of NIH3T3s in hybrid fibrin-microgel networks polymerized with varying concentrations of thrombin. Averge migration speed per cell is shown for fibrin 8 mg/mL only, or fibrin 8 mg/mL with ϕ=0.112 ULC microgels polymerized with 1.0 U/mL thrombin (n=4 independent experiments), or fibrin 8 mg/mL with ϕ=0.112 ULC microgels polymerized with 10

U/mL thrombin (n=1 independent experiment). Points represent average migration speed calculated from the instantaneous speed of a cell over the course of the 12 hour experiment and data is represented box and whiskers plots, which extend from the 25th to 75th percentiles with a line at the median and error bars to the minimum and maximum values. A Kruskal-Wallis non-parametric test with Dunn's multiple comparisons post-test was used. Both microgel containing groups had average migration speeds statistically significantly greater than the fibrin along group ($p<0.0001$) and the 10 U/mL thrombin sample was significantly less than the 1.0 U/mL thrombin ($*p<0.05$).

When cell motility was analyzed in these composite systems with different architectures, cells in the ULC microgel groups polymerized with 1.0 U/mL thrombin displayed significantly higher average migration speeds compared to cells polymerized in 10 U/mL thrombin, with average speeds of 15.82 μm/hr and 9.09 μm/hr respectively. Thus, these results suggest that microgel network average radius may be an important factor in enabling enhanced cell motility in these hybrid fibrin-microgel constructs.

5.3.3 Depletion induced pre-clustering of microgels in alginate solutions

The route towards generating these hybrid materials is not limited to exploiting the polymerization dynamics of fibrin. Similar materials were generated by inducing microgel-cluster formation via depletion interactions, i.e. attractive forces between microgels due to osmotic pressure induced by local depletants [253], specifically in alginate (Figure 23). A solution of the anionic polysaccharide alginate was mixed with a ϕ=0.112 ULC microgel solution, and prior to gelation (Figure 23 C-E), effects of

depletion were observed, i.e. clustering of microgels induced from local alginate polysaccharide chains. Alginate concentration was decreased incrementally (from 1% to 0.5%) and at significantly low concentrations (0.1%, Figure 23F), depletion was no longer observed — microgels remained homogenously dispersed.

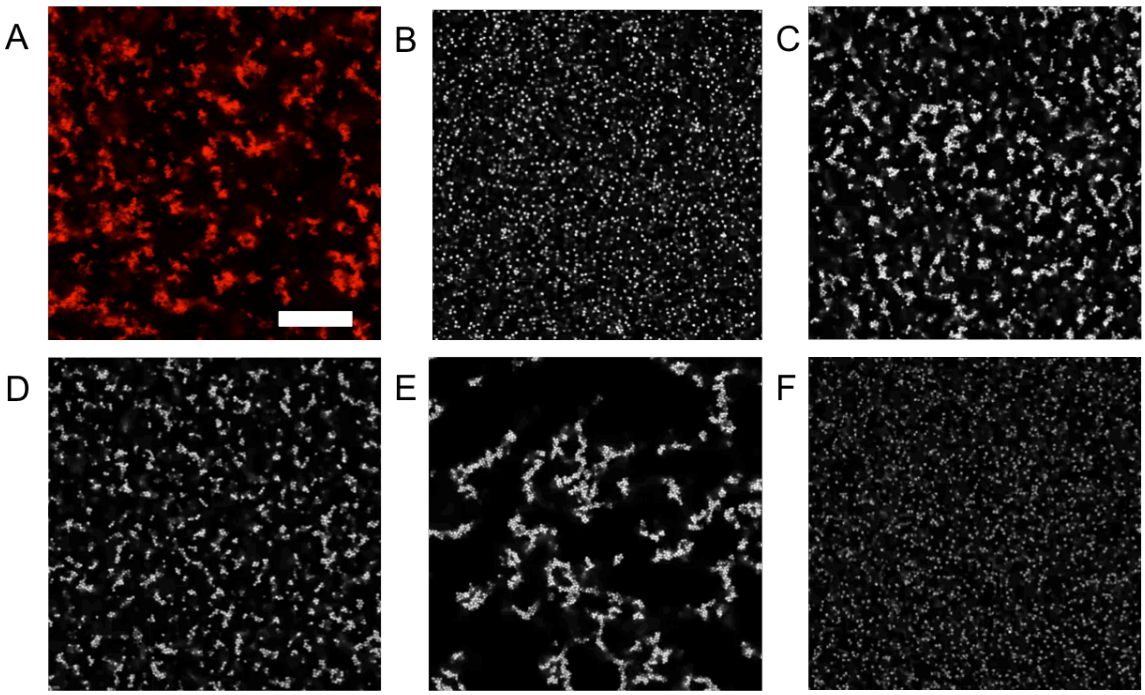

Figure 23: Clustering of microgels within alginate-microgel hybrid constructs. Confocal slices of composite gels with ULC microgels (ϕ=0.112), scale bar 20 μm. A) Ca^{2+} crosslinked alginate with ULC microgels. B) ULC microgels (ϕ=0.112) in buffer prior to the adition of alginate. C) Pre-clustering of ULC microgels (ϕ=0.112) with 1% alginate added to the solution. D) Pre-clustering of ULC microgels (ϕ=0.112) with 0.5% alginate added to the solution. E) Time-evolved pre-clustering of ULC microgels (ϕ=0.112) with 0.5% alginate added to the solution after 15 minutes. F) ULC microgels (ϕ=0.112) with 0.1% alginate added to the solution.

Thus, when microgels were mixed with high molecular weight alginate solutions, pre-clusters of microgels formed that could later be immobilized upon initiation ionic crosslinking of the network with the addition of Ca^{2+} (Crosslinked gel shown in Figure 23A). Additionally, clusters of microgels were observed to grow over time (Figure 23E), thus these structures could be tuned through changing the time at which the network is crosslinked with the addition of divalent cations.

5.3.4 PEG-microgel composite materials and interactions

Results from the confocal image slices and stacks of hybrid PEGDA and PEG-4MAL gels (4% PEG final weight percent) with ULC microgels (ϕ=0.112) displayed in Figure 24 demonstrate no microgel clustering.

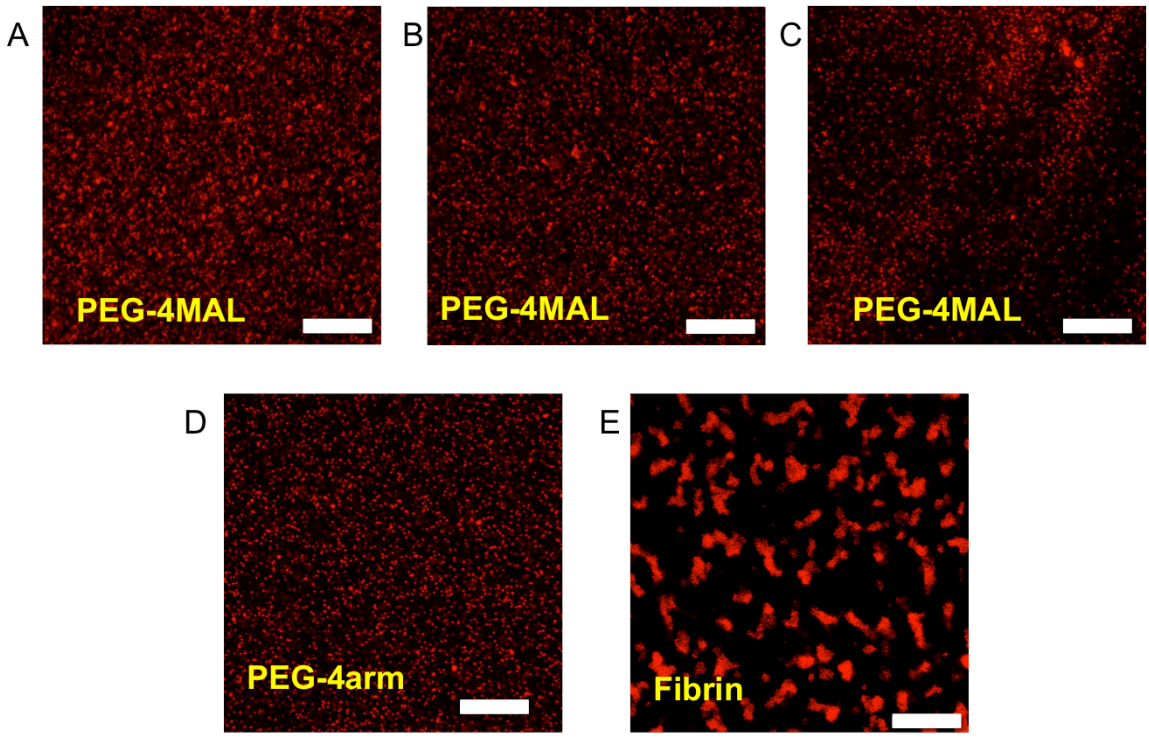

Figure 24: Imaging of microgels within crosslinked PEG-microgel hybrid constructs. Confocal slices of composite gels with ULC microgels (ϕ=0.112), scale

bar 20 µm. A) PEG-4MAL GDQ crosslinked gels formed with CLP in pH 3 HEPES buffer. B) PEG-4MAL GDQ crosslinked gels formed with CLP in pH 5 HEPES buffer. C) PEG-4MAL GDQ crosslinked gels formed with CLP in pH 7.4 HEPES buffer. D) PEGDA gel with microgels formed via UV free radical polymerization initiated by Igracure 2959 exposed to UV for 10 minutes. E) Fibrin 8 mg/mL gel with clustered microgels, for comparison.

Microgels remain homogenously dispersed throughout the gel solution throughout the duration of the experiment (both prior to gelation and after addition of the crosslinking peptide). As it was expected that the presence of PEG may induce a depletion attraction, the experiment was repeated without the addition of the cross-linking peptide and microgels were mixed with PEG and imaged (Figure 25).

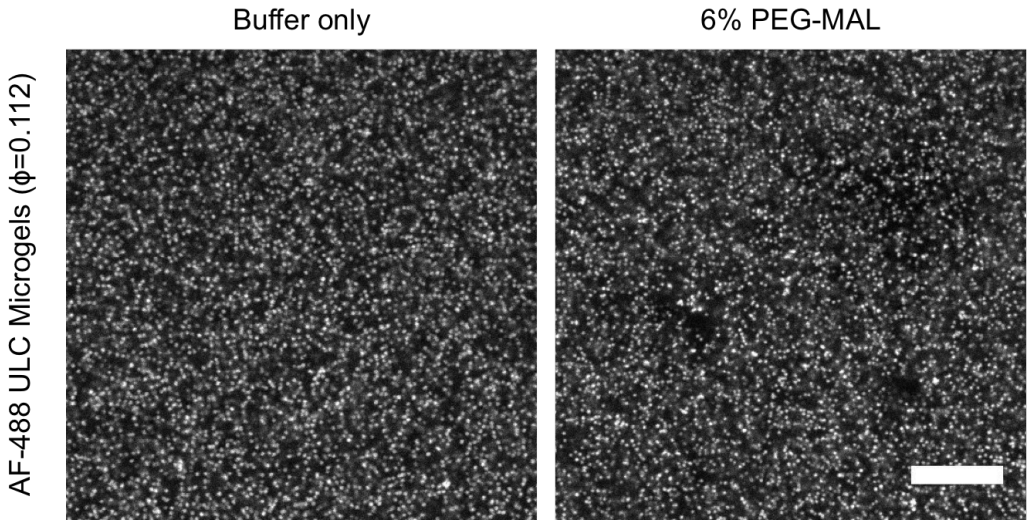

Figure 25: Imaging of microgels within PEG-microgel hybrid suspensions. Confocal slices of solutions of ULC microgels (ϕ=0.112) A) in buffer or B) in a 6% solution of PEG-MAL, scale bar 20 µm. Images (videos) were acquired after the solutions had been allowed to sit and equilibrate for 1 hour.

After the samples had equilibrated for an hour, there were still no indications of depletion in the group that contained 6% PEG-4MAL added to the solution. However, when time-lapse images were acquired of the sample, compared to the microgels only in buffer, it was apparent that the PEG was in fact slowing diffusion/Brownian motion of the particles.

5.4 Discussion

This work demonstrated microgel network formation in fibrin is governed by fibrin polymerization rate. If polymerization is fast, the microgels do not have time to rearrange and the resultant average radius of the structures is small, while if slow, the microgels can gradually be driven together forming larger structures. As a result, the mechanism of microgel domain assembly is governed by the polymerization dynamics of fibrin and allows for tunability of network architecture for a given application. When cell motility was analyzed in these composite systems with different architectures (but identical fibrin and microgel concentration), there were no significant differences in migration speed. However, due to the slow polymerization rate of the 0.1 U/mL thrombin hybrid gels, cells would settle to the gel-culture dish interface and thus these materials could not be analyzed. It was found that fibrin 8 mg/mL gels with ULC microgels (ϕ=0.112) polymerized with 1.0 U/mL thrombin displayed significantly greater average migration speeds compared to a 10 U/mL thrombin sample. This is likely because the microgel networks formed at higher thrombin concentrations have smaller network diameters (3.47 μm compared to 4.5 μm) and thus require more matrix degradation prior to cell motility.

While alginate was able to support the formation of microgel networks, the attempts to form them within PEG failed. For undetermined reasons, it appears that depletion does not occur in the PEG system, yet one may expect this to occur based on the physical principles of the phenomena. However, PEG is a relatively uncharged molecule while alginate is highly anionic. Perhaps there is additional swelling of alginate in salt solutions compared to PEG where the effective volume fraction of alginate is in the end, much larger than for the PEG. When simply mixing PEG-4MAL and microgels, it was observed however that the diffusion and thermal fluctuations of ULC microgels (ϕ=0.112) in buffer solutions was greater than in solutions with increasing concentrations of PEG-4MAL. Thus, PEG may hinder diffusion and serve as a molecular crowder, yet the osmotic pressure is not quite high enough to drive the formation of clustered microgel domains.

Overall, these results demonstrate the ability of microgel networks to form in other materials, such as alginate. Thus one could view these findings to suggest a paradigm shift in the way that composite ECM mimetic materials are designed. In the future of this project, more work could be done to test other ECM mimicking biomaterials that may allow for interconnected microgel network formation. However, in order to recapitulate the native ECM using synthetic engineering strategies, colloids provide a unique opportunity provide alterations to the bulk gel structure within dense materials [171].

CHAPTER 6 DETERMINE THE POTENTIAL OF HYBRID FIBRIN-MICROGEL CONSTRUCTS TO ENHANCE CELL INFILTRATION USING IN VIVO SYSTEMS

6.1 Introduction

To demonstrate *in vivo* feasibility of this composite gel tissue engineering strategy, the hybrid constructs were tested using a subcutaneous implant model. This animal model is utilized as an initial test of a material for biocompatibility and vascularization. While it may not be wholly applicable for deducing information to apply to a specific disease state, it is a simple surgery that provides a general outlook on the ability of the material to integrate with the host tissue and can also serve to identify the potential problems with the foreign body reaction [109]. Many others have utilized subcutaneous implants to assess vascularization in engineered materials [223, 254-256]. However, for concerns that growth factor mediated angiogenic cues would overwhelm the potential differences, and knowing that fibrin degradation products are pro-angiogenic, fibrin alone and fibrin-microgel constructs were tested in this model. The hypothesis for this aim was that the presence of microgels would enhance angiogenesis and vascularization due to the ability of microgels to enhance migration. After four weeks, to quantify vascularization of the implant, micro-CT and lectin perfusions were performed in order to label vasculature within the embedded tissues. Cell infiltration was also quantified through histological staining and imaging.

Additionally, to better understand the *in vivo* results, *in vitro* angiogenesis assays were investigated. First, an *ex vivo* microvessel fragment angiogenesis assay was

performed, which has been utilized previously for the testing of engineered fibrin matrices [7]. *In vitro* sprouting and neovessel formation of primary multicellular vessel fragments has been extensively studied [7, 211-217, 257-259]. Upon primary isolation and digestion from the tissue, these fragments comprised of endothelial cells, pericytes, and red blood cells have been shown to growth and form interconnected tubule networks, which can then anastomose with host vasculature when implanted *in vivo*. Thus, this assay represents a more complex angiogenesis model system to study these processes.

To investigate the process of angiogenesis at an even more simplified level, human umbilical vein endothelial cells were cultured on collagen coated microbeads [260] embedded within the fibrin-microgel hybrid constructs to observe sprouting of single cell type structures. Through the collection of these experiments, the angiogenic potential of these hybrid constructs was measured and quantified.

6.2 Materials and methods

6.2.1 Rat subcutaneous implant model

6.2.1.1 Electrospinning PCL nanofiber mesh scaffolds

In order to create the poly(caprolactone) (PCL) nanofiber meshes, 12% w/v PCL was dissolved in a 90:10 mixture of HFP:DMF (1,1,1,3,3,3-Hexafluoro-2-propanol : *N,N*-Dimethylformamide). After overnight dissolution, 5 mL of the solution was loaded into a 10mL syringe and placed on a syringe pump facing the copper collecting surface connected to a voltage supply. The positive wire from the voltage supply was wrapped around the needle on the end of the syringe containing the polymer solution. Polymer was infused at 0.75 mL/hr and the voltage source was turned on (10-15 kV) after a few

minutes to ensure initial polymer flow out of the syringe and stable Taylor cone formation. Electrospun polymer was generated on aluminum sheets taped to the copper coated collecting surface over the course of five hours. Sheets of electrospun polymer were then laser cut into rectangular meshes with 1 mm diameter cut out holes. Rectangular meshes are then formed into 12 mm x 5 mm diameter cylinders using UV curable glue. Meshes were sterilized in 100% absolute ethanol overnight and stored in PBS until use.

6.2.1.2 Pre-forming polymerized fibrin gels in scaffolds

Fibrin gels of the various groups (8 mg/mL fibrin, 8 mg/mL fibrin + ULC microgels ϕ=0.112, 25 mg/mL fibrin, 25 mg/mL fibrin + ULC microgels ϕ=0.112, and 2.5 mg/mL fibrin) were formed as previously described, but filled within the PCL nanofiber meshes that were placed in 96 well plates. After 1 hour of polymerization, constructs were then removed and surgically implanted into the rats. Containment of the hydrogels within the PCL tubes allowed for convenient determination of scaffold location at the end of the study. For the lectin perfusion groups, the microgel containing constructs contained ϕ=0.112 of AF647 ULC microgels.

6.2.1.3 Implantation surgical procedure

In order to test vascularization potential of the composite gels, male Sprague Dawley rats (n=8-10 Micro-Fil perfusion, n=3 lectin perfusion) approximately 8 weeks of age underwent a subcutaneous implant procedure (Harlan, Tampa, FL). Two 2 cm incisions were made on the dorsal side of the rat, and two pockets in the subcutaneous space were made lateral to the incision sites by blunt dissection. The constructs were inserted into the subcutaneous pockets away from the incision site, and incisions were

closed with sutures and wound clips. Aseptic procedures were followed throughout the surgery, and the Georgia Institute of Technology Institute Animal Care and Use Committee approved all procedures.

6.2.1.4 Perfusion and tissue harvesting

After four weeks, the vasculature was cleared with 0.9% saline containing 0.4% papaverine hydrochloride (Sigma-Aldrich), perfusion fixed with 10% neutral buffered formalin, rinsed again with 0.9% saline. For the Micro-Fil perfusion (n=8-10 per group), 15-25 mL of lead chromate-based radiopaque contrast agent (Microfil MV-122, FlowTech) prepared according to manufacturer's instructions with a 2:1 dilution of contrast agent with diluent was injected with a syringe [261, 262]. Samples were stored at 4° C overnight for polymerization of the contrast agent after which constructs were excised from the animal and fixed for three hours in 10% formalin. Constructs were then transferred into 30% sucrose solutions in PBS for two days and stored at 4° C. Next samples were OCT vacuum-embedded for one hour periods in various ratios of 30% sucrose to OCT (1:0, 4:1, 3:1, 2:1, 1:1, 1:2, 0:1). Once the sample was in 100% OCT it was left to vacuum-embed overnight and then was moved into the -80° C freezer for storage.

For the lectin perfusion, the animals (n=3 per group excluding 2.5 mg/mL fibrin) were injected with either 10mL lectin dye at 0.1 mg/mL (DyLight 488 Lycopersicon Escuentum (Tomato) Lectin, Vector Laboratories), which incubated in the vasculature for 10 minutes to allow for adequate staining. Post-perfusion, explants were harvested and fixed in 10% neutral buffered formalin overnight, switched into PBS, and sectioned for imaging.

6.2.2 Micro-CT angiography

Tissue explants were placed into a sample holder within the Micro-CT 40 (Scanco Medical) machine and imaged in batch scans with medium resolution (12 micron voxel size (isotropic/cube elements), X-ray source and detector: energy = 55 kVp, intensity = 145 μA, 250 ms integration time, pixel matrix 1024x1024). Scans were contoured and evaluated with a sigma of 1.2 and a Gaussian blur of 1.0 at a threshold value set at 85 for all of the samples (which was found to most accurately capture vessels without artificially enlarging them). Data was acquired and analyzed in a blinded fashion. Evaluations of the 3D vessel structure were performed in three different ways: contouring the volume and analyzing the entire construct, contouring the volume and analyzing the middle portion of the construct by cutting 25% off the each end of the cylinder (thus eliminating potential variability in the vascularization of the ends of the constructs), and contouring the volume but shrinking the contour radially by 10% (thus eliminating variability in whether or not the contours potentially contain tissue on the outside of the PCL mesh).

6.2.3 Cell infiltration histological analysis

6.2.3.1 H&E staining of frozen tissue sections

Tissue explants were frozen in OCT in blocks that were then cut into 7 μm sections on the CryoStar cryostat. OCT did not adequately infiltrate the constructs, especially the high fibrin concentration groups, thus some sections were cut onto cryostat sectioning tape. These tape sections were then stained rinsed with water, and stained with hematoxylin and eosin, cleared with 100% absolute ethanol, and mounted to plastic slides still in contact with the tape using a UV curable mounting media.

6.2.3.2 Quantification of cell infiltration distance in subcutaneous implants

Images of H&E stained slides were imaged on a Nikon E600 light microscope (Nikon; Tokyo, Japan) using the 2X or 4X objective and color camera. For quantitative measurements, entire longitudinal cross sections of the tissue were imaged with a 10X (Plan-Apochromat NA 0.25) objective for magnification with a Nikon TiE microscope (Nikon; Tokyo, Japan) and CoolSNAP HQ2 monochromatic CCD camera (Photometrics; Tucson, AZ) with an automated stage to perform tile scanning at stitching of 10X images to form a larger composite image. Cell infiltration distance was quantified in a blinded fashion for each image from 3 locations on both the ends of the construct (top and bottom of the cylinder) and both of the sides (cell infiltrate through the pores/holes in the PCL mesh). Distances were averaged per construct and 3-4 slices (from different implants) were pooled.

6.2.4 Analysis of lectin perfusion of smaller diameter vessels

The 12 mm explanted tissue was sectioned into 6 cross-sections each 2 mm thick. Cross-sections were placed on glass coverslips and volumes of the whole tissue area were tile scanned. Using a LSM 700 series fluorescent confocal microscope (Carl Zeiss Microscopy Ltd) with a 10X objective (EC Plan-Neofluar NA 0.3), image stacks (200um) were acquired 2 mm from each end of the PCL mesh/gel border. Images are represented as maximum intensity projections from the same regions within the gels for each condition. Dotted lines represent the region within the interior of the PCL nanofiber mesh and squares illustrate the region of interest that is magnified.

6.2.5 Microvessel fragment angiogenesis assay

6.2.5.1 Microvessel fragment isolation and culture

Epididymal adipose tissue of male Sprague Dawley rats was collected under anesthesia and processed by mincing, followed by limited digestion with collagenase (Worthington Biochemicals, Lakewood, NJ), and sequential filtration through a 500 μm and a 70 μm mesh to remove large tissue debris and smaller fragments and single cells, as previously described in the literature [7, 211-217, 257-259]. MVFs were suspended at a concentration of 20,000 fragments/mL, in the fibrinogen solutions (+/- ULC microgels), and immediately mixed with appropriate volumes of thrombin, cast into a 3D gel, and polymerized for 1 hour prior to addition of MVF media. Microvessel fragments were cultured in 50% DMEM and 50% F10 media supplemented with VEGF, PDGF, micronutrients, and penicillin-streptomycin. Media was changed the day after gel formation, and every other day subsequently. After 10 days in culture, samples were be fixed in 4% formaldehyde, permeabilized with 0.2% Triton X-100, blocked in 5% non-fat milk in PBS with 1% BSA, and stained with FITC-GSL-1 (Vector Laboratories) for cellular visualization. Neovessel sprouts from the parent fragments begin to appear by the 4th day in culture and gradually form an interconnected network at low fibrin concentrations by day 10 [7, 212, 213].

6.2.5.2 Quantifying microvessel sprouting and network formation in composite gels

Confocal 10X tile scans (2560x2560 μm) of 100 μm thick maximum intensity projections of GSL1 stained microvessel networks cultures were obtained and imported into MATLAB. The network analysis software from Chapter 3 was used to analyze various parameters of the 3D networks including total vessel volume, vessel length, and number of branches.

6.2.6 HUVEC sprouting and network formation

6.2.6.1 GFP-HUVEC culture

GFP-HUVECs lentivirally transduced with the CytoLight green plasmid controlled under the CMV promoter were obtained from Essen Bioscience at passage 2. Cells were grown and expanded to passage 5 in EGM-2 media (Clonetics, Lonza).

6.2.6.2 hMSC culture and Human Foreskin Fibroblast (HFF)

Prior to experimentation, Human MSCs (Lonza) were cultured up to passage 6 in DMEM with L-glutamine, sodium pyruvate, 1.0 g/L glucose, 10% FBS, and 1% penicillin-streptomycin. HFF's were cultured in DMEM with L-glutamine, sodium pyruvate, 4.5 g/L glucose, 10% FBS, and 1% penicillin-streptomycin. Upon initiation of the sprouting assay, all cells were cultured in EGM-2.

6.2.7 HUVEC coated bead angiogenesis assay

In this assay, endothelial cells were coated onto microbeads and embedded into a fibrin matrix to measure cell sprouting and growth away from the bead surface [260, 263-266]. Cytodex-3 collagen coated microbeads (GE Life Sciences) were resuspended at 0.5g per 50mL in PBS for three hours. Beads were then allowed to settle, rinsed in PBS three times, and autoclaved for sterilization. GFP-HUVECs were incubated with Cytodex-3 beads for 4 hours (shaking every 20 minutes) in EGM-2 at a concentration of 1 million cells per 2500 beads (which can be counted under a microscope in a 10ul aliquot to determine concentration) in a flow cytometry round bottom tube at 37°C. After coating, beads were transferred into a T-flask with additional media and left overnight in the incubator. The following day, beads were suspended into fibrin gels with and without

microgels at a concentration of approximately 400 beads/mL of gel solution. 25,000 hMSCs/mL of gel were also incorporated into the polymerizing constructs. Gels were polymerized for 20 minutes and HFF's were plated on top of the gels in EGM-2 media at 8,000 cells/mL of gel solution. After 7 days in culture, samples were fixed in 4% formaldehyde for 20 minutes, stored in PBS and imaged with the LSM 700 confocal microscope (with either 10X EC Plan-Neofluar NA/0.3 or 20X Plan Apochromat NA/0.8 M27).

6.2.8 Statistical Analysis

All statistical analyses were performed in GraphPad Prism (GraphPad Software, San Diego, CA). All alpha values were set to 0.05. For samples that did not pass a normality test, data is represented in box and whisker plots, which extends from the 25th to 75th percentiles with a line at the median and error bars to the minimum and maximum values. For micro-CT angiography vascular volume and volume fraction (which were non-normal distributions), a Kruskal-Wallis non-parametric test with Dunn's post-test was performed, *$p<0.05$, **$p<0.01$. For total volume micro-CT analysis, data fit a normal distribution; therefore the data was analyzed using an ordinary one-way ANOVA with Tukey's multiple comparisons test. For cell infiltration, a Kruskal-Wallis non-parametric test with Dunn's post-test was performed. For microvessel sprouting network analysis, a Kruskal-Wallis non-parametric test with Dunn's post-test was performed, *$p<0.05$, **$p<0.01$, ***$p<0.001$, ****$p<0.0001$.

6.3 Results

6.3.1 Micro-CT angiography

All methods of quantification of the micro-CT evaluations resulted in similar trends show in Figure 26, where results from the full construct are in panel A, middle half are in panel B, and 10% radial reduction are in panel C. Quantitative outputs including vascular volume, total volume, and vascular volume fraction were obtained. Because the constructs likely change shape while in vivo (due to degradation or mechanical insult from the rats skin), the main parameter of interest is vascular volume fraction, which accounts for slight differences in construct volume. However, no significant differences were found in vascular volume fraction or vascular volume between any of the groups except with the 2.5 mg/mL fibrin physiological control, which had increased vascularization compared with the other groups. There were no significant differences in total volume of the constructs across all groups tested.

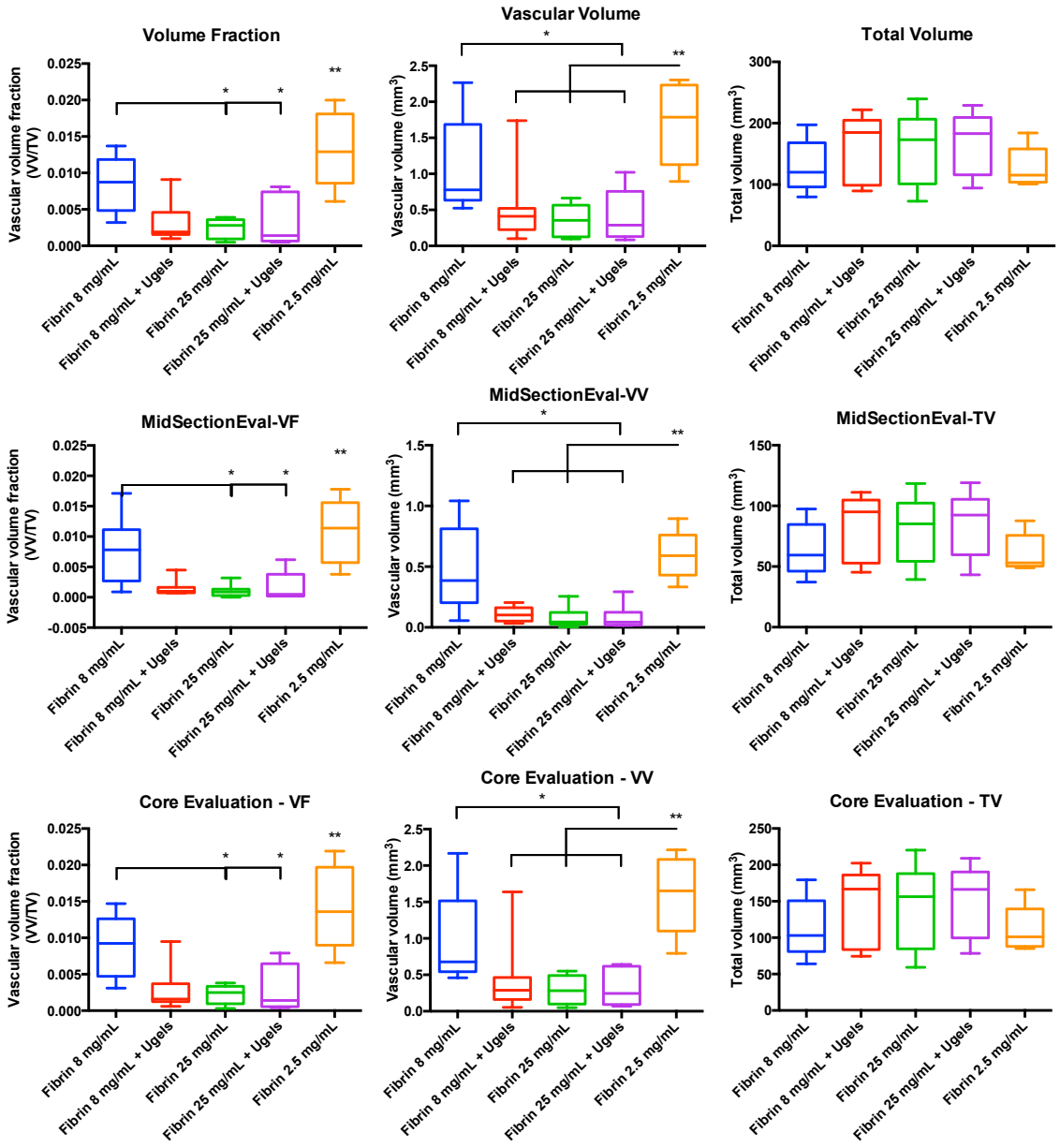

Figure 26: Micro-CT angiography of 4 week in vivo vascularization of hybrid fibrin-microgel constructs. A) Quantification of volume fraction, vascular volume, and total volume from the analysis of the entire contoured construct. B) Quantification of volume fraction, vascular volume, and total volume from the analysis of the middle section (25% off of each end lengthwise removed) of the contoured construct. C) Quantification of volume fraction (VF), vascular volume (VV) , and

total volume (TV) from the analysis of the entire length of the construct with the contour diameter reduced by 10% radially. Box and whiskers plot extends from the 25th to 75th percentiles with a line at the median and error bars to the minimum and maximum values, n=7-10 independent gels from separate animals; For VV & VF, Kruskal-Wallis non-parametric test with Dunn's post-test was performed, *p<0.05, **p<0.01. For TV analysis, data fit a normal distribution, but no significant differences were detected using an ordinary one-way ANOVA with Tukey's multiple comparisons test.

Representative angiograms from each group can be seen in Figure 27 below. Qualitatively, no striking differences were observed between the 8 mg/mL fibrin groups and little vascularization was observed in the 25 mg/mL fibrin groups with and without microgels. Physiological concentrations of fibrin (2.5 mg/mL) displayed robust vascularization that often bridged the implant.

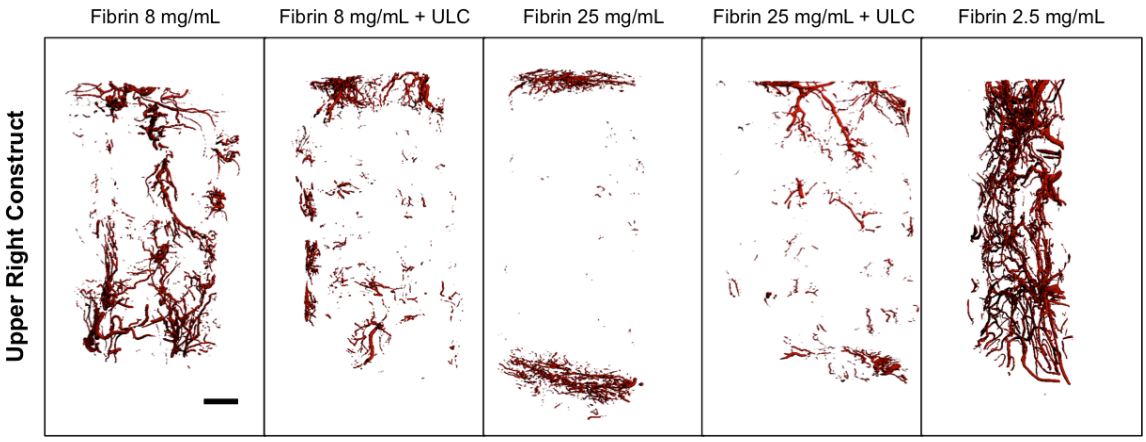

Figure 27: Representative micro-CT angiograms of 4 week in vivo vascularization of hybrid fibrin-microgel constructs. Fibrin only 2.5 mg/mL. B) Fibrin only 8 mg/mL. C) Fibrin 8 mg/mL + ULC microgels (ϕ=0.112). D) Fibrin only 25 mg/mL. E) Fibrin 25 mg/mL + ULC microgels (ϕ=0.112).

When examining angiograms from different animals that were placed at different anatomical locations, a large amount of variability is present within the data. This can be appreciated in Figure 28, which shows 4 different implants from the fibrin 8 mg/mL group with ULC microgels ϕ=0.112. In general, upper constructs tended to display more vascularization compared to constructs implanted on the lower portion of the rat.

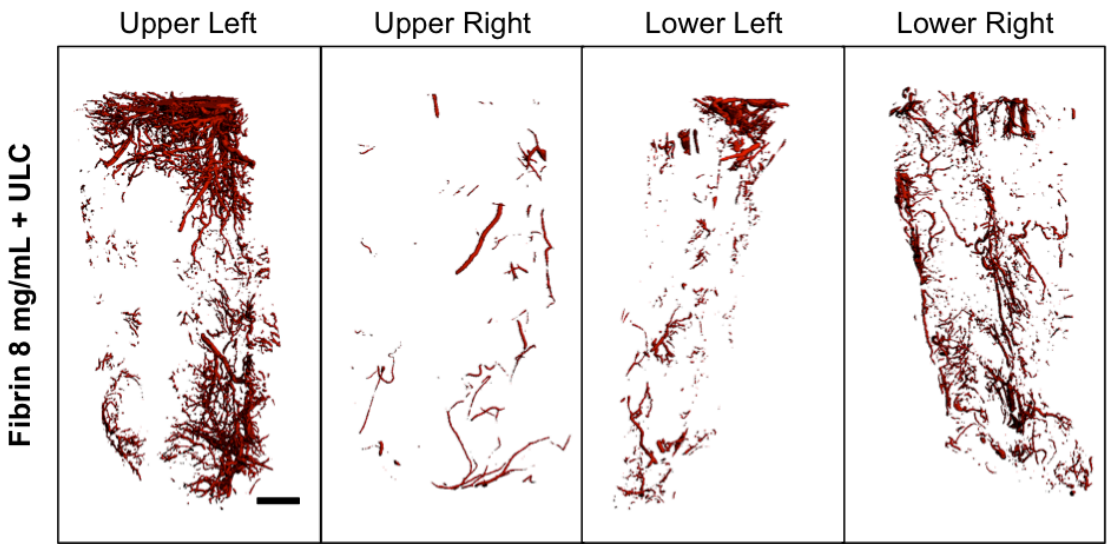

Figure 28: Representative micro-CT angiograms of 4 week in vivo vascularization of fibrin 8 mg/mL + ULC microgels (ϕ=0.112) in different anatomical locations. The variability in A) upper left implanted construct B) upper right implanted construct C) lower left implanted construct and D) lower right implanted construct demonstrate the diversity in the vascularization response of these anatomical locations.

6.3.2 Histological quantification of rat subcutaneous implant model

Representative images of H&E stained sections can be seen in Figure 29. Yellow dotted lines represent the middle of the construct, black dotted lines represent the cell infiltration border, 'P' represents regions where the PCL nanofiber mesh is present, and 'F' represents region where residual fibrin gel is remaining. Fibrin 8 mg/mL groups with and without microgels displayed more robust cell infiltration compared to both 25 mg/mL groups, which was expected.

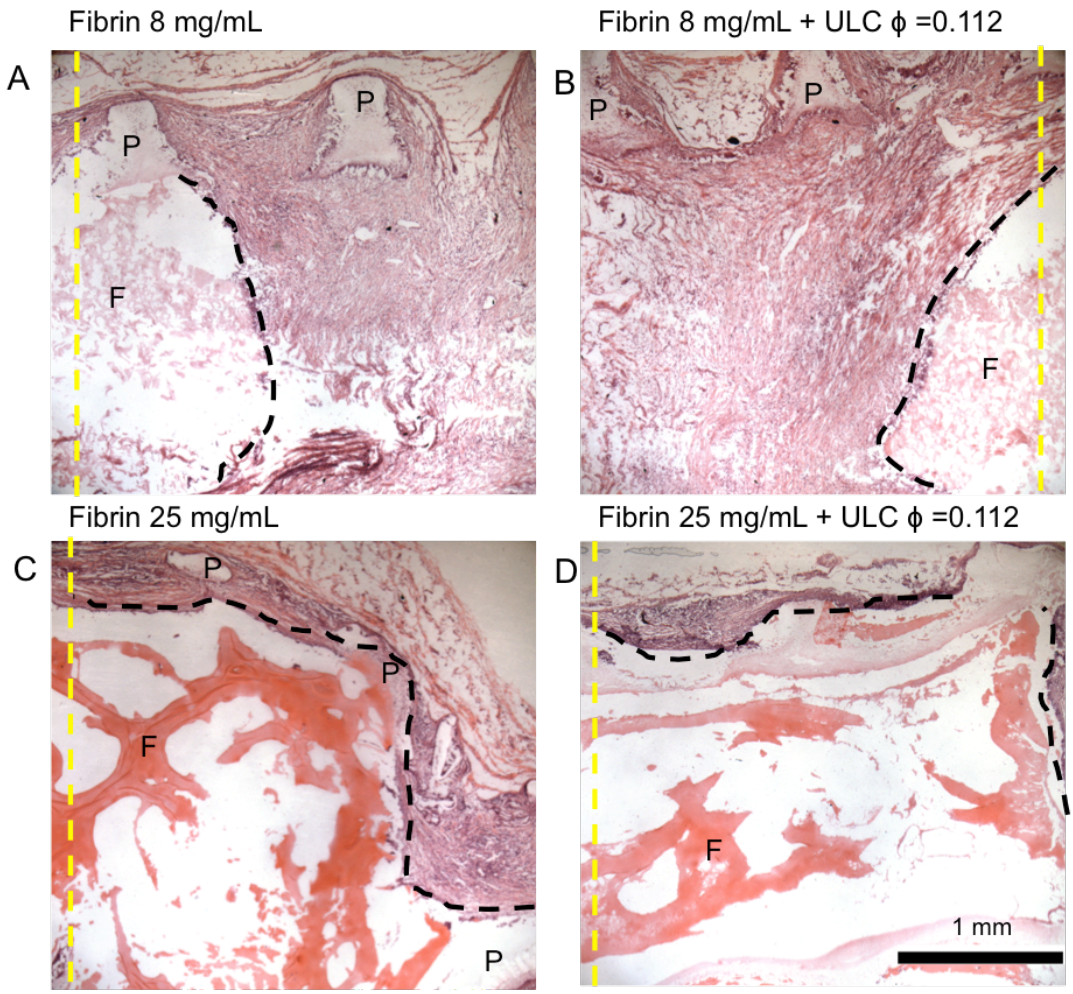

Figure 29: Representative H&E histological sections of 4 week in vivo vascularization of hybrid fibrin-microgel constructs. 2X images of tissue sections were acquired of A) Fibrin 8 mg/mL B) Fibrin 8 mg/mL + ULC microgels ϕ=0.112 C) Fibrin 25 mg/mL D) Fibrin 25 mg/mL + ULC microgels ϕ=0.112. Yellow dotted lines represent the middle of the construct, black dotted lines represent the cell infiltration border, 'P' represents regions where the PCL nanofiber mesh is present, and 'F' represents region where residual fibrin gel is remaining.

From H&E stained sections, cell infiltration distance was measured and results are shown in Figure 30. No significant differences in infiltration distance were found in any of the groups, from either the ends of the cylindrical constructs or through the holes in the PCL mesh on the sides. Most of the 2.5 mg/mL control samples had complete bridging of the infiltrating cells across the entire implant and thus were not included in this analysis (data not shown).

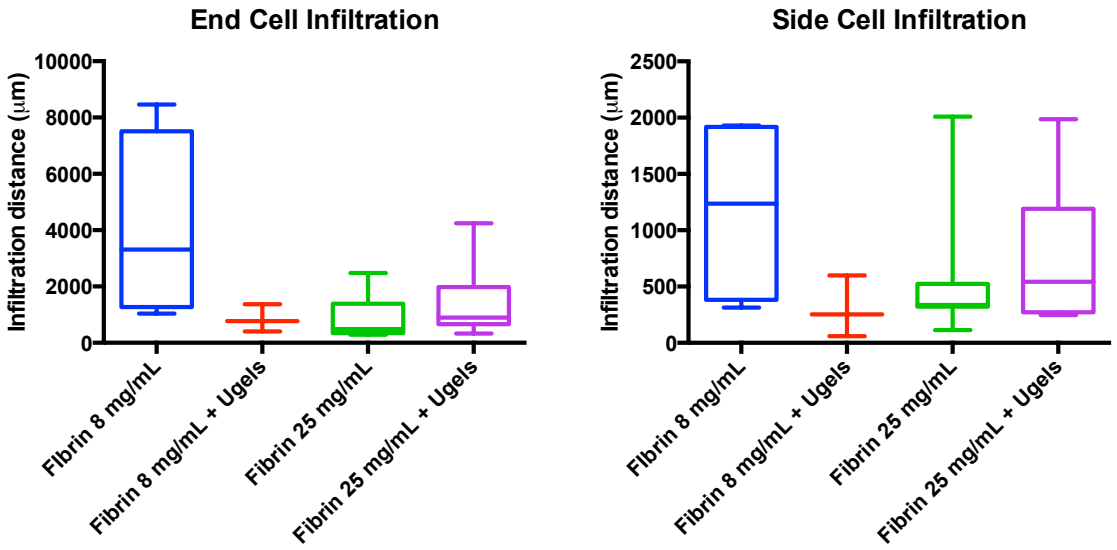

Figure 30: Cell infiltration quantiation from H&E histological sections of 4 week in vivo vascularization of hybrid fibrin-microgel constructs. Tiled 10X images of tissue sections were acquired from Fibrin 8 mg/mL, Fibrin 8 mg/mL + ULC microgels ϕ=0.112, Fibrin 25 mg/mL, Fibrin 25 mg/mL + ULC microgels ϕ=0.112, and Fibrin 2.5 mg/mL. Infiltration distance (μm) was quantified from 3 locations on either side of the construct from A) the sides of the construct (which contained the laser cut holes in the PCL nanofiber mesh, or B) the ends of the cylinder, which contained a larger surface area exposed to the subcutaneous space. Box and whiskers plot

extends from the 25th to 75th percentiles with a line at the median and error bars to the minimum and maximum values, n= 3-7; Kruskal-Wallis non parametric test with Dunn's post-test show no significant differences between any of the groups.

6.3.3 Lectin vessel confocal imaging of explanted tissue from rat subcutaneous implant model

While the micro-CT data allows for robust quantitation of vessel volumes and other parameters, there are some limitations of the system including: 1) the voxel size is more ideal for larger diameter vessels, and 2) the viscosity of the contrast agent (Micro-Fil) can inhibit infiltration of smaller diameter vessels. With these concerns in mind, a small molecule lectin dye was diluted in saline and perfused for visualization of smaller diameter vessels that had infiltrated the constructs. Maximum intensity projections of 200 μm thick sections at each 2 mm section were acquired, and Figure 31 shows representative whole scans (n=3) from each group 2 mm within the construct. No qualitative differences in the lectin perfusion were observed in the 8 mg/mL fibrin constructs with or without microgels. However, little to no infiltrating blood vessels were observed in the 25 mg/mL fibrin groups whereas many small vessels were observed at the 2 mm depth were observed in the 25 mg/mL construct containing microgels. These small vessels ranged from approximately 10-20 μm in diameter. Additionally, microgels were still found within the constructs after 4 weeks and vessels were seen to be growing in areas where microgels were present. Thus, the addition of ULC microgels into fibrin biomaterials made at supraphysiological concentrations enhanced the in growth of native

blood vessels within the biomaterial compared to minimal infiltration a observed in fibrin only control groups at 25 mg/mL.

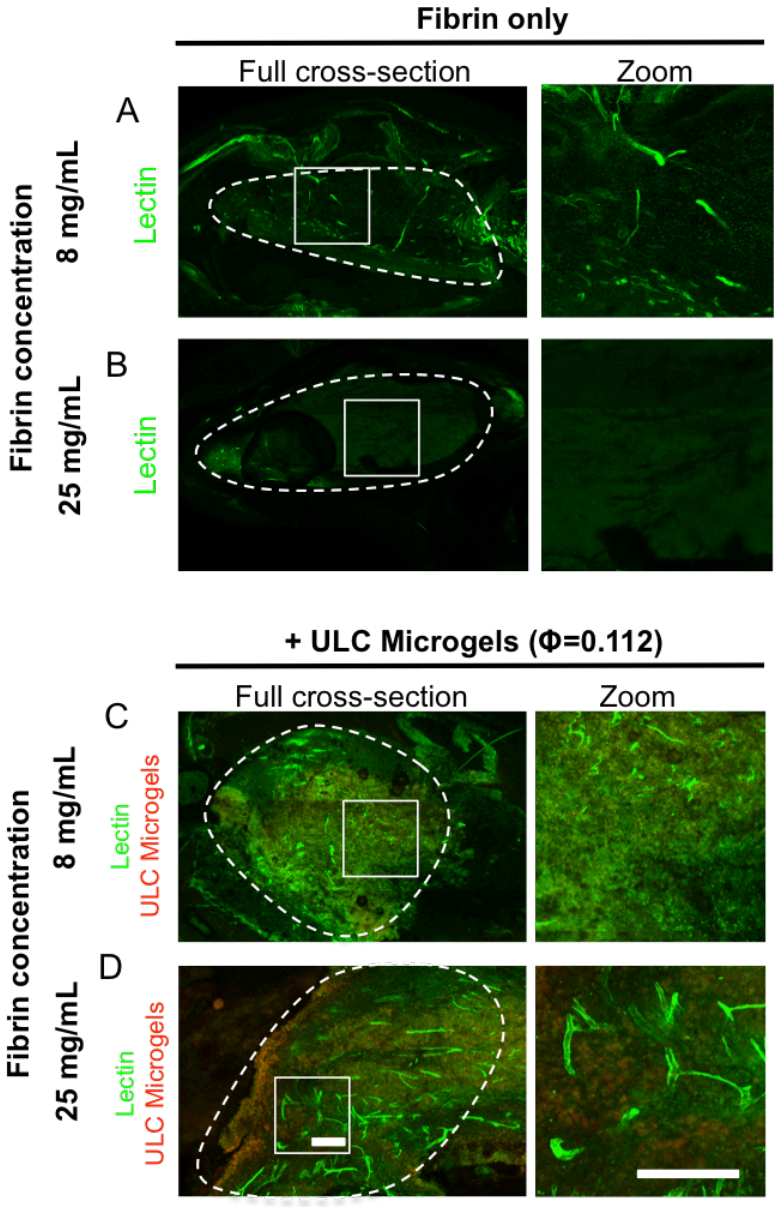

Figure 31: Maximum intensity projections of lectin perfused subcutaneous implants hybrid fibrin-microgel constructs at 4 weeks. Tiled 10X images of 200 µm thick tissue sections were acquired from Fibrin 8 mg/mL, Fibrin 8 mg/mL + AF-647 ULC

microgels ϕ=0.112, Fibrin 25 mg/mL, Fibrin 25 mg/mL + AF-647 ULC microgels ϕ=0.112. (Scale bar 200 µm.)

6.3.4 Microvessel fragment angiogenesis and sprouting quantification

Microvessel fragments were embedded in fibrin gels with and without microgels and a representative day 0 image of the GSL1 lectin stained fragments can be viewed below in Figure 32. Fragments are variable in size, but are multicellular capillary fragments that contain red blood cells, pericytes, and sometimes red blood cells.

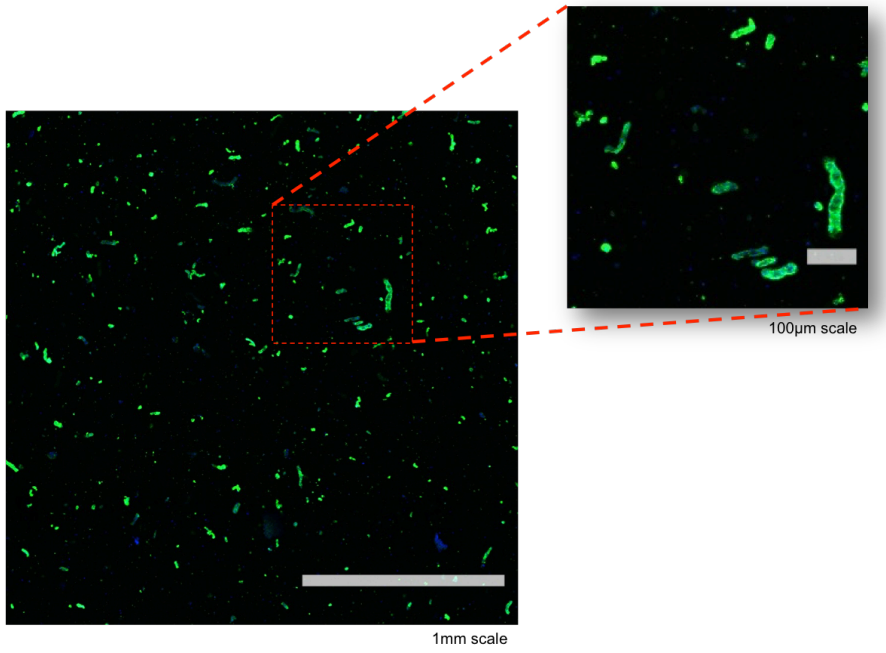

Figure 32: Microvessel fragment morphology on Day 0 immediately after encapsulation in hybrid fibrin-microgel constructs. Tiled 10X images of 100 µm thickness were acquired from lectin stained MVF cultures embedded in Fibrin 8 mg/mL, gel. Scale bar 1 mm on tiled image and 100 µm on zoom in portion.

Robust microvessel networks were formed in the 2.5 mg/mL and 8 mg/mL fibrin, whereas the density of the fibrin at 25 mg/mL prohibited complete network sprouting and connectivity in the gels after 10 days in culture (Figure 33). A zoom in from Figure 33E is shown in panel F of Figure 33 where the multicellular nature, tube-like structure, and size of the microvessel fragment can be appreciated.

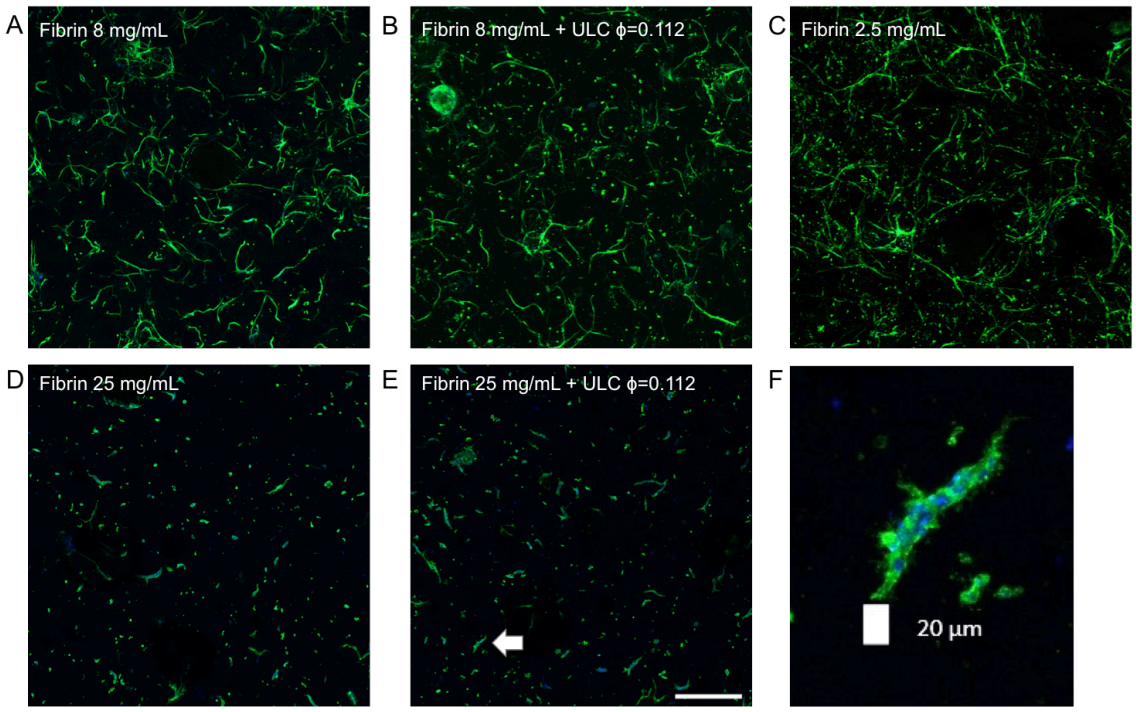

Figure 33: Microvessel fragment sprouting over 10 days in hybrid fibrin-microgel constructs. Tiled 10X images of 150 µm thickness were acquired from lectin stained MVF cultures embedded in A) Fibrin 8 mg/mL, B) Fibrin 8 mg/mL + ULC microgels ϕ=0.112, C) Fibrin 2.5 mg/mL, D) Fibrin 25 mg/mL, E) Fibrin 25 mg/mL + ULC microgels ϕ=0.112, 500 µm scale, F) Zoom in on individual fragment next to arrow in E, 25 mg/mL + ULC microgels ϕ=0.112 sample, 20 µm scale.

Large tile scans (2560 x 2560 μm) from at least four different gels were analyzed in MATLAB using similar methods as described in Chapter 3 for microgel network analysis and vessel arc length, total vessel volume, and number of branches. When quantified, the main differences that were observed were found between the different fibrin concentrations and thus independent of the presence of ULC microgels as shown in Figure 34.

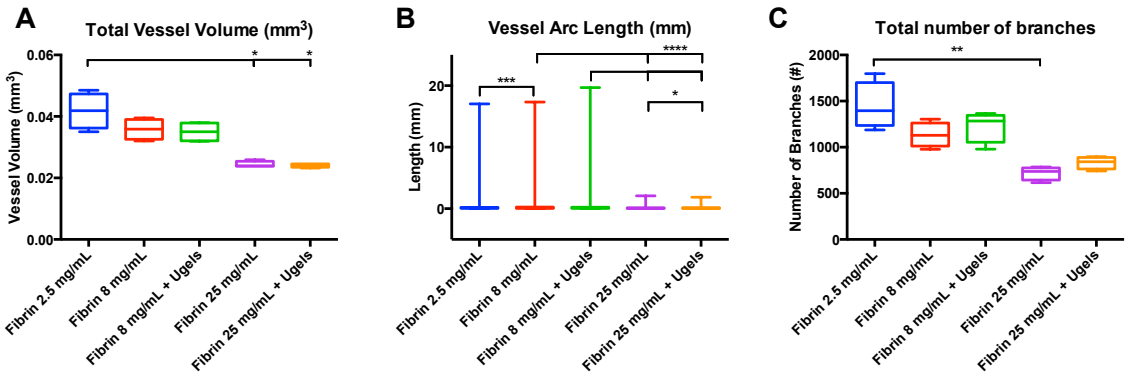

Figure 34: Quantification of microvessel fragment sprouting over 10 days in hybrid fibrin-microgel constructs (ULC microgels ϕ=0.112). A) Quantification of total vessel volume for the various constructs (pooled data from n=4 samples) B) Quantification of total number of branches summed for each sample (n=4) for each group and C) vessel arc length. Box and whiskers plot extends from the 25th to 75th percentiles with a line at the median and error bars to the minimum and maximum values, n=4 independent gels (n=994-1398 vessels/branches analyzed in B); Kruskal-Wallis non-parametric test with Dunn's post-test was performed, *p<0.05, **p<0.01, ***p<0.001, ****p<0.0001.

No differences in the ± microgel groups at the same fibrin concentration were observed in analysis of total vessel volume or number of branches. However, the non-parametric analysis of vessel arc length demonstrated that there were significant differences in vessel arc length between fibrin 25 mg/mL and fibrin 25 mg/mL + ULC microgels ϕ=0.112 (*$p<0.01$). While the differences shown between the 8 mg/mL samples are inconclusive, and the total number of branches and total volumes of the 25 mg/mL samples ± microgels are not significantly different, this data does present potential for microgels to enhance vessel arc length within this *in vitro* angiogenesis model.

6.3.5 GFP-HUVEC coated bead sprouting/angiogenesis qualitative observations

HUVEC coated beads were imaged on the confocal microscope and no qualitative differences were observed between groups with and without ULC microgels after 7 days. While some sprouting was seen at 8 mg/mL fibrin with and without microgels, no significant outgrowths were observed in the 25 mg/mL fibrin samples as shown in Figure 35.

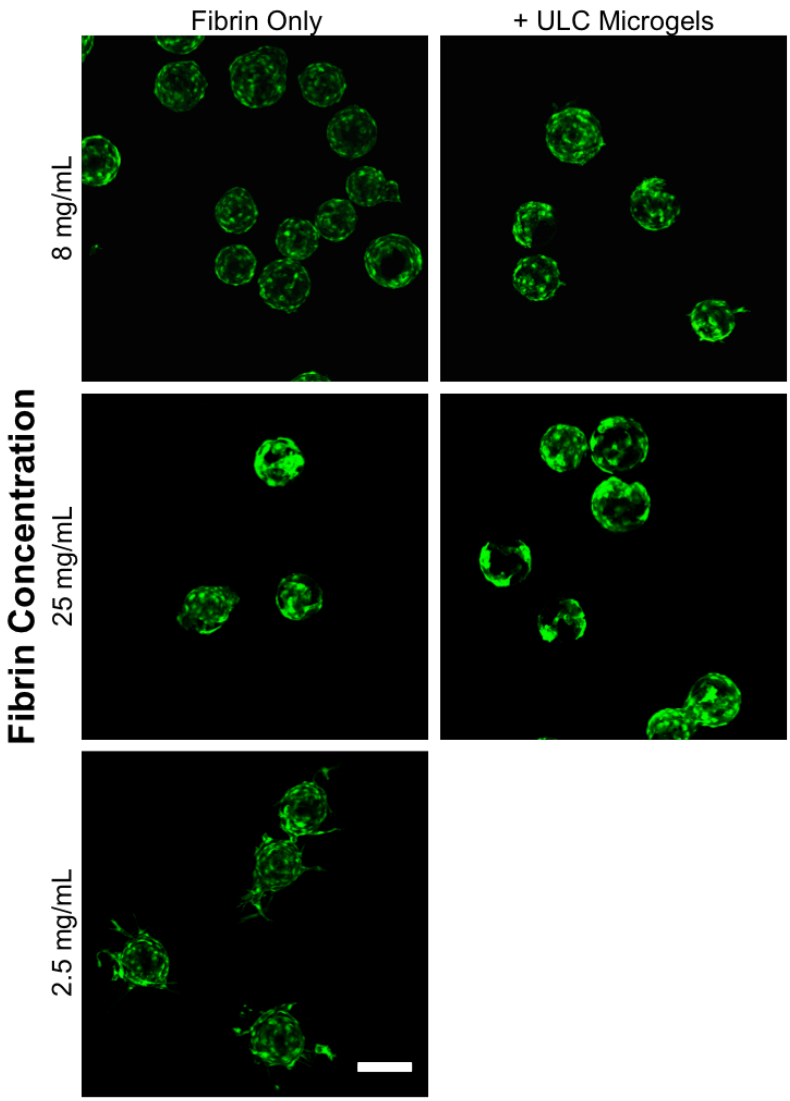

Figure 35: Representative GFP-HUVEC sprouting from collagen coated beads after 7 days in hybrid fibrin-microgel constructs. A) Fibrin 8 mg/mL, B) Fibrin 8 mg/mL + ULC microgels ϕ=0.112, C) Fibrin 25 mg/mL, D) Fibrin 25 mg/mL + ULC microgels ϕ=0.112. E) Fibrin 2.5 mg/mL, scale bar 200 μm.

Additionally, there appeared to be differences in fibrin degradation surrounding the microbeads that was observable in the samples with labeled fibrinogen (8 mg/mL fibrin +/- microgels, n=1). Where in Figure 36A the fibrin only group shows little fibrin

degradation around the bead with small amounts of sprouting, panel B shows significant degradation and cell-mediated deformation of fibrin fibers distant from the bead and GFP-HUVEC surface. This will be examined in more detail within the discussion.

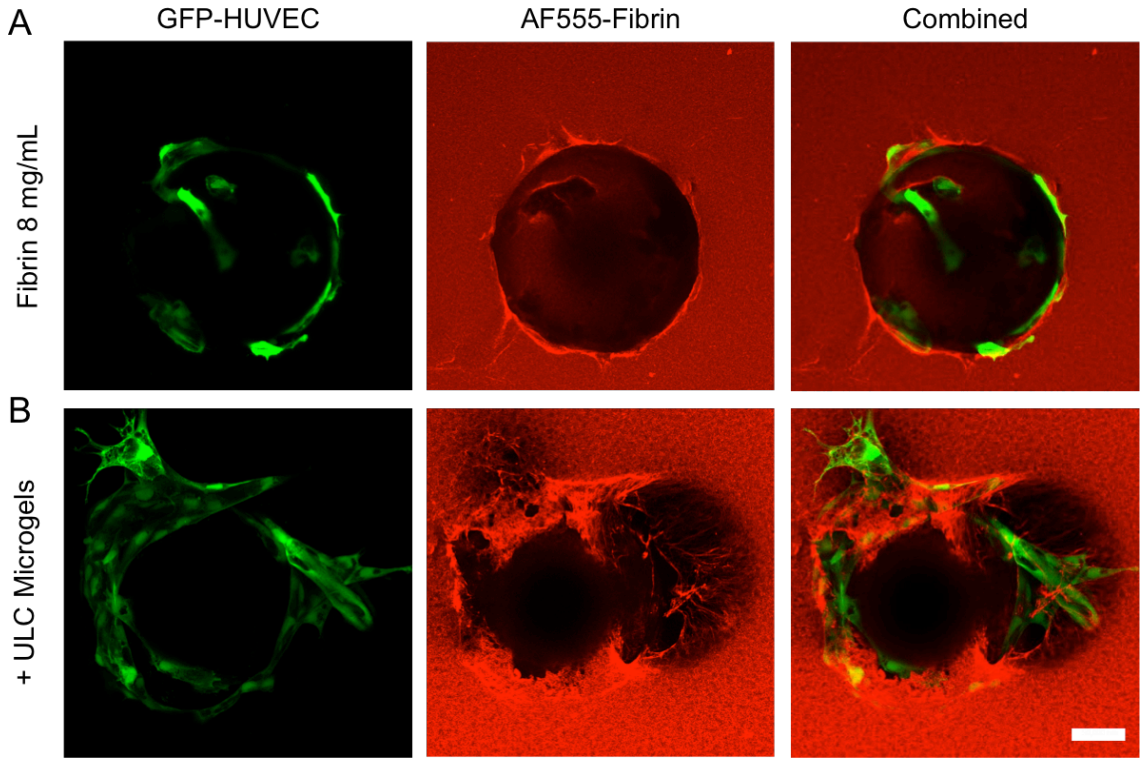

Figure 36: Evidence of variable degradation in GFP-HUVEC sprouting from collagen coated beads after 7 days in hybrid fibrin-microgel constructs. A) Fibrin 8 mg/mL, B) Fibrin 8 mg/mL + ULC microgels ϕ=0.112, scale 50 µm.

6.4 Discussion

The data acquired with micro-CT angiography illustrating the vascularization of the subcutaneous implants was inconclusive. In general, there appeared to be more vascularization at the ends of the PCL nanofiber meshes as opposed to in the center, with

little vascular bridging in any of the groups except for the physiological fibrin controls. This data thus suggests that the lowest fibrin concentration samples perform the best with respect to vascularization. This is not surprising as it is an excellent positive control for in growth into a porous matrix with quick turnover. Additionally, the literature supports these results with respect to fibrin gels at 2.5 mg/mL being capable of supporting sprouting in vitro. However, in reality these structures will not be maintained *in vivo* without the stability and structural support of the PCL mesh. Fibrin gels at physiological concentration will be degraded and resorbed quickly in vivo [9, 267, 268], but the stiffness and ability for the PCL mesh to hold its shape may have significantly altered the interpretation of these results. This is evident as there are no statistical differences in the total volumes of the tissue explants, whereas a hypothesis strongly supported by the literature would be that the physiological fibrin gels should have collapsed and fully degraded after 1 month *in vivo* [9, 88, 269-271]. For example, in the *in vitro* microvessel fragment assay, at the 10 day time point intact gel regions still persisted, but there was noticeable degradation of the 2.5 mg/mL fibrin only gels. While the other fibrin gels may have received structural support from the PCL mesh as well, histological evidence of the 25 mg/mL samples suggested the presence of fibrin within the center of the explants indicating that these gels had not fully degraded. Additionally, while not tested within this work, it is known that the mechanical and adhesive properties of physiological fibrin gels are not sufficient to stop major bleeds, seal large wounds, or facilitate stable anastomoses compared to fibrin sealants (thus initially rationalizing the generation of fibrin sealants with high fibrinogen concentrations to improve mechanics) [92].

Ultimately, results from the Micro-Fil micro-CT perfusions did not correlate with qualitative results obtained from the lectin perfusion. The hypothesis for these differences is that the micro-CT was unable to detect vessels with diameters smaller than 50 μm due to the higher viscosity of Micro-Fil, which is unable to flow through into these smaller vessels [272]. However, as the lectin dye is suspended in saline, smaller vessels and capillaries that have infiltrated the constructs can be visualized in the imaged tissue cross-sections.

The presence of microgels on microvessel spouting in the *in vitro* model of angiogenesis primarily demonstrated effects between different fibrin concentrations. These results could have been a product of the matrix architecture not being conducive to the growth and migration of larger multicellular structures. One could also hypothesize that the adhesive environment within the microvessel may have been more desirable than the surrounding matrix architecture, causing there to be less of a driving force for proliferation and migration. However, vessel arc length demonstrated that there were significant differences in vessel arc length between fibrin 25 mg/mL and fibrin 25 mg/mL + ULC microgels ϕ=0.112, suggesting potential for enhanced vessel growth with microgels incorporated into constructs at high fibrin concentrations.

The presence of microgels had no significant effects on the sprouting of HUVECs from collagen-coated beads. When analyzing gels that were polymerized with fluorescently labeled fibrinogen, striking observations were made with the cells interaction with the fibrin matrix surrounding the bead. Significant degradation and deformation of the matrix was observed in the groups containing microgels. It is known that porosity can affect polymer degradation as pores represent additional stress raisers

and increase the available surface area of the material to environmental factors that may cause degradation [36]. HUVECs appeared to have generated significant traction forces on the matrix as visualized in the strain of fibrin fibers and deformation of the microgel network architecture around the bead interface.

These results shed light into the fact that perhaps there is a baseline level of degradation that must occur in order to allow space for these cellular structures to generate traction and contractile forces to initiate migration. Even though microgel networks are present within the 3D matrix, perhaps in situations where cells are connected as a part of a larger multicellular structure, the microgel network diameter is still not large enough to enable spreading and the generation of contractility from the collective cell group to facilitate differences between groups with and without microgels. In a somewhat unrelated study, Khetan and co-workers sought to understand the differences in mesenchymal stem cell fate decisions based on matrix stiffness, degradation, and spreading/confinement [49]. They found that cells in confined spaces (in hydrogels that inhibited local matrix degradation) would differentiate down an adipogeneic lineage independent of matrix elasticity. When cells were able to degrade the matrix and had high spread areas and tractions, they differentiated towards and osteogenic lineage. Interestingly, switching the permissive hydrogel (that allowed local matrix degradation) to a restrictive state through delayed additional matrix crosslinking or inhibition of tension-mediated signaling, caused the spread osteogenic cells to switch towards an adipogenic phenotype even with no changes in cellular morphology. This work illustrates a similar idea that perhaps the presence of microgels enable cells to become more contractile through enabling protrusions to reach out and bind fibrin at

more distant locations (additionally causing increased spreading). Alternatively, perhaps microgels enable increased local degradation of the matrix in proximity to the cell body, which further increases cell spreading, contractility, and initiation of cell migration. Additionally, it has also been shown that multiple proteolytic mechanisms including MMP dependent and serine protease dependent degradation enables endothelial cell sprouting angiogenesis [266].

The results of this work allowed for a detailed understanding of how these composite materials perform in various tests of angiogenesis and vascularization and have provided much insight to inform future iterations of this system.

CHAPTER 7 CONCLUSIONS AND FUTURE DIRECTIONS

There remains a challenge in regenerative medicine to design engineered tissues that have optimal mechanical properties for the target site, allow for adequate host-material interaction/integration, and enable stabilized vascularization to promote longevity of the construct. We have generated a novel technology to enable cell infiltration and motility in dense biomaterial systems, specifically fibrin. Compared to the state of the native provisional fibrin matrix, this increased density requirement arises from the need for mechanical strength to either glue tissues, halt bleeding/heal wounds, or tune the mechanical properties of the construct for a specific therapy. Microgel-laden engineered fibrin matrices maintain the robust mechanical properties of dense fibrin matrices and yet are capable of cell infiltration *in vitro* and *in vivo* contrary to fibrin only controls.

Through harnessing the polymerization dynamics of fibrin, we were able to tune the architecture of microgel assemblies to form interconnected networks, which allowed for enhanced cell spreading, motility, and infiltration. Further investigation of the formation of these microgel tunnels has shown that the process is dependent on the bulk polymer used in the biomaterial composite system. We additionally have demonstrated polymers such as alginate are able to generate similar microgel tunneling structures, yet through different mechanisms, specifically depletion. When microgels are mixed with high molecular weight alginate solutions, pre-clusters of microgels form that then can be immobilized upon initiation ionic crosslinking. Thus, this technology is not limited to fibrin, but is applicable in other systems as long as pre-clustering or polymerization induced microgel clustering is observed.

Others in the field have sought to augment biomaterials with or even generate tissue engineering constructs from colloidal assemblies. However, each of these approaches contains a fundamental challenge or limitation, which will be subsequently described. Hwang et al generated a composite fibrin gel doped with alginate microparticles for applications in soft tissue reconstruction where volume retention of the implant is necessary after traumatic injury or tumor resection [20]. While the polydisperse alginate beads (ranging from 50-500 μm) enabled the implant to maintain its structure compared to the fibrin only implant that was completely resorbed after 12 weeks, the presence of the alginate beads significantly diminished the compression modulus of the composite material. Additionally, alginate beads did not enhance initial cell spreading or infiltration into the dense fibrin composites.

Another colloid based tissue engineering strategy was recently reported by Griffin et al., describing microporous annealed particle (MAP) gels inspired by porogens [273]. PEG based microparticles were generated using a water-in-oil droplet segmentation microfluidic set up for the self-assembly of monodisperse microgels (crosslinked with Michael addition reaction) with diameters of 30 to 150 μm. Particles were then annealed together utilizing FXIII crosslinking to form shape-molding colloidal gels with a porosity arising from the spaces in between the microparticles. The constructs were able to promote accelerated wound closure rates in vivo compared to non-porous controls. However, microfluidic approaches for the generation of these monodisperse functionalized colloids suffer from low throughput (100 μl of microgels in 1 hour) while precipitation polymerization of pNIPAM microgels can result in liters of product within a few hours.

A similar technology to MAP gels was reported in 2010 with the generation of 'modugels' by Scott et al [274]. Here, differentially functionalized PEG-RGD microgels were centrifuged to form a compact colloidal gel around cells, which maintained initial viability in the constructs. However, the constructs were not tested *in vivo*, and several drawbacks relating to the difficulty of their fabrication for in situ shape-molding applications is immediately apparent. Finally, work from Buddy Ratner utilized sphere-templated biomaterial implants with uniform interconnected pores [275]. While these implants displayed reduced fibrosis and increased vascularization, it is a fundamental porogen system, where extensive processing of the material with harsh solvents must be performed.

Our approach remains unique in that microgels form interconnected networks upon the dynamic assembly of fibrin and their structures can be tuned through adjustments in fibrin polymerization. High volume fractions of microgels are additionally used to structurally modify the base polymer system just upon simple mixing and addition of the catalytic enzyme thrombin. In systems where depletion could be expected to occur based on the size/molecular weight of the monomer and volume fraction, these clusters/ microgel networks can be formed even upon simple mixing (as in the example of alginate). The gel structure can then be subsequently frozen with the addition of a crosslinking solution containing a divalent cation. Additionally, the microgels did not affect the rheological properties of the fibrin composites, contrary to what is seen in most porogen/ porous systems [36]. Due to the unique softness of the pNIPAM-based microgels used in this work, cells are able to harness the interconnected microgel networks for enhanced cell spreading and motility. While significant enhancements in

vascularization among the groups remains to be fully realized, the fundamental groundwork characterizing the system in this project allows for future tuning of the system to succeed in different therapeutic areas. Additionally, many questions about the details of the system still remain, especially with respect to the cellular mechanism of action.

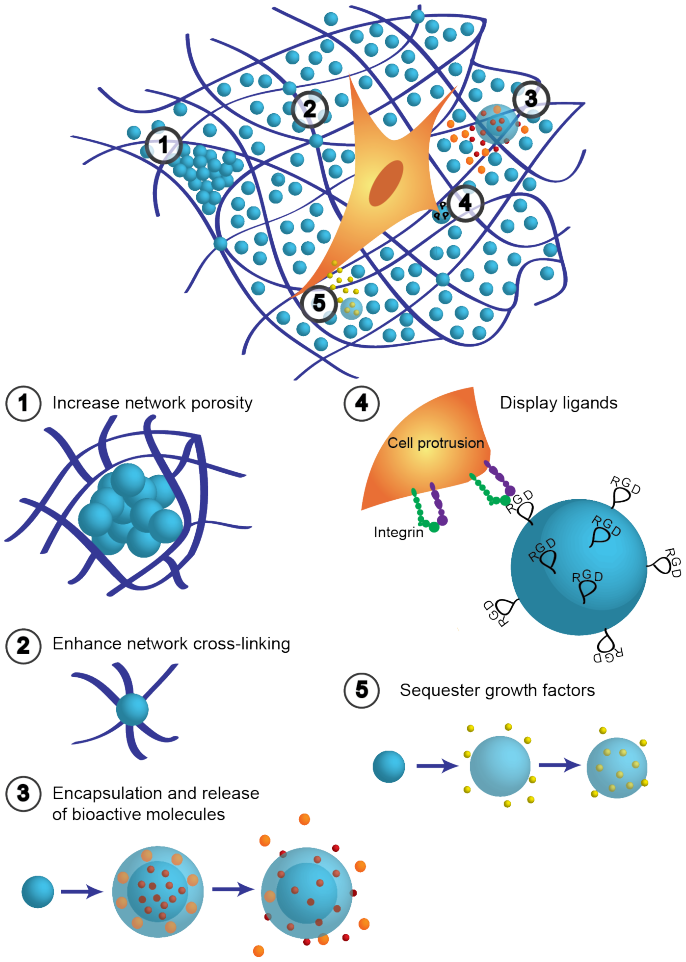

Figure 37: Schematic of the potential of composite ECM-microgel colloidal assemblies in regenerative medicine. (Reproduced from [171], Copyright Elsevier 2013.)

In the future, this work could be expanded upon in many ways to further understand the microenvironmental cues that exist in these composite matrices that influence cell infiltration and vascularization. As shown in Figure 37, while this work is immediately relevant to strategy 1, strategies 2-5 represent other directions that this work could follow in order to achieve other desired therapeutic outcomes.

From *in vivo* and *in vitro* investigations in aim 3, it was determined that potentially greater benefits could be realized from these materials if the diameters of the interconnected microgel networks could be increased. This could potentially be achieved through the formation of composite networks using a newly realized microgel particle termed Giant ULC microgels (GULCs), which are 3-5 μm in diameter [180]. Once materials are generated with larger microgel network architectures, these materials could be tested in an animal model to assess vascularization.

Testing within the subcutaneous implant model, could also be enhanced through providing the endogenous cells with a more prevalent angiogenic signal or cell recruitment cue, such as VEGF or SDF-1 [276]. VEGF is a native growth factor that is instrumental in angiogenesis in vivo and has demonstrated the ability to enhance vascularization in the subcutaneous model [223]. Stromal cell-derived factor-1α (SDF-1α) is a well-studied CXCR4 receptor-related chemokine, known to be involved in hematopoietic stem cell activation, mobilization, and homing [277], and that has also been employed in various tissue engineering studies to recruit mesenchymal stem cells (MSCs) [278], endothelial progenitor cells (EPCs) [279], promote angiogenesis [280], and enhance wound healing [281]. Upon injury to tissues, stem cells are recruited from the bone marrow to home to the site of injury to aid in tissue repair [276, 282, 283].

SDF-1α has also been shown to induce VEGF secretion in endothelial cells [284, 285], a known pro-angiogenic factor, which will enhance recruitment and proliferation of endothelial cells and progenitors. Others have used local delivery of SDF-1α in controlled release hydrogel based systems for the recruitment of progenitor cells [286], but the hydrogels used do not display microstructures or pore sizes amenable for robust cell infiltration.

In addition, previous work has demonstrated the ability to use pNIPAm-based microgels as tunable delivery vehicles for therapeutic molecules [174]. Based on the negative charge of the microgels, cationic proteins can be non-covalently encapsulated within the loose microgel particles. SDF-1α, like many chemokines, is positively charged and has also been administered to tissues via controlled release based on its charge [286, 287]. This combinatorial approach would allow for not only a structural benefit to the matrix architecture, but also a therapeutic benefit through enhanced recruitment of progenitor cells to the implanted tissue. Before these studies are to be performed, it would be advised however that there may be some concern with loading these particles for controlled growth factor release. Due to the ultra low crosslinked nature of these particles, theoretically their internal polymer structure is a more open mesh compared to more highly crosslinked comparable pNIPAM-AAc. Thus, the growth factor may be more susceptible to burst release if diffusion out of the particle is less hindered.

Alternatively, in contrast to the study outlined in this dissertation, it may be beneficial to test the efficacy of the engineered material in an animal model where more vessels are present, such as the mesenteric fat pad [206, 207], or intramuscularly [9]. Comparatively to the subcutaneous space, these regions are more highly vascularized and

native tissue would have a higher incentive to infiltrate the constructs implanted within these regions. Although a convenient and straightforward test for an initial characterization of a new material, the subcutaneous implant model suffers from an overall lack of significant vascularization, animal-to-animal variability, and even variability based on anatomical location of the implant within the animal as found in these studies.

If larger microgel network structures are unable to be generated, this work still could have significant benefit in the field of cell delivery. Many therapeutic approaches of the future to heal wounded soft tissues or for the generation of organ structures will rely on the delivery of cells within complex biomaterial systems. Fibroblasts and other mesenchymal cells make up the dominant portion of the cell population within many soft tissues, and mesenchymal stem cells are one cell type of interest that is commonly investigated in tissue engineering. Mesenchymal cells, being adhesion-dependent, rely on cell-matrix interactions for survival and proliferation. When these cells are unable to spread, polarize, and migrate, their phenotype and survival is limited [288]. Studies investigating in vivo delivery of MSCs in animals have demonstrated large amounts of cell death upon implantation and proven difficulty in maintaining cell viability over the long term [251, 289-291]. Additionally, diffusion of nutrients and removal of waste products within dense matrices that inhibit spreading also becomes a challenge to overcome. Composite ECM-microgel materials could enable initial cell spreading and maintenance of natural phenotype in cell delivery systems where normally these processes are hindered or delayed. This could potentially lead to increased cell viability over the long term or enhance initial cell survival post-implantation. The delivery of

cardiac progenitor cells (CPCs) in hybrid fibrin-microgel matrices detailed in this dissertation is being tested currently in a model of myocardial infarction.

Overall, this work illustrates a new clinically relevant colloid-matrix assembly [171] that decouples stiffness and cell-viewed mesh size to enable cell infiltration and motility using ultra soft colloidal assemblies.

APPENDIX

A.1. Supplemental experiments for insights into future directions

A.1.1. Investigation of cell motility in microgel laden RGD-alginate gels

A.1.1.1. Rationale

Alginate is popular biomaterial used in tissue engineering that is derived from seaweed [248]. Although it presents no native adhesion ligands for mammalian cells, it can be functionalized to present ligands such as RGD, in order to promote cell attachment, growth, and viability. Additionally, mammalian cells do not possess the enzyme (alginase) capable of degrading alginate [249]. Thus, it was hypothesized that adding microgels into RGD-alginate networks would enable cell spreading and migration contrary to RGD-alginate only constructs.

A.1.1.2. Methods

A.1.1.2.1. Cell seeded RGD-alginate gel formation and monitoring cell motility

RGD-Alginate was mixed with CMFDA-labeled NIH3T3 cells (methods previously described) with and without ULC microgels (ϕ=0.112) and cell culture media for a final cell concentration of 200,000 cells per mL in a 1% RGD-alginate gel. Calcium sulfate (final concentration of 6 mM) was added to the solution and mixed quickly before pipetting onto a tissue culture dish for subsequent gelation. Additional media was supplemented over top of the gels 30 minutes later and cells were left to grow and spread overnight. The next morning cells were subsequently monitored in the Nikon Biostation (imaged every 10 minutes for 12 hours).

A.1.1.3. Results

When cells were incubated in 1% RGD-alginate gels with and without ULC microgels, differences in cell morphology were found at the end of the experiment (~24 hour time point). Cell migration (characterized as translocation of the cell body/nucleus) was only observed in a select few cells per region in the gels containing microgels, while no cells within RGD-alginate alone moved within these experiments. In the groups containing microgels, cells displayed robust protrusions compared to RGD-alginate only gels, but maintained a rounded morphology in general, only sprouting a few thin and long protrusions at a time. Examples of these morphologies can be seen below in Figure 38, where NIH3T3s in 1% RGD-alginate gels can be seen in panels A and B and are completely rounded. Microgel network formation is apparent from the granular quality of the phase contrast image in C, which shows cells in a 1% RGD-alginate gel with ULC microgels (ϕ=0.112). Additionally, protrusions can be seen (yellow arrows) in panel D, which shows the CMFDA labeled cells in the FITC channel.

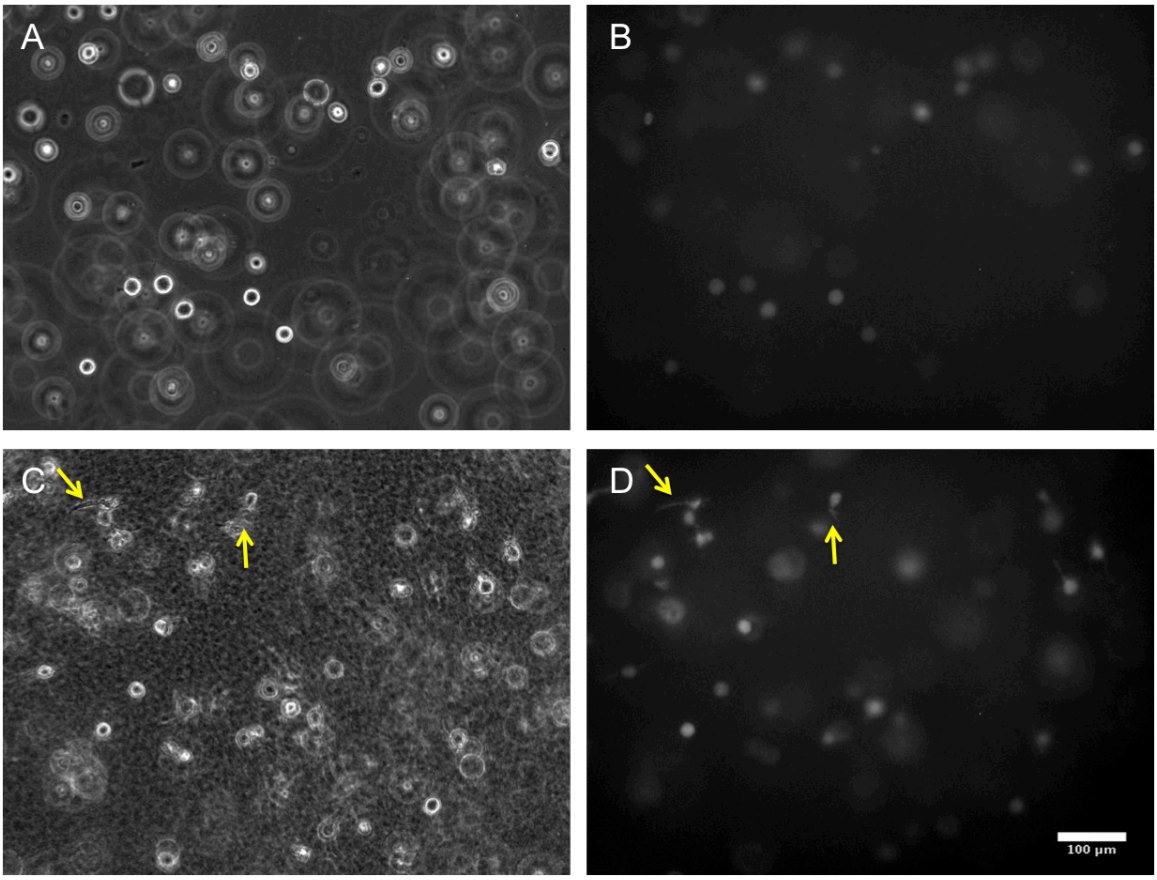

Figure 38: Phase contrast and fluorescence images of NIH3T3s in RGD-alginate gels with and without microgels. Images from end of 12 hour experiment in the Nikon Biostation taken with a 10X objective, A) phase contrast of 1% RGD-alginate only gel, B) FITC image of CMFDA labeled NIH3T3s in 1% RGD-alginate only gel, C) phase contrast of 1% RGD-alginate gel with ULC microgels (ϕ=0.112), B) FITC image of CMFDA labeled NIH3T3s in 1% RGD-alginate gel with ULC microgels (ϕ=0.112).

A.1.1.4. Discussion

Cells do not possess the adequate enzymes (alginases) to degrade alginate on their own, thus it degrades slowly over long time scales as ion exchange occurs. Therefore, these results are unique and demonstrate the potential for ULC microgels to enable cell

spreading (elongation of protrusions) and motility (observed qualitatively) within hydrogels that are not degradable by cellular mechanisms. Cell spreading and motility is visualized within the first 12 hours of incubation in the gels, thus the cells are leveraging the microgel networks through an unknown process. Future work could investigate this finding in more detail to better understand the mechanism.

A.1.2. Formation of hybrid fibrin-microgel constructs with giant ultra low crosslinked microgels (GULCs)

A.1.2.1. Rationale

The results from this dissertation suggest that to enable processes in which collective cell migration occurs, fibrin gels may require larger diameter microgel network tunnels to better support angiogenesis. Thus, one potential solution to this problem would be to use larger microgel, specifically giant ultra low crosslinked microgels (GULCs), which have diameters ranging from 3-5 μm [180]. In order to determine if larger microgels would create larger interconnected structures, confocal microscopy was performed on composite fibrin-GULC gels with fluorescently labeled fibrinogen.

A.1.2.2. Methods

A.1.2.2.1. GULC synthesis[7]

The synthesis of GULC microgels is similar to that of ULC microgels described in chapter 3 except that a temperature ramp is performed at the beginning of the reaction. Briefly, the reaction was initiated at 45 °C followed by an increase in temperature to 60 °C at a rate of 30 °C/hr. After completion, the reaction solution was cooled to room temperature and filtered through glass wool. Microgels were centrifugally pelleted and redispersed in deionized H_2O 3-6 times to purify and then lyophilized before use.

[7] Adapted from Bachman et al. Ultrasoft, highly deformable microgels, Soft Matter, 11 (2015) 2018-2028. Adapted from with permission by The Royal Society of Chemistry.

A.1.2.2.2. Hybrid gel formation and confocal microscopy

Gels were formed similarly as previously described in chapter 3, however, a final concentration of 4 mg/mL GULCs was utilized in the place of ULC microgels.

A.1.2.3. Results

GULCs formed connected networks within dense fibrin gels as observed in Figure 39 below. As GULCs average approximately 5 μm in diameter, outlines of individual particles can be viewed in the confocal image as thin fibrin fibers wrap around the periphery of the particles.

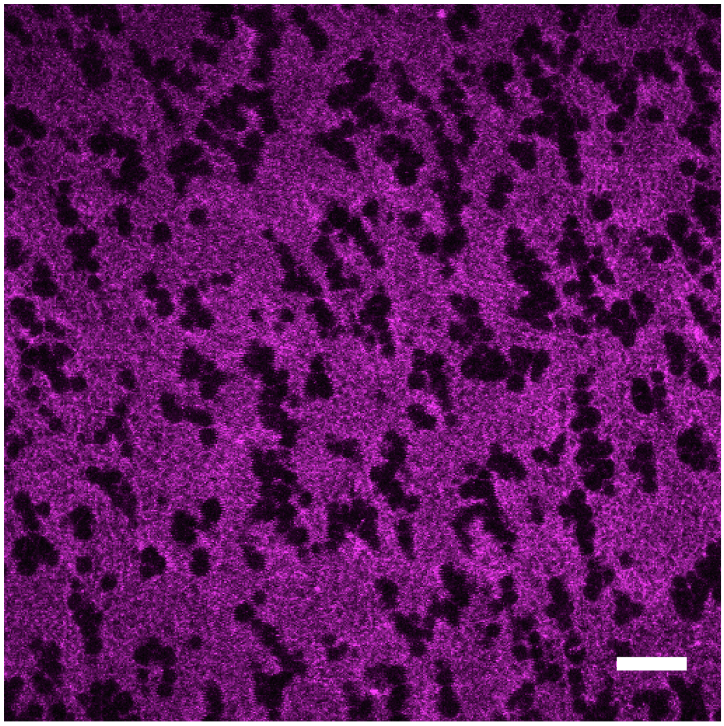

Figure 39: Confocal image of fibrin gel 15 mg/mL with Giant ULC microgels (4 mg/mL) incorporated during polymerization with 2 U/mL thrombin.Made with 2.5% Alexa Fluor 647 fibrinogen, scale bar 20 μm.

Quantitative analysis of this image gives an average network radius of 4.05 μm compared to ULC microgels, which on average formed tunnels with a radius of 4.5 μm.

A.1.2.4. Discussion

Although the data represented is only from a single independent experiment, the similar values in microgel network radius suggest that using larger microgels may not enable the formation of larger microgel network tunnels and as seen in the image, the GULCs seem to form more single microgel strings or lines of small clusters throughout the gel as opposed to large clusters. While the cluster size may be similar to cases where ULC microgels are used, ULC microgels have more particles per cluster, and thus potentially allow for cells to rearrange the grouping of microgels as opposed to a cell interrogating 1 larger microgel, which may be inhibitory to deformation/relaxation. However, microgel volume fraction is necessarily at ϕ_c in this experiment because viscometric experiments have not been performed on the GULCs. Thus, microgel concentration could be increased to ϕ_c for future experiments once it is determined and potentially larger diameter microgel networks could be formed.

REFERENCES

[1] I. Levental, P.C. Georges, P.A. Janmey, Soft biological materials and their impact on cell function, Soft Matter, 3 (2007) 299.

[2] J.W. Weisel, The mechanical properties of fibrin for basic scientists and clinicians, Biophysical chemistry, 112 (2004) 267-276.

[3] M.E. Carr, Jr., S.L. Carr, Fibrin structure and concentration alter clot elastic modulus but do not alter platelet mediated force development, Blood Coagulation & Fibrinolysis, 6 (1995) 79.

[4] M.A. LeRoux, F. Guilak, L.A. Setton, Compressive and shear properties of alginate gel: Effects of sodium ions and alginate concentration, Journal of Biomedical Materials Research, 47 (1999) 46-53.

[5] N. Reddy, R. Reddy, Q. Jiang, Crosslinking biopolymers for biomedical applications, Trends in Biotechnology.

[6] M. Gonen-Wadmany, R. Goldshmid, D. Seliktar, Biological and mechanical implications of PEGylating proteins into hydrogel biomaterials, Biomaterials, 32 (2011) 6025-6033.

[7] S.E. Stabenfeldt, M. Gourley, L. Krishnan, J.B. Hoying, T.H. Barker, Engineering fibrin polymers through engagement of alternative polymerization mechanisms, Biomaterials, 33 (2012) 535-544.

[8] M.M. Martino, F. Tortelli, M. Mochizuki, S. Traub, D. Ben-David, G.A. Kuhn, R. Müller, E. Livne, S.A. Eming, J.A. Hubbell, Engineering the Growth Factor Microenvironment with Fibronectin Domains to Promote Wound and Bone Tissue Healing, Science translational medicine, 3 (2011) 100ra189.

[9] V. Sacchi, R. Mittermayr, J. Hartinger, M.M. Martino, K.M. Lorentz, S. Wolbank, A. Hofmann, R.A. Largo, J.S. Marschall, E. Groppa, R. Gianni-Barrera, M. Ehrbar, J.A. Hubbell, H. Redl, A. Banfi, Long-lasting fibrin matrices ensure stable and functional angiogenesis by highly tunable, sustained delivery of recombinant VEGF164, Proceedings of the National Academy of Sciences of the United States of America, 111 (2014) 6952-6957.

[10] W. Hayen, M. Goebeler, S. Kumar, R. Riessen, V. Nehls, Hyaluronan stimulates tumor cell migration by modulating the fibrin fiber architecture, Journal of cell science, 112 (1999) 2241-2251.

[11] J.K. Mouw, G. Ou, V.M. Weaver, Extracellular matrix assembly: a multiscale deconstruction, Nature reviews. Molecular cell biology, 15 (2014) 771-785.

[12] D. Seliktar, Designing cell-compatible hydrogels for biomedical applications, Science, 336 (2012) 1124-1128.

[13] A. Atala, F.K. Kasper, A.G. Mikos, Engineering complex tissues, Science translational medicine, 4 (2012) 160rv112.

[14] E.T. Pashuck, M.M. Stevens, Designing Regenerative Biomaterial Therapies for the Clinic, Science translational medicine, 4 (2012) 160sr164.

[15] J.M. Karp, F. Sarraf, M.S. Shoichet, J.E. Davies, Fibrin-filled scaffolds for bone-tissue engineering: An in vivo study, Journal of biomedical materials research. Part A, 71 (2004) 162-171.

[16] A.J. Hanson, M.T. Quinn, Effect of fibrin sealant composition on human neutrophil chemotaxis, Journal of Biomedical Materials Research, 61 (2002) 474-481.

[17] M. Ahearne, D.J. Kelly, A comparison of fibrin, agarose and gellan gum hydrogels as carriers of stem cells and growth factor delivery microspheres for cartilage regeneration, Biomedical materials, 8 (2013) 035004.

[18] P. Losi, E. Briganti, C. Errico, A. Lisella, E. Sanguinetti, F. Chiellini, G. Soldani, Fibrin-based scaffold incorporating VEGF- and bFGF-loaded nanoparticles stimulates wound healing in diabetic mice, Acta biomaterialia, 9 (2013) 7814-7821.

[19] Y. Han, Q. Zeng, L. E, D. Wang, H. He, H. Liu, Sustained topical delivery of insulin from fibrin gel loaded with poly(lactic-co-glycolic Acid) microspheres improves the biomechanical retention of titanium implants in type 1 diabetic rats, Journal of oral and maxillofacial surgery : official journal of the American Association of Oral and Maxillofacial Surgeons, 70 (2012) 2299-2308.

[20] C.M. Hwang, B. Ay, D.L. Kaplan, J.P. Rubin, K.G. Marra, A. Atala, J.J. Yoo, S.J. Lee, Assessments of injectable alginate particle-embedded fibrin hydrogels for soft tissue reconstruction, Biomedical materials, 8 (2013) 014105.

[21] H. Layman, X. Li, E. Nagar, X. Vial, S.M. Pham, F.M. Andreopoulos, Enhanced angiogenic efficacy through controlled and sustained delivery of FGF-2 and G-CSF from fibrin hydrogels containing ionic-albumin microspheres, Journal of biomaterials science. Polymer edition, 23 (2012) 185-206.

[22] L.A. Lyon, A. Fernandez-Nieves, The polymer/colloid duality of microgel suspensions, Annual review of physical chemistry, 63 (2012) 25-43.

[23] Z. Meng, J.K. Cho, V. Breedveld, L.A. Lyon, Physical aging and phase behavior of multiresponsive microgel colloidal dispersions, The journal of physical chemistry. B, 113 (2009) 4590-4599.

[24] A.C. Brown, S.E. Stabenfeldt, B. Ahn, R.T. Hannan, K.S. Dhada, E.S. Herman, V. Stefanelli, N. Guzzetta, A. Alexeev, W.A. Lam, L.A. Lyon, T.H. Barker, Ultrasoft

microgels displaying emergent platelet-like behaviours, Nature materials, advance online publication (2014).

[25] C. Frantz, K.M. Stewart, V.M. Weaver, The extracellular matrix at a glance, Journal of cell science, 123 (2010) 4195-4200.

[26] M. Humphries, The molecular basis and specificity of integrin-ligand interactions, Journal of cell science, 97 (1990) 585-592.

[27] G.S. Schultz, A. Wysocki, Interactions between extracellular matrix and growth factors in wound healing, Wound repair and regeneration : official publication of the Wound Healing Society [and] the European Tissue Repair Society, 17 (2009) 153-162.

[28] J.D. Humphries, A. Byron, M.J. Humphries, Integrin ligands at a glance, Journal of cell science, 119 (2006) 3901-3903.

[29] P.A. Janmey, J.P. Winer, J.W. Weisel, Fibrin gels and their clinical and bioengineering applications, Journal of the Royal Society, Interface / the Royal Society, 6 (2009) 1-10.

[30] M. Mörgelin, D. Heinegård, J. Engel, M. Paulsson, The cartilage proteoglycan aggregate: assembly through combined protein—carbohydrate and protein—protein interactions, Biophysical chemistry, 50 (1994) 113-128.

[31] S. Lally, R. Liu, C. Supasuteekul, B.R. Saunders, T. Freemont, Using osmotic deswelling of microgel particles to control the mechanical properties of pH-responsive hydrogel composites, Journal of Materials Chemistry, 21 (2011) 17719-17728.

[32] J.J. Rice, M.M. Martino, L. De Laporte, F. Tortelli, P.S. Briquez, J.A. Hubbell, Engineering the regenerative microenvironment with biomaterials, Advanced healthcare materials, 2 (2013) 57-71.

[33] B. Trappmann, C.S. Chen, How cells sense extracellular matrix stiffness: a material's perspective, Current opinion in biotechnology, 24 (2013) 948-953.

[34] M. Guvendiren, J.A. Burdick, Engineering synthetic hydrogel microenvironments to instruct stem cells, Current opinion in biotechnology, 24 (2013) 841-846.

[35] J.L. West, Protein-patterned hydrogels: Customized cell microenvironments, Nature materials, 10 (2011) 727 - 729.

[36] J.S. Temenoff, A.G. Mikos, Biomaterials: The Intersection of Biology and Materials Science, Pearson Prentice Hall, Upper Saddle River, New Jersey 07458, 2008.

[37] B. Geiger, J.P. Spatz, A.D. Bershadsky, Environmental sensing through focal adhesions, Nature reviews. Molecular cell biology, 10 (2009) 21-33.

[38] E. Ruoslahti, M.D. Pierschbacher, New Perspectives in Cell Adhesion: RGD and Integrins, Science, 238 (1987) 491-497.

[39] M.D. Pierschbacher, E. Ruoslahti, Cell attachment activity of fibronectin can be duplicated by small synthetic fragments of the molecule, Nature, 309 (1984) 30-33.

[40] U. Hersel, C. Dahmen, H. Kessler, RGD modified polymers: biomaterials for stimulated cell adhesion and beyond, Biomaterials, 24 (2003) 4385-4415.

[41] E. Ruoslahti, The RGD story: a personal account, Matrix Biology, 22 (2003) 459-465.

[42] A.S. Gobin, J.L. West, Cell migration through defined, synthetic extracellular matrix analogues, The FASEB Journal, (2002).

[43] S.-H. Lee, J.J. Moon, J.L. West, Three-dimensional micropatterning of bioactive hydrogels via two-photon laser scanning photolithography for guided 3D cell migration, Biomaterials, 29 (2008) 2962-2968.

[44] M.P. Lutolf, J.L. Lauer-Fields, H.G. Schmoekel, A.T. Metters, F.E. Weber, G.B. Fields, J.A. Hubbell, Synthetic matrix metalloproteinase-sensitive hydrogels for the conduction of tissue regeneration: engineering cell-invasion characteristics, Proceedings of the National Academy of Sciences of the United States of America, 100 (2003) 5413-5418.

[45] M.P. Lutolf, J.A. Hubbell, Synthetic biomaterials as instructive extracellular microenvironments for morphogenesis in tissue engineering, Nat Biotech, 23 (2005) 47-55.

[46] G.P. Raeber, M.P. Lutolf, J.A. Hubbell, Molecularly engineered PEG hydrogels: a novel model system for proteolytically mediated cell migration, Biophysical journal, 89 (2005) 1374-1388.

[47] M.P. Lutolf, G.P. Raeber, A.H. Zisch, N. Tirelli, J.A. Hubbell, Cell-Responsive Synthetic Hydrogels, Advanced Materials, 15 (2003) 888-892.

[48] J.S. Miller, C.J. Shen, W.R. Legant, J.D. Baranski, B.L. Blakely, C.S. Chen, Bioactive hydrogels made from step-growth derived PEG-peptide macromers, Biomaterials, 31 (2010) 3736-3743.

[49] S. Khetan, M. Guvendiren, W.R. Legant, D.M. Cohen, C.S. Chen, J.A. Burdick, Degradation-mediated cellular traction directs stem cell fate in covalently crosslinked three-dimensional hydrogels, Nature materials, 12 (2013) 458-465.

[50] K.S. Anseth, A.T. Metters, S.J. Bryant, P.J. Martens, J.H. Elisseeff, C.N. Bowman, In situ forming degradable networks and their application in tissue engineering and drug delivery, Journal of Controlled Release, 78 (2002) 199-209.

[51] X. Liu, J.M. Holzwarth, P.X. Ma, Functionalized Synthetic Biodegradable Polymer Scaffolds for Tissue Engineering, Macromolecular bioscience, 12 (2012) 911-919.

[52] F. Ramirez, D.B. Rifkin, Cell signaling events: a view from the matrix, Matrix Biology, 22 (2003) 101-107.

[53] P.J. Wipff, D.B. Rifkin, J.J. Meister, B. Hinz, Myofibroblast contraction activates latent TGF-beta1 from the extracellular matrix, The Journal of cell biology, 179 (2007) 1311-1323.

[54] M.W. Tibbitt, K.S. Anseth, Dynamic Microenvironments: The Fourth Dimension, Science translational medicine, 4 (2012) 160ps124.

[55] M. Mehta, K. Schmidt-Bleek, G.N. Duda, D.J. Mooney, Biomaterial delivery of morphogens to mimic the natural healing cascade in bone, Advanced Drug Delivery Reviews, 64 (2012) 1257-1276.

[56] C.-C. Lin, K. Anseth, PEG Hydrogels for the Controlled Release of Biomolecules in Regenerative Medicine, Pharm Res, 26 (2009) 631-643.

[57] W.W. Yuen, N.R. Du, C.H. Chan, E.A. Silva, D.J. Mooney, Mimicking nature by codelivery of stimulant and inhibitor to create temporally stable and spatially restricted angiogenic zones, Proceedings of the National Academy of Sciences, 107 (2010) 17933-17938.

[58] S.A. DeLong, J.J. Moon, J.L. West, Covalently immobilized gradients of bFGF on hydrogel scaffolds for directed cell migration, Biomaterials, 26 (2005) 3227-3234.

[59] A.H. Zisch, M.P. Lutolf, M. Ehrbar, G.P. Raeber, S.C. Rizzi, N. Davies, H. Schmökel, D. Bezuidenhout, V. Djonov, P. Zilla, J.A. Hubbell, Cell-demanded release of VEGF from synthetic, biointeractive cell-ingrowth matrices for vascularized tissue growth, The FASEB Journal, (2003).

[60] N. Yamaguchi, K.L. Kiick, Polysaccharide−Poly(ethylene glycol) Star Copolymer as a Scaffold for the Production of Bioactive Hydrogels, Biomacromolecules, 6 (2005) 1921-1930.

[61] N. Laurens, P. Koolwijk, M.P. de Maat, Fibrin structure and wound healing, Journal of thrombosis and haemostasis : JTH, 4 (2006) 932-939.

[62] J. Ceccarelli, A.J. Putnam, Sculpting the blank slate: how fibrin's support of vascularization can inspire biomaterial design, Acta biomaterialia, 10 (2014) 1515-1523.

[63] M. Radosevich, H.A. Goubran, T. Burnouf, Fibrin Sealant: Scientific Rationale, Production Methods, Properties, and Current Clinical Use, Vox Sanguinis, 72 (1997) 133-143.

[64] H.F. Dvorak, V.S. Harvey, P. Estrella, L.F. Brown, J. McDonagh, A.M. Dvorak, Fibrin containing gels induce angiogenesis. Implications for tumor stroma generation and wound healing, Laboratory investigation; a journal of technical methods and pathology, 57 (1987) 673-686.

[65] B.N. Brown, S.F. Badylak, Extracellular matrix as an inductive scaffold for functional tissue reconstruction, Translational Research, 163 (2014) 268-285.

[66] R. Londono, S. Badylak, Biologic Scaffolds for Regenerative Medicine: Mechanisms of In vivo Remodeling, Annals of biomedical engineering, 43 (2015) 577-592.

[67] B. Sicari, L. Zhang, R. Londono, S. Badylak, An Assay to Quantify Chemotactic Properties of Degradation Products from Extracellular Matrix, in: G. Vunjak-Novakovic, K. Turksen (Eds.) Biomimetics and Stem Cells, Springer New York, 2014, pp. 103-110.

[68] A.J. Beattie, T.W. Gilbert, J.P. Guyot, A.J. Yates, S.F. Badylak, Chemoattraction of Progenitor Cells by Remodeling Extracellular Matrix Scaffolds, Tissue Engineering Part A, 15 (2008) 1119-1125.

[69] J.E. Valentin, A.M. Stewart-Akers, T.W. Gilbert, S.F. Badylak, Macrophage Participation in the Degradation and Remodeling of Extracellular Matrix Scaffolds, Tissue Engineering Part A, 15 (2009) 1687-1694.

[70] R.F. Doolittle, Fibrinogen and Fibrin, Annual review of biochemistry, 53 (1984) 195-229.

[71] A.S. Soon, C.S. Lee, T.H. Barker, Modulation of fibrin matrix properties via knob:hole affinity interactions using peptide-PEG conjugates, Biomaterials, 32 (2011) 4406-4414.

[72] J.W. Weisel, R.I. Litvinov, Mechanisms of fibrin polymerization and clinical implications, Blood, 121 (2013) 1712-1719.

[73] I.N. Chernysh, C. Nagaswami, P.K. Purohit, J.W. Weisel, Fibrin clots are equilibrium polymers that can be remodeled without proteolytic digestion, Scientific reports, 2 (2012) 879.

[74] L. Muszbek, V.C. Yee, Z. Hevessy, Blood Coagulation Factor XIII: Structure and Function, Thrombosis Research, 94 (1999) 271-305.

[75] R.A. Ariens, T.S. Lai, J.W. Weisel, C.S. Greenberg, P.J. Grant, Role of factor XIII in fibrin clot formation and effects of genetic polymorphisms, Blood, 100 (2002) 743-754.

[76] L. Lorand, D. Chenoweth, A. Gray, TITRATION OF THE ACCEPTOR CROSS-LINKING SITES IN FIBRIN*, Annals of the New York Academy of Sciences, 202 (1972) 155-171.

[77] K.B. Lewis, D.C. Teller, J. Fry, G.W. Lasser, P.D. Bishop, Crosslinking Kinetics of the Human Transglutaminase, Factor XIII[A2], Acting on Fibrin Gels and γ-Chain Peptides, Biochemistry, 36 (1997) 995-1002.

[78] T. Tamaki, N. Aoki, Cross-linking of alpha 2-plasmin inhibitor and fibronectin to fibrin by fibrin-stabilizing factor, Biochimica et biophysica acta, 661 (1981) 280-286.

[79] C.S. Greenberg, M.A. Shuman, The zymogen forms of blood coagulation factor XIII bind specifically to fibrinogen, Journal of Biological Chemistry, 257 (1982) 6096-6101.

[80] G. Dickneite, H.J. Metzner, M. Kroez, B. Hein, U. Nicolay, The Importance of Factor XIII as a Component of Fibrin Sealants, Journal of Surgical Research, 107 (2002) 186-195.

[81] J.W. Weisel, C. Nagaswami, Computer modeling of fibrin polymerization kinetics correlated with electron microscope and turbidity observations: clot structure and assembly are kinetically controlled, Biophysical journal, 63 (1992) 111-128.

[82] E.A. Ryan, L.F. Mockros, J.W. Weisel, L. Lorand, Structural Origins of Fibrin Clot Rheology, Biophysical journal, 77 (1999) 2813-2826.

[83] M.W. Mosesson, Fibrinogen and fibrin structure and functions, Journal of thrombosis and haemostasis : JTH, 3 (2005) 1894-1904.

[84] J.B. Walker, M.E. Nesheim, The molecular weights, mass distribution, chain composition, and structure of soluble fibrin degradation products released from a fibrin clot perfused with plasmin, The Journal of biological chemistry, 274 (1999) 5201-5212.

[85] S. Nürnberger, S. Wolbank, A. Peterbauer-Scherb, T. Morton, G. Feichtinger, A. Gugerell, A. Meinl, K. Labuda, M. Bittner, W. Pasteiner, L. Nikkola, C. Gabriel, M. van Griensven, H. Redl, Properties and Potential Alternative Applications of Fibrin Glue, in: J. von Byern, I. Grunwald (Eds.) Biological Adhesive Systems, Springer Vienna, 2010, pp. 237-259.

[86] J. Ferguson, S. Nürnberger, H. Redl, Fibrin: The Very First Biomimetic Glue — Still a Great Tool, in: J. von Byern, I. Grunwald (Eds.) Biological Adhesive Systems, Springer Vienna, 2010, pp. 225-236.

[87] H.C. Hedrich, M. Simunek, S. Reisinger, J. Ferguson, H. Gulle, A. Goppelt, H. Redl, Fibrin chain cross-linking, fibrinolysis, and in vivo sealing efficacy of differently structured fibrin sealants, Journal of biomedical materials research. Part B, Applied biomaterials, 100 (2012) 1507-1512.

[88] T.A. Ahmed, E.V. Dare, M. Hincke, Fibrin: a versatile scaffold for tissue engineering applications, Tissue engineering. Part B, Reviews, 14 (2008) 199-215.

[89] T. Osathanon, M.L. Linnes, R.M. Rajachar, B.D. Ratner, M.J. Somerman, C.M. Giachelli, Microporous nanofibrous fibrin-based scaffolds for bone tissue engineering, Biomaterials, 29 (2008) 4091-4099.

[90] H.G. Schmoekel, F.E. Weber, J.C. Schense, K.W. Gratz, P. Schawalder, J.A. Hubbell, Bone repair with a form of BMP-2 engineered for incorporation into fibrin cell ingrowth matrices, Biotechnology and bioengineering, 89 (2005) 253-262.

[91] W.D. Spotnitz, Hemostats, Sealants, and Adhesives: A Practical Guide for the Surgeon, The American Surgeon, 78 (2012) 1305-1321.

[92] M.-G.M. Lee, D. Jones, Applications of Fibrin Sealant in Surgery, Surgical Innovation, 12 (2005) 203-213.

[93] A.T. Committee, Y.M. Bhat, S. Banerjee, B.A. Barth, S.S. Chauhan, K.T. Gottlieb, V. Konda, J.T. Maple, F.M. Murad, P.R. Pfau, D.K. Pleskow, U.D. Siddiqui, J.L. Tokar, A. Wang, S.A. Rodriguez, Tissue adhesives: cyanoacrylate glue and fibrin sealant, Gastrointestinal endoscopy, 78 (2013) 209-215.

[94] G. Marx, X. Mou, Characterizing fibrin glue performance as modulated by heparin, aprotinin, and factor XIII, Journal of Laboratory and Clinical Medicine, 140 (2002) 152-160.

[95] C.M. Ghajar, X. Chen, J.W. Harris, V. Suresh, C.C. Hughes, N.L. Jeon, A.J. Putnam, S.C. George, The effect of matrix density on the regulation of 3-D capillary morphogenesis, Biophysical journal, 94 (2008) 1930-1941.

[96] J.D. Smith, M.E. Melhem, K.T. Magge, A.S. Waggoner, P.G. Campbell, Improved growth factor directed vascularization into fibrin constructs through inclusion of additional extracellular molecules, Microvascular research, 73 (2007) 84-94.

[97] N.U. Bang, A.H. Freiman, E.E. Cliffton, Effect of Increased Fibrinogen Concentration on the Lysis of In Vivo Thrombi, Circulation Research, 8 (1960) 419-422.

[98] P.D. Kim, S.R. Peyton, A.J. VanStrien, A.J. Putnam, The influence of ascorbic acid, TGF-beta1, and cell-mediated remodeling on the bulk mechanical properties of 3-D PEG-fibrinogen constructs, Biomaterials, 30 (2009) 3854-3864.

[99] D. Seliktar, Extracellular stimulation in tissue engineering, Ann N Y Acad Sci, 1047 (2005) 386-394.

[100] L. Almany, D. Seliktar, Biosynthetic hydrogel scaffolds made from fibrinogen and polyethylene glycol for 3D cell cultures, Biomaterials, 26 (2005) 2467-2477.

[101] D. Dikovsky, H. Bianco-Peled, D. Seliktar, The effect of structural alterations of PEG-fibrinogen hydrogel scaffolds on 3-D cellular morphology and cellular migration, Biomaterials, 27 (2006) 1496-1506.

[102] D. Dikovsky, H. Bianco-Peled, D. Seliktar, Defining the Role of Matrix Compliance and Proteolysis in Three-Dimensional Cell Spreading and Remodeling, Biophysical journal, 94 (2008) 2914-2925.

[103] I. Frisman, D. Seliktar, H. Bianco-Peled, Nanostructuring biosynthetic hydrogels for tissue engineering: A cellular and structural analysis, Acta biomaterialia, 8 (2012) 51-60.

[104] I. Frisman, D. Seliktar, H. Bianco-Peled, Nanostructuring PEG-fibrinogen hydrogels to control cellular morphogenesis, Biomaterials, 32 (2011) 7839-7846.

[105] G. Zhang, X. Wang, Z. Wang, J. Zhang, L. Suggs, A PEGylated fibrin patch for mesenchymal stem cell delivery, Tissue engineering, 12 (2006) 9-19.

[106] C.T. Drinnan, G. Zhang, M.A. Alexander, A.S. Pulido, L.J. Suggs, Multimodal release of transforming growth factor-β1 and the BB isoform of platelet derived growth factor from PEGylated fibrin gels, Journal of Controlled Release, 147 (2010) 180-186.

[107] E. Chung, J.A. Rytlewski, A.G. Merchant, K.S. Dhada, E.W. Lewis, L.J. Suggs, Fibrin-based 3D matrices induce angiogenic behavior of adipose-derived stem cells, Acta biomaterialia, 17 (2015) 78-88.

[108] E.A. Phelps, A.J. García, Engineering more than a cell: vascularization strategies in tissue engineering, Current opinion in biotechnology, 21 (2010) 704-709.

[109] J.M. Anderson, A. Rodriguez, D.T. Chang, FOREIGN BODY REACTION TO BIOMATERIALS, Seminars in immunology, 20 (2008) 86-100.

[110] B.G. Keselowsky, A.W. Bridges, K.L. Burns, C.C. Tate, J.E. Babensee, M.C. LaPlaca, A.J. García, Role of plasma fibronectin in the foreign body response to biomaterials, Biomaterials, 28 (2007) 3626-3631.

[111] C.J. Wilson, R.E. Clegg, D.I. Leavesley, M.J. Pearcy, Mediation of biomaterial-cell interactions by adsorbed proteins: a review, Tissue engineering, 11 (2005) 1-18.

[112] Z. Xia, J.T. Triffitt, A review on macrophage responses to biomaterials, Biomedical materials, 1 (2006) R1-9.

[113] J.M. Anderson, BIOLOGICAL RESPONSES TO MATERIALS, Annual Review of Materials Research, 31 (2001) 81-110.

[114] J.D. Bryers, C.M. Giachelli, B.D. Ratner, Engineering biomaterials to integrate and heal: the biocompatibility paradigm shifts, Biotechnology and bioengineering, 109 (2012) 1898-1911.

[115] K. Wolf, M. Te Lindert, M. Krause, S. Alexander, J. Te Riet, A.L. Willis, R.M. Hoffman, C.G. Figdor, S.J. Weiss, P. Friedl, Physical limits of cell migration: control by

ECM space and nuclear deformation and tuning by proteolysis and traction force, The Journal of cell biology, 201 (2013) 1069-1084.

[116] K. Wolf, P. Friedl, Extracellular matrix determinants of proteolytic and non-proteolytic cell migration, Trends in cell biology, 21 (2011) 736-744.

[117] A.J. Marshall, B.D. Ratner, Quantitative characterization of sphere-templated porous biomaterials, AIChE Journal, 51 (2005) 1221-1232.

[118] B.D. Ratner, A paradigm shift: biomaterials that heal, Polymer International, 56 (2007) 1183-1185.

[119] S.J. Bryant, J.L. Cuy, K.D. Hauch, B.D. Ratner, Photo-patterning of porous hydrogels for tissue engineering, Biomaterials, 28 (2007) 2978-2986.

[120] M.P. Linnes, B.D. Ratner, C.M. Giachelli, A fibrinogen-based precision microporous scaffold for tissue engineering, Biomaterials, 28 (2007) 5298-5306.

[121] W.M. Elbjeirami, E.O. Yonter, B.C. Starcher, J.L. West, Enhancing mechanical properties of tissue-engineered constructs via lysyl oxidase crosslinking activity, Journal of Biomedical Materials Research Part A, 66A (2003) 513-521.

[122] H. Enderling, N.R. Alexander, E.S. Clark, K.M. Branch, L. Estrada, C. Crooke, J. Jourquin, N. Lobdell, M.H. Zaman, S.A. Guelcher, A.R.A. Anderson, A.M. Weaver, Dependence of Invadopodia Function on Collagen Fiber Spacing and Cross-Linking: Computational Modeling and Experimental Evidence, Biophysical journal, 95 (2008) 2203-2218.

[123] M. Ehrbar, A. Sala, P. Lienemann, A. Ranga, K. Mosiewicz, A. Bittermann, S.C. Rizzi, F.E. Weber, M.P. Lutolf, Elucidating the role of matrix stiffness in 3D cell migration and remodeling, Biophysical journal, 100 (2011) 284-293.

[124] K. Wolf, Y.I. Wu, Y. Liu, J. Geiger, E. Tam, C. Overall, M.S. Stack, P. Friedl, Multi-step pericellular proteolysis controls the transition from individual to collective cancer cell invasion, Nature cell biology, 9 (2007) 893-904.

[125] P.P. Provenzano, D.R. Inman, K.W. Eliceiri, S.M. Trier, P.J. Keely, Contact Guidance Mediated Three-Dimensional Cell Migration is Regulated by Rho/ROCK-Dependent Matrix Reorganization, Biophysical journal, 95 (2008) 5374-5384.

[126] K.R. Levental, H. Yu, L. Kass, J.N. Lakins, M. Egeblad, J.T. Erler, S.F. Fong, K. Csiszar, A. Giaccia, W. Weninger, M. Yamauchi, D.L. Gasser, V.M. Weaver, Matrix crosslinking forces tumor progression by enhancing integrin signaling, Cell, 139 (2009) 891-906.

[127] A.J. Ridley, M.A. Schwartz, K. Burridge, R.A. Firtel, M.H. Ginsberg, G. Borisy, J.T. Parsons, A.R. Horwitz, Cell Migration: Integrating Signals from Front to Back, Science, 302 (2003) 1704-1709.

[128] P. Friedl, K. Wolf, Proteolytic interstitial cell migration: a five-step process, Cancer Metastasis Rev, 28 (2009) 129-135.

[129] P. Friedl, S. Alexander, Cancer Invasion and the Microenvironment: Plasticity and Reciprocity, Cell, 147 (2011) 992-1009.

[130] Y.-J. Liu, M. Le Berre, F. Lautenschlaeger, P. Maiuri, A. Callan-Jones, M. Heuzé, T. Takaki, R. Voituriez, M. Piel, Confinement and Low Adhesion Induce Fast Amoeboid Migration of Slow Mesenchymal Cells, Cell, 160 (2015) 659-672.

[131] P. Friedl, K. Wolf, Tumour-cell invasion and migration: diversity and escape mechanisms, Nat Rev Cancer, 3 (2003) 362-374.

[132] K. Wolf, R. Müller, S. Borgmann, E.-B. Bröcker, P. Friedl, Amoeboid shape change and contact guidance: T-lymphocyte crawling through fibrillar collagen is independent of matrix remodeling by MMPs and other proteases, 2003.

[133] T. Lämmermann, M. Sixt, Mechanical modes of 'amoeboid' cell migration, Current opinion in cell biology, 21 (2009) 636-644.

[134] R.J. Petrie, N. Gavara, R.S. Chadwick, K.M. Yamada, Nonpolarized signaling reveals two distinct modes of 3D cell migration, The Journal of cell biology, 197 (2012) 439-455.

[135] P. Friedl, K. Wolf, J. Lammerding, Nuclear mechanics during cell migration, Current opinion in cell biology, 23 (2011) 55-64.

[136] T. Harada, J. Swift, J. Irianto, J.-W. Shin, K.R. Spinler, A. Athirasala, R. Diegmiller, P.C.D.P. Dingal, I.L. Ivanovska, D.E. Discher, Nuclear lamin stiffness is a barrier to 3D migration, but softness can limit survival, The Journal of cell biology, 204 (2014) 669-682.

[137] B.R. Saunders, B. Vincent, Microgel particles as model colloids: theory, properties and applications, Advances in colloid and interface science, 80 (1999) 1-25.

[138] R. Pelton, Temperature-sensitive aqueous microgels, Advances in colloid and interface science, 85 (2000) 1-33.

[139] X. Wang, X. Qiu, C. Wu, Comparison of the Coil-to-Globule and the Globule-to-Coil Transitions of a Single Poly(N-isopropylacrylamide) Homopolymer Chain in Water, Macromolecules, 31 (1998) 2972-2976.

[140] P.N. Pusey, W. van Megen, Phase behaviour of concentrated suspensions of nearly hard colloidal spheres, Nature, 320 (1986) 340-342.

[141] J. Mattsson, H.M. Wyss, A. Fernandez-Nieves, K. Miyazaki, Z. Hu, D.R. Reichman, D.A. Weitz, Soft colloids make strong glasses, Nature, 462 (2009) 83-86.

[142] H.M. Wyss, T. Franke, E. Mele, D.A. Weitz, Capillary micromechanics: Measuring the elasticity of microscopic soft objects, Soft Matter, 6 (2010) 4550-4555.

[143] R.A. Petros, J.M. DeSimone, Strategies in the design of nanoparticles for therapeutic applications, Nat Rev Drug Discov, 9 (2010) 615-627.

[144] R.P. Brinkhuis, F.P.J.T. Rutjes, J.C.M. van Hest, Polymeric vesicles in biomedical applications, Polymer Chemistry, 2 (2011) 1449-1462.

[145] G.S. Kwon, K. Kataoka, Block copolymer micelles as long-circulating drug vehicles, Advanced Drug Delivery Reviews, 16 (1995) 295-309.

[146] B. Städler, A.D. Price, A.N. Zelikin, A Critical Look at Multilayered Polymer Capsules in Biomedicine: Drug Carriers, Artificial Organelles, and Cell Mimics, Advanced Functional Materials, 21 (2011) 14-28.

[147] M. Malmsten, Soft drug delivery systems, Soft Matter, 2 (2006) 760-769.

[148] M.H. Smith, L.A. Lyon, Multifunctional Nanogels for siRNA Delivery, Accounts of Chemical Research, 45 (2011) 985-993.

[149] H. Bysell, R. Månsson, P. Hansson, M. Malmsten, Microgels and microcapsules in peptide and protein drug delivery, Advanced Drug Delivery Reviews, 63 (2011) 1172-1185.

[150] A.V. Kabanov, S.V. Vinogradov, Nanogels as Pharmaceutical Carriers: Finite Networks of Infinite Capabilities, Angewandte Chemie International Edition, 48 (2009) 5418-5429.

[151] B.-S. Kim, S.W. Park, P.T. Hammond, Hydrogen-Bonding Layer-by-Layer-Assembled Biodegradable Polymeric Micelles as Drug Delivery Vehicles from Surfaces, ACS Nano, 2 (2008) 386-392.

[152] C. Mendoza-Palomares, A. Ferrand, S. Facca, F. Fioretti, G. Ladam, S. Kuchler-Bopp, T. Regnier, D. Mainard, N. Benkirane-Jessel, Smart Hybrid Materials Equipped by Nanoreservoirs of Therapeutics, ACS Nano, 6 (2012) 483-490.

[153] S.M. Gutowski, K.L. Templeman, A.B. South, J.C. Gaulding, J.T. Shoemaker, M.C. LaPlaca, R.V. Bellamkonda, L.A. Lyon, A.J. Garcia, Host response to microgel coatings on neural electrodes implanted in the brain, Journal of biomedical materials research. Part A, 102 (2014) 1486-1499.

[154] G. Eng, B.W. Lee, H. Parsa, C.D. Chin, J. Schneider, G. Linkov, S.K. Sia, G. Vunjak-Novakovic, Assembly of complex cell microenvironments using geometrically docked hydrogel shapes, Proceedings of the National Academy of Sciences, 110 (2013) 4551-4556.

[155] E.A. Scott, M.D. Nichols, R. Kuntz-Willits, D.L. Elbert, Modular scaffolds assembled around living cells using poly(ethylene glycol) microspheres with macroporation via a non-cytotoxic porogen, Acta biomaterialia, 6 (2010) 29-38.

[156] G. Villar, A.D. Graham, H. Bayley, A tissue-like printed material, Science, 340 (2013) 48-52.

[157] J.P. Gong, Why are double network hydrogels so tough?, Soft Matter, 6 (2010) 2583.

[158] N. Huebsch, P.R. Arany, A.S. Mao, D. Shvartsman, O.A. Ali, S.A. Bencherif, J. Rivera-Feliciano, D.J. Mooney, Harnessing traction-mediated manipulation of the cell/matrix interface to control stem-cell fate, Nature materials, 9 (2010) 518-526.

[159] M. Guvendiren, J.A. Burdick, Engineering synthetic hydrogel microenvironments to instruct stem cells, Current opinion in biotechnology, 24 (2013) 841-846.

[160] M.B. Browning, T. Wilems, M. Hahn, E. Cosgriff-Hernandez, Compositional control of poly(ethylene glycol) hydrogel modulus independent of mesh size, Journal of biomedical materials research. Part A, 98 (2011) 268-273.

[161] A.K. Gaharwar, N.A. Peppas, A. Khademhosseini, Nanocomposite hydrogels for biomedical applications, Biotechnology and bioengineering, 111 (2014) 441-453.

[162] K. Haraguchi, T. Takada, Synthesis and Characteristics of Nanocomposite Gels Prepared by In Situ Photopolymerization in an Aqueous System, Macromolecules, 43 (2010) 4294-4299.

[163] P. Schexnailder, E. Loizou, L. Porcar, P. Butler, G. Schmidt, Heterogeneity in nanocomposite hydrogels from poly(ethylene oxide) cross-linked with silicate nanoparticles, Physical chemistry chemical physics : PCCP, 11 (2009) 2760-2766.

[164] N. Lin, J. Huang, A. Dufresne, Preparation, properties and applications of polysaccharide nanocrystals in advanced functional nanomaterials: a review, Nanoscale, 4 (2012) 3274-3294.

[165] K.K. Gupta, A. Kundan, P.K. Mishra, P. Srivastava, S. Mohanty, N.K. Singh, A. Mishra, P. Maiti, Polycaprolactone composites with TiO2 for potential nanobiomaterials: tunable properties using different phases, Physical chemistry chemical physics : PCCP, 14 (2012) 12844-12853.

[166] J. Hu, T. Kurokawa, T. Nakajima, T.L. Sun, T. Suekama, Z.L. Wu, S.M. Liang, J.P. Gong, High Fracture Efficiency and Stress Concentration Phenomenon for Microgel-Reinforced Hydrogels Based on Double-Network Principle, Macromolecules, 45 (2012) 9445-9451.

[167] J. Meid, F. Dierkes, J. Cui, R. Messing, A.J. Crosby, A. Schmidt, W. Richtering, Mechanical properties of temperature sensitive microgel/polyacrylamide composite hydrogels-from soft to hard fillers, Soft Matter, 8 (2012) 4254-4263.

[168] R. Liu, J.M. Saunders, T.J. Freemont, B.R. Saunders, Doubly crosslinked microgel-polyelectrolyte complexes: three simple methods to tune and improve gel mechanical properties, Soft Matter, 8 (2012) 10932-10940.

[169] C. Supasuteekul, A.H. Milani, J.M. Saunders, S. Lally, T. Freemont, B.R. Saunders, A study of hydrogel composites containing pH-responsive doubly crosslinked microgels, Soft Matter, 8 (2012) 7234-7242.

[170] A.H. Milani, A.J. Freemont, J.A. Hoyland, D.J. Adlam, B.R. Saunders, Injectable doubly cross-linked microgels for improving the mechanical properties of degenerated intervertebral discs, Biomacromolecules, 13 (2012) 2793-2801.

[171] K.C. Clarke, A.M. Douglas, A.C. Brown, T.H. Barker, L.A. Lyon, Colloid-matrix assemblies in regenerative medicine, Current Opinion in Colloid & Interface Science, 18 (2013) 393-405.

[172] J. Gao, B.J. Frisken, Cross-Linker-Free N-Isopropylacrylamide Gel Nanospheres, Langmuir : the ACS journal of surfaces and colloids, 19 (2003) 5212-5216.

[173] J. Gao, B.J. Frisken, Influence of Reaction Conditions on the Synthesis of Self-Cross-Linked N-Isopropylacrylamide Microgels, Langmuir : the ACS journal of surfaces and colloids, 19 (2003) 5217-5222.

[174] M.H. Smith, L.A. Lyon, Tunable Encapsulation of Proteins within Charged Microgels, Macromolecules, 44 (2011) 8154-8160.

[175] R. Pelton, T. Hoare, Microgels and Their Synthesis: An Introduction, in: Microgel Suspensions, Wiley-VCH Verlag GmbH & Co. KGaA, 2011, pp. 1-32.

[176] A. Galperin, T.J. Long, S. Garty, B.D. Ratner, Synthesis and fabrication of a degradable poly(N-isopropyl acrylamide) scaffold for tissue engineering applications, Journal of biomedical materials research. Part A, 101 (2013) 775-786.

[177] A. Galperin, T.J. Long, B.D. Ratner, Degradable, thermo-sensitive poly(N-isopropyl acrylamide)-based scaffolds with controlled porosity for tissue engineering applications, Biomacromolecules, 11 (2010) 2583-2592.

[178] M. Cloitre, Yielding, Flow, and Slip in Microgel Suspensions: From Microstructure to Macroscopic Rheology, in: Microgel Suspensions, Wiley-VCH Verlag GmbH & Co. KGaA, 2011, pp. 283-309.

[179] C. Macosko, Rheology: principles, measurements, and applications, Advances in interfacial engineering series, (1994).

[180] H. Bachman, A.C. Brown, K.C. Clarke, K.S. Dhada, A. Douglas, C.E. Hansen, E. Herman, J.S. Hyatt, P. Kodlekere, Z. Meng, S. Saxena, M.W. Spears Jr, N. Welsch, L.A. Lyon, Ultrasoft, highly deformable microgels, Soft Matter, 11 (2015) 2018-2028.

[181] S. Asakura, F. Oosawa, On Interaction between Two Bodies Immersed in a Solution of Macromolecules, The Journal of Chemical Physics, 22 (1954) 1255-1256.

[182] P.J. Lu, J.C. Conrad, H.M. Wyss, A.B. Schofield, D.A. Weitz, Fluids of Clusters in Attractive Colloids, Physical Review Letters, 96 (2006) 028306.

[183] D. Marenduzzo, K. Finan, P.R. Cook, The depletion attraction: an underappreciated force driving cellular organization, The Journal of cell biology, 175 (2006) 681-686.

[184] R.H. Adams, K. Alitalo, Molecular regulation of angiogenesis and lymphangiogenesis, Nature reviews. Molecular cell biology, 8 (2007) 464-478.

[185] M. Potente, H. Gerhardt, P. Carmeliet, Basic and Therapeutic Aspects of Angiogenesis, Cell, 146 873-887.

[186] S. Balaji, A. King, T.M. Crombleholme, S.G. Keswani, The Role of Endothelial Progenitor Cells in Postnatal Vasculogenesis: Implications for Therapeutic Neovascularization and Wound Healing, Advances in Wound Care, 2 (2013) 283-295.

[187] M. Eguchi, H. Masuda, T. Asahara, Endothelial progenitor cells for postnatal vasculogenesis, Clin Exp Nephrol, 11 (2007) 18-25.

[188] M. Kioi, H. Vogel, G. Schultz, R.M. Hoffman, G.R. Harsh, J.M. Brown, Inhibition of vasculogenesis, but not angiogenesis, prevents the recurrence of glioblastoma after irradiation in mice, The Journal of Clinical Investigation, 120 (2010) 694-705.

[189] S. Purhonen, J. Palm, D. Rossi, N. Kaskenpää, I. Rajantie, S. Ylä-Herttuala, K. Alitalo, I.L. Weissman, P. Salven, Bone marrow-derived circulating endothelial precursors do not contribute to vascular endothelium and are not needed for tumor growth, Proceedings of the National Academy of Sciences, 105 (2008) 6620-6625.

[190] M. Heil, I. Eitenmüller, T. Schmitz-Rixen, W. Schaper, Arteriogenesis versus angiogenesis: similarities and differences, Journal of Cellular and Molecular Medicine, 10 (2006) 45-55.

[191] P. Carmeliet, Angiogenesis in health and disease, Nat Med, 9 (2003) 653-660.

[192] P. Carmeliet, R.K. Jain, Molecular mechanisms and clinical applications of angiogenesis, Nature, 473 (2011) 298-307.

[193] B.H. Annex, Therapeutic angiogenesis for critical limb ischaemia, Nat Rev Cardiol, 10 (2013) 387-396.

[194] D. Mozaffarian, E.J. Benjamin, A.S. Go, D.K. Arnett, M.J. Blaha, M. Cushman, S. de Ferranti, J.-P. Després, H.J. Fullerton, V.J. Howard, M.D. Huffman, S.E. Judd, B.M. Kissela, D.T. Lackland, J.H. Lichtman, L.D. Lisabeth, S. Liu, R.H. Mackey, D.B. Matchar, D.K. McGuire, E.R. Mohler, C.S. Moy, P. Muntner, M.E. Mussolino, K. Nasir, R.W. Neumar, G. Nichol, L. Palaniappan, D.K. Pandey, M.J. Reeves, C.J. Rodriguez, P.D. Sorlie, J. Stein, A. Towfighi, T.N. Turan, S.S. Virani, J.Z. Willey, D. Woo, R.W. Yeh, M.B. Turner, Heart Disease and Stroke Statistics—2015 Update: A Report From the American Heart Association, Circulation, 131 (2015) e29-e322.

[195] V. van Weel, R.B. van Tongeren, V.W.M. van Hinsbergh, J.H. van Bockel, P.H.A. Quax, Vascular Growth in Ischemic Limbs: A Review of Mechanisms and Possible Therapeutic Stimulation, Annals of Vascular Surgery, 22 (2008) 582-597.

[196] B.H. Annex, M. Simons, Growth factor-induced therapeutic angiogenesis in the heart: protein therapy, 2005.

[197] J. Tongers, J.G. Roncalli, D.W. Losordo, Therapeutic Angiogenesis for Critical Limb Ischemia: Microvascular Therapies Coming of Age, Circulation, 118 (2008) 9-16.

[198] E.A. Phelps, A.J. Garcia, Update on therapeutic vascularization strategies, Regenerative Medicine, 4 (2008) 65-80.

[199] M.M. Martino, S. Brkic, E. Bovo, M. Burger, D.J. Schäfer, T. Wolff, L. Gürke, P.S. Briquez, H.M. Larsson, R. Gianni Barrera, J.A. Hubbell, A. Banfi, Extracellular matrix and growth factor engineering for controlled angiogenesis in regenerative medicine, Frontiers in Bioengineering and Biotechnology, 3 (2015).

[200] O. Ilina, P. Friedl, Mechanisms of collective cell migration at a glance, Journal of cell science, 122 (2009) 3203-3208.

[201] P. Friedl, D. Gilmour, Collective cell migration in morphogenesis, regeneration and cancer, Nature reviews. Molecular cell biology, 10 (2009) 445-457.

[202] P. Friedl, K. Wolf, M.M. Zegers, Rho-directed forces in collective migration, Nature cell biology, 16 (2014) 208-210.

[203] U.R. Michaelis, Mechanisms of endothelial cell migration, Cell. Mol. Life Sci., 71 (2014) 4131-4148.

[204] A. Haeger, M. Krause, K. Wolf, P. Friedl, Cell jamming: Collective invasion of mesenchymal tumor cells imposed by tissue confinement, Biochimica et Biophysica Acta (BBA) - General Subjects, 1840 (2014) 2386-2395.

[205] J.S. Miller, K.R. Stevens, M.T. Yang, B.M. Baker, D.-H.T. Nguyen, D.M. Cohen, E. Toro, A.A. Chen, P.A. Galie, X. Yu, R. Chaturvedi, S.N. Bhatia, C.S. Chen, Rapid casting of patterned vascular networks for perfusable engineered three-dimensional tissues, Nature materials, 11 (2012) 768-774.

[206] J.D. Baranski, R.R. Chaturvedi, K.R. Stevens, J. Eyckmans, B. Carvalho, R.D. Solorzano, M.T. Yang, J.S. Miller, S.N. Bhatia, C.S. Chen, Geometric control of vascular networks to enhance engineered tissue integration and function, Proceedings of the National Academy of Sciences of the United States of America, 110 (2013) 7586-7591.

[207] R.R. Chaturvedi, K.R. Stevens, R.D. Solorzano, R.E. Schwartz, J. Eyckmans, J.D. Baranski, S.C. Stapleton, S.N. Bhatia, C.S. Chen, Patterning Vascular Networks In Vivo for Tissue Engineering Applications, Tissue Engineering Part C: Methods, 21 (2014) 509-517.

[208] I. Arnaoutova, J. George, H. Kleinman, G. Benton, The endothelial cell tube formation assay on basement membrane turns 20: state of the science and the art, Angiogenesis, 12 (2009) 267-274.

[209] D.G. Chalupowicz, Z.A. Chowdhury, T.L. Bach, C. Barsigian, J. Martinez, Fibrin II induces endothelial cell capillary tube formation, The Journal of cell biology, 130 (1995) 207-215.

[210] M.N. Nakatsu, R.C.A. Sainson, J.N. Aoto, K.L. Taylor, M. Aitkenhead, S. Pérez-del-Pulgar, P.M. Carpenter, C.C.W. Hughes, Angiogenic sprouting and capillary lumen formation modeled by human umbilical vein endothelial cells (HUVEC) in fibrin gels: the role of fibroblasts and Angiopoietin-1 ☆, Microvascular research, 66 (2003) 102-112.

[211] L. Krishnan, C.J. Underwood, S. Maas, B.J. Ellis, T.C. Kode, J.B. Hoying, J.A. Weiss, Effect of mechanical boundary conditions on orientation of angiogenic microvessels, Cardiovasc Res, 78 (2008) 324-332.

[212] L. Krishnan, J.B. Hoying, H. Nguyen, H. Song, J.A. Weiss, Interaction of angiogenic microvessels with the extracellular matrix, American journal of physiology. Heart and circulatory physiology, 293 (2007) H3650-3658.

[213] B.R. Shepherd, H.Y. Chen, C.M. Smith, G. Gruionu, S.K. Williams, J.B. Hoying, Rapid perfusion and network remodeling in a microvascular construct after implantation, Arterioscler Thromb Vasc Biol, 24 (2004) 898-904.

[214] N.D. Kirkpatrick, S. Andreou, J.B. Hoying, U. Utzinger, Live imaging of collagen remodeling during angiogenesis, American journal of physiology. Heart and circulatory physiology, 292 (2007) H3198-3206.

[215] C.C. Chang, J.B. Hoying, Directed three-dimensional growth of microvascular cells and isolated microvessel fragments, Cell transplantation, 15 (2006) 533-540.

[216] C.C. Chang, L. Krishnan, S.S. Nunes, K.H. Church, L.T. Edgar, E.D. Boland, J.A. Weiss, S.K. Williams, J.B. Hoying, Determinants of microvascular network topologies in implanted neovasculatures, Arterioscler Thromb Vasc Biol, 32 (2012) 5-14.

[217] J.B. Hoying, C.A. Boswell, S.K. Williams, Angiogenic potential of microvessel fragments established in three-dimensional collagen gels, In vitro cellular & developmental biology. Animal, 32 (1996) 409-419.

[218] K. Lee, E.A. Silva, D.J. Mooney, Growth factor delivery-based tissue engineering: general approaches and a review of recent developments, 2011.

[219] J.J. Moon, J.L. West, Vascularization of engineered tissues: approaches to promote angio-genesis in biomaterials, Current topics in medicinal chemistry, 8 (2008) 300-310.

[220] S. Ylä-Herttuala, J.E. Markkanen, T.T. Rissanen, Gene Therapy for Ischemic Cardiovascular Diseases: Some Lessons Learned from the First Clinical Trials, Trends in Cardiovascular Medicine, 14 (2004) 295-300.

[221] R. Gupta, J. Tongers, D.W. Losordo, Human Studies of Angiogenic Gene Therapy, Circulation Research, 105 (2009) 724-736.

[222] M.M. Martino, P.S. Briquez, A. Ranga, M.P. Lutolf, J.A. Hubbell, Heparin-binding domain of fibrin(ogen) binds growth factors and promotes tissue repair when incorporated within a synthetic matrix, Proceedings of the National Academy of Sciences, 110 (2013) 4563-4568.

[223] E.A. Phelps, N. Landázuri, P.M. Thulé, W.R. Taylor, A.J. García, Bioartificial matrices for therapeutic vascularization, Proceedings of the National Academy of Sciences, 107 (2010) 3323-3328.

[224] J.J. Moon, J.E. Saik, R.A. Poche, J.E. Leslie-Barbick, S.H. Lee, A.A. Smith, M.E. Dickinson, J.L. West, Biomimetic hydrogels with pro-angiogenic properties, Biomaterials, 31 (2010) 3840-3847.

[225] J.K.G. Dhont, An Introduction to Dynamics of Colloids, Elsevier, 1996.

[226] K. Schatzel, Suppression of Multiple-Scattering by Photon Cross-Correlation Techniques, J Mod Optic, 38 (1991) 1849-1865.

[227] K. Kratz, T. Hellweg, W. Eimer, Influence of charge density on the swelling of colloidal poly(N-isopropylacrylamide-co-acrylic acid) microgels, Colloid Surface A, 170 (2000) 137-149.

[228] B.H. Tan, K.C. Tam, Review on the dynamics and micro-structure of pH-responsive nano-colloidal systems, Adv Colloid Interfac, 136 (2008) 25-44.

[229] A. Torsello, E.R. Hancock, A skeletal measure of 2D shape similarity, Computer Vision and Image Understanding, 95 (2004) 1-29.

[230] M.S. Hassouna, MultiStencils Fast Marching Methods: A Highly Accurate Solution to the Eikonal Equation on Cartesian Domains, IEEE Transactions on Pattern Analysis and Machine Intelligence, 29 (2007) 1563-1574.

[231] C. Storm, J.J. Pastore, F.C. MacKintosh, T.C. Lubensky, P.A. Janmey, Nonlinear elasticity in biological gels, Nature, 435 (2005) 191-194.

[232] G. Jell, C. Minelli, M.M. Stevens, Biomaterial-Related Approaches: Surface Structuring, in: U. Meyer, J. Handschel, H.P. Wiesmann, T. Meyer (Eds.) Fundamentals of Tissue Engineering and Regenerative Medicine, Springer Berlin Heidelberg, 2009, pp. 469-484.

[233] D.E. Discher, P. Janmey, Y.L. Wang, Tissue cells feel and respond to the stiffness of their substrate, Science, 310 (2005) 1139-1143.

[234] A.J. Engler, S. Sen, H.L. Sweeney, D.E. Discher, Matrix Elasticity Directs Stem Cell Lineage Specification, Cell, 126 (2006) 677-689.

[235] M.P. Lutolf, P.M. Gilbert, H.M. Blau, Designing materials to direct stem-cell fate, Nature, 462 (2009) 433-441.

[236] P.M. Gilbert, K.L. Havenstrite, K.E.G. Magnusson, A. Sacco, N.A. Leonardi, P. Kraft, N.K. Nguyen, S. Thrun, M.P. Lutolf, H.M. Blau, Substrate Elasticity Regulates Skeletal Muscle Stem Cell Self-Renewal in Culture, Science, 329 (2010) 1078-1081.

[237] I.L. Ivanovska, J.-W. Shin, J. Swift, D.E. Discher, Stem cell mechanobiology: diverse lessons from bone marrow, Trends in cell biology, (2015).

[238] J. Swift, I.L. Ivanovska, A. Buxboim, T. Harada, P.C.D.P. Dingal, J. Pinter, J.D. Pajerowski, K.R. Spinler, J.-W. Shin, M. Tewari, F. Rehfeldt, D.W. Speicher, D.E. Discher, Nuclear Lamin-A Scales with Tissue Stiffness and Enhances Matrix-Directed Differentiation, Science, 341 (2013).

[239] A.J. Engler, M.A. Griffin, S. Sen, C.G. Bonnemann, H.L. Sweeney, D.E. Discher, Myotubes differentiate optimally on substrates with tissue-like stiffness: pathological implications for soft or stiff microenvironments, The Journal of cell biology, 166 (2004) 877-887.

[240] B.D. Cosgrove, P.M. Gilbert, E. Porpiglia, F. Mourkioti, S.P. Lee, S.Y. Corbel, M.E. Llewellyn, S.L. Delp, H.M. Blau, Rejuvenation of the muscle stem cell population restores strength to injured aged muscles, Nat Med, 20 (2014) 255-264.

[241] Y. Tang, R.G. Rowe, Elliot L. Botvinick, A. Kurup, Andrew J. Putnam, M. Seiki, Valerie M. Weaver, Evan T. Keller, S. Goldstein, J. Dai, D. Begun, T. Saunders, Stephen J. Weiss, MT1-MMP-Dependent Control of Skeletal Stem Cell Commitment via a β1-Integrin/YAP/TAZ Signaling Axis, Developmental cell, 25 (2013) 402-416.

[242] A. Jacob, R. Prekeris, The regulation of MMP targeting to invadopodia during cancer metastasis, Frontiers in Cell and Developmental Biology, 3 (2015) 4.

[243] S.E.A. Gratton, P.A. Ropp, P.D. Pohlhaus, J.C. Luft, V.J. Madden, M.E. Napier, J.M. DeSimone, The effect of particle design on cellular internalization pathways, Proceedings of the National Academy of Sciences, 105 (2008) 11613-11618.

[244] K. Kettler, K. Veltman, D. van de Meent, A. van Wezel, A.J. Hendriks, Cellular uptake of nanoparticles as determined by particle properties, experimental conditions, and cell type, Environmental Toxicology & Chemistry, 33 (2014) 481-492.

[245] J.-W. Yoo, S. Mitragotri, Polymer particles that switch shape in response to a stimulus, Proceedings of the National Academy of Sciences, 107 (2010) 11205-11210.

[246] S. Sayedyahossein, L. Dagnino, Chapter Six - Integrins and Small GTPases as Modulators of Phagocytosis, in: W.J. Kwang (Ed.) International Review of Cell and Molecular Biology, Academic Press, 2013, pp. 321-354.

[247] E.A. Phelps, N.O. Enemchukwu, V.F. Fiore, J.C. Sy, N. Murthy, T.A. Sulchek, T.H. Barker, A.J. García, Maleimide Cross-Linked Bioactive PEG Hydrogel Exhibits Improved Reaction Kinetics and Cross-Linking for Cell Encapsulation and In Situ Delivery, Advanced Materials, 24 (2012) 64-70.

[248] J.A. Rowley, G. Madlambayan, D.J. Mooney, Alginate hydrogels as synthetic extracellular matrix materials, Biomaterials, 20 (1999) 45-53.

[249] K.Y. Lee, D.J. Mooney, Alginate: properties and biomedical applications, Progress in polymer science, 37 (2012) 106-126.

[250] Y. Fang, S. Al-Assaf, G.O. Phillips, K. Nishinari, T. Funami, P.A. Williams, L. Li, Multiple Steps and Critical Behaviors of the Binding of Calcium to Alginate, The Journal of Physical Chemistry B, 111 (2007) 2456-2462.

[251] A.B. Allen, Z. Gazit, S. Su, H.Y. Stevens, R.E. Guldberg, In Vivo Bioluminescent Tracking of Mesenchymal Stem Cells Within Large Hydrogel Constructs, Tissue engineering. Part C, Methods, (2014).

[252] C.R. Dosier, B.A. Uhrig, N.J. Willett, L. Krishnan, M.-T.A. Li, H.Y. Stevens, Z. Schwartz, B.D. Boyan, R.E. Guldberg, Effect of Cell Origin and Timing of Delivery for Stem Cell-Based Bone Tissue Engineering Using Biologically Functionalized Hydrogels, Tissue Engineering Part A, 21 (2014) 156-165.

[253] S. Asakura, F. Oosawa, On interaction between two bodies immersed in a solution of macromolecules, Chemical Physics, (1954) 1255-1256.

[254] T.T. Lee, J.R. García, J.I. Paez, A. Singh, E.A. Phelps, S. Weis, Z. Shafiq, A. Shekaran, A. del Campo, A.J. García, Light-triggered in vivo activation of adhesive peptides regulates cell adhesion, inflammation and vascularization of biomaterials, Nature materials, 14 (2015) 352-360.

[255] B.M. Baker, R.P. Shah, A.M. Silverstein, J.L. Esterhai, J.A. Burdick, R.L. Mauck, Sacrificial nanofibrous composites provide instruction without impediment and enable functional tissue formation, Proceedings of the National Academy of Sciences, 109 (2012) 14176-14181.

[256] R.J. Wade, E.J. Bassin, C.B. Rodell, J.A. Burdick, Protease-degradable electrospun fibrous hydrogels, Nature communications, 6 (2015).

[257] C.C. Chang, S.S. Nunes, S.C. Sibole, L. Krishnan, S.K. Williams, J.A. Weiss, J.B. Hoying, Angiogenesis in a microvascular construct for transplantation depends on the method of chamber circulation, Tissue engineering. Part A, 16 (2010) 795-805.

[258] R.P. Rhoads, R.M. Johnson, C.R. Rathbone, X. Liu, C. Temm-Grove, S.M. Sheehan, J.B. Hoying, R.E. Allen, Satellite cell-mediated angiogenesis in vitro coincides with a functional hypoxia-inducible factor pathway, American journal of physiology. Cell physiology, 296 (2009) C1321-1328.

[259] K.B. Vartanian, H.Y. Chen, J. Kennedy, S.K. Beck, J.T. Ryaby, H. Wang, J.B. Hoying, The non-proteolytically active thrombin peptide TP508 stimulates angiogenic sprouting, Journal of cellular physiology, 206 (2006) 175-180.

[260] C.M. Ghajar, K.S. Blevins, C.C. Hughes, S.C. George, A.J. Putnam, Mesenchymal stem cells enhance angiogenesis in mechanically viable prevascularized tissues via early matrix metalloproteinase upregulation, Tissue engineering, 12 (2006) 2875-2888.

[261] C.L. Duvall, W.R. Taylor, D. Weiss, R.E. Guldberg, Quantitative microcomputed tomography analysis of collateral vessel development after ischemic injury, 2004.

[262] J.D. Boerckel, B.A. Uhrig, N.J. Willett, N. Huebsch, R.E. Guldberg, Mechanical regulation of vascular growth and tissue regeneration in vivo, Proceedings of the National Academy of Sciences, (2011).

[263] V. Nehls, D. Drenckhahn, A microcarrier-based cocultivation system for the investigation of factors and cells involved in angiogenesis in three-dimensional fibrin matrices in vitro, Histochemistry and cell biology, 104 (1995) 459-466.

[264] V. Nehls, D. Drenckhahn, A Novel, Microcarrier-Based in Vitro Assay for Rapid and Reliable Quantification of Three-Dimensional Cell Migration and Angiogenesis, Microvascular research, 50 (1995) 311-322.

[265] M.N. Nakatsu, J. Davis, C.C.W. Hughes, Optimized Fibrin Gel Bead Assay for the Study of Angiogenesis, Journal of Visualized Experiments : JoVE, (2007) 186.

[266] C.M. Ghajar, S. Kachgal, E. Kniazeva, H. Mori, S.V. Costes, S.C. George, A.J. Putnam, Mesenchymal cells stimulate capillary morphogenesis via distinct proteolytic mechanisms, Experimental cell research, 316 (2010) 813-825.

[267] D. Whelan, N.M. Caplice, A.J.P. Clover, Fibrin as a delivery system in wound healing tissue engineering applications, Journal of Controlled Release, 196 (2014) 1-8.

[268] K.M. Lorentz, S. Kontos, P. Frey, J.A. Hubbell, Engineered aprotinin for improved stability of fibrin biomaterials, Biomaterials, 32 (2011) 430-438.

[269] M. Ehrbar, V.G. Djonov, C. Schnell, S.A. Tschanz, G. Martiny-Baron, U. Schenk, J. Wood, P.H. Burri, J.A. Hubbell, A.H. Zisch, Cell-Demanded Liberation of VEGF121 From Fibrin Implants Induces Local and Controlled Blood Vessel Growth, Circulation Research, 94 (2004) 1124-1132.

[270] M. Ehrbar, S.M. Zeisberger, G.P. Raeber, J.A. Hubbell, C. Schnell, A.H. Zisch, The role of actively released fibrin-conjugated VEGF for VEGF receptor 2 gene activation and the enhancement of angiogenesis, Biomaterials, 29 (2008) 1720-1729.

[271] Q. Ye, G. Zünd, P. Benedikt, S. Jockenhoevel, S.P. Hoerstrup, S. Sakyama, J.A. Hubbell, M. Turina, Fibrin gel as a three dimensional matrix in cardiovascular tissue engineering, European Journal of Cardio-Thoracic Surgery, 17 (2000) 587-591.

[272] S.X. Vasquez, F. Gao, F. Su, V. Grijalva, J. Pope, B. Martin, J. Stinstra, M. Masner, N. Shah, D.M. Weinstein, R. Farias-Eisner, S.T. Reddy, Optimization of MicroCT Imaging and Blood Vessel Diameter Quantitation of Preclinical Specimen Vasculature with Radiopaque Polymer Injection Medium, PloS one, 6 (2011) e19099.

[273] D.R. Griffin, W.M. Weaver, P.O. Scumpia, D. Di Carlo, T. Segura, Accelerated wound healing by injectable microporous gel scaffolds assembled from annealed building blocks, Nature materials, 14 (2015) 737-744.

[274] E.A. Scott, M.D. Nichols, R. Kuntz-Willits, D.L. Elbert, Modular scaffolds assembled around living cells using poly(ethylene glycol) microspheres with macroporation via a non-cytotoxic porogen, Acta biomaterialia, 6 (2010) 29-38.

[275] E. Sussman, M. Halpin, J. Muster, R. Moon, B. Ratner, Porous Implants Modulate Healing and Induce Shifts in Local Macrophage Polarization in the Foreign Body Reaction, Annals of biomedical engineering, 42 (2014) 1508-1516.

[276] M. Grunewald, I. Avraham, Y. Dor, E. Bachar-Lustig, A. Itin, S. Jung, S. Chimenti, L. Landsman, R. Abramovitch, E. Keshet, VEGF-induced adult neovascularization: recruitment, retention, and role of accessory cells, Cell, 124 (2006) 175-189.

[277] T.T. Lau, D.-A. Wang, Stromal cell-derived factor-1 (SDF-1): homing factor for engineered regenerative medicine, Expert Opinion on Biological Therapy, 11 (2011) 189-197.

[278] J.T. Schantz, H. Chim, M. Whiteman, Cell guidance in tissue engineering: SDF-1 mediates site-directed homing of mesenchymal stem cells within three-dimensional polycaprolactone scaffolds, Tissue engineering, 13 (2007) 2615-2624.

[279] E. Chavakis, S. Dimmeler, Homing of Progenitor Cells to Ischemic Tissues, Antioxidants & Redox Signaling, 15 (2010) 967-980.

[280] G. Zhang, Y. Nakamura, X. Wang, Q. Hu, L.J. Suggs, J. Zhang, Controlled release of stromal cell-derived factor-1 alpha in situ increases c-kit+ cell homing to the infarcted heart, Tissue engineering, 13 (2007) 2063-2071.

[281] S.Y. Rabbany, J. Pastore, M. Yamamoto, T. Miller, S. Rafii, R. Aras, M. Penn, Continuous delivery of stromal cell-derived factor-1 from alginate scaffolds accelerates wound healing, Cell transplantation, 19 (2010) 399-408.

[282] K. Hattori, B. Heissig, K. Tashiro, T. Honjo, M. Tateno, J.-H. Shieh, N.R. Hackett, M.S. Quitoriano, R.G. Crystal, S. Rafii, M.A.S. Moore, Plasma elevation of stromal cell–derived factor-1 induces mobilization of mature and immature hematopoietic progenitor and stem cells, 2001.

[283] M. Kucia, J. Ratajczak, R. Reca, A. Janowska-Wieczorek, M.Z. Ratajczak, Tissue-specific muscle, neural and liver stem/progenitor cells reside in the bone marrow, respond to an SDF-1 gradient and are mobilized into peripheral blood during stress and tissue injury, Blood Cells, Molecules, and Diseases, 32 (2004) 52-57.

[284] J. Kijowski, M. Baj-Krzyworzeka, M. Majka, R. Reca, L.A. Marquez, M. Christofidou-Solomidou, A. Janowska-Wieczorek, M.Z. Ratajczak, The SDF-1-CXCR4 Axis Stimulates VEGF Secretion and Activates Integrins but does not Affect Proliferation and Survival in Lymphohematopoietic Cells, Stem cells, 19 (2001) 453-466.

[285] T. Neuhaus, S. Stier, G. Totzke, E. Gruenewald, S. Fronhoffs, A. Sachinidis, H. Vetter, Y.D. Ko, Stromal cell-derived factor 1α (SDF-1α) induces gene-expression of early growth response-1 (Egr-1) and VEGF in human arterial endothelial cells and enhances VEGF induced cell proliferation, Cell Proliferation, 36 (2003) 75-86.

[286] S. Prokoph, E. Chavakis, K.R. Levental, A. Zieris, U. Freudenberg, S. Dimmeler, C. Werner, Sustained delivery of SDF-1α from heparin-based hydrogels to attract circulating pro-angiogenic cells, Biomaterials, 33 (2012) 4792-4800.

[287] Y. Wang, D.J. Irvine, Engineering chemoattractant gradients using chemokine-releasing polysaccharide microspheres, Biomaterials, 32 (2011) 4903-4913.

[288] C.S. Chen, M. Mrksich, S. Huang, G.M. Whitesides, D.E. Ingber, Geometric Control of Cell Life and Death, Science, 276 (1997) 1425-1428.

[289] M. Rodrigues, L.G. Griffith, A. Wells, Growth factor regulation of proliferation and survival of multipotential stromal cells, Stem cell research & therapy, 1 (2010) 32.

[290] P. Giannoni, S. Scaglione, A. Daga, C. Ilengo, M. Cilli, R. Quarto, Short-Time Survival and Engraftment of Bone Marrow Stromal Cells in an Ectopic Model of Bone Regeneration, Tissue Engineering Part A, 16 (2009) 489-499.

[291] R. Tasso, A. Augello, S. Boccardo, S. Salvi, M. Caridà, F. Postiglione, F. Fais, M. Truini, R. Cancedda, G. Pennesi, Recruitment of a Host's Osteoprogenitor Cells Using Exogenous Mesenchymal Stem Cells Seeded on Porous Ceramic, Tissue Engineering Part A, 15 (2009) 2203-2212.